

# Notes on Wave Propagation in Anisotropic Elastic Solids

Michael Conry  
michael.conry@acronymchile.com

Apr 2005

## Abstract

The aim of this document is to summarise the information on elastic material properties, and wave propagation which I have found in my recent reading. The books and papers read are listed at the end of this document, and cited throughout. First, the basic constitutive equations governing elastic solids are presented. Once the concept of elastic properties has been established, our attention turns to the various symmetry classes which exist. These symmetries simplify the material properties. I have written more on symmetry than I had expected to, as the area turned out to be surprisingly interesting. Following on from the exposition of the material properties of various symmetry classes, we look at solving the dynamic elastic equations for specific materials. Slowness curves are introduced and calculated for particular cases.

Finally, following the discussion of Slowness curves in bulk anisotropic materials, attention is turned towards the problem of Lamb waves: guided waves in plates. This phenomenon is studied for isotropic plates, and also for anisotropic and inhomogeneous (layered) plates.

It is important to note that this document is still a work in progress. If anyone actually *does* read it, and has suggestions/corrections, I would be very glad to hear from them at michael.conry@acronymchile.com

# Contents

<b>1</b>	<b>Bulk Waves</b>	<b>6</b>
1.1	Basic Equations . . . . .	6
1.2	Reduced Notation . . . . .	7
1.3	Material Symmetry . . . . .	8
1.3.1	Triclinic Symmetry . . . . .	10
1.3.2	Monoclinic Symmetry . . . . .	10
1.3.3	Orthotropic Symmetry . . . . .	11
1.3.4	Tetragonal Symmetry . . . . .	12
1.3.5	Trigonal Symmetry . . . . .	15
1.3.6	Transversely Isotropic Symmetry . . . . .	17
1.3.7	Cubic Symmetry . . . . .	19
1.3.8	Isotropic Symmetry . . . . .	19
1.4	Bulk Waves . . . . .	20
1.4.1	Bulk Waves Background . . . . .	20
1.4.2	Computation of Slowness and Skew Curves Background . . . . .	22
1.4.3	Examples of Slowness and Skew Curves . . . . .	23
<b>2</b>	<b>Guided Waves in Plates</b>	<b>45</b>
2.1	Introduction . . . . .	45
2.2	Lamb Waves . . . . .	45
2.2.1	Lamb Waves in Aluminium Plate . . . . .	46
2.2.2	Boundary Conditions . . . . .	48
2.3	Isotropic Dispersion . . . . .	52
2.3.1	Introduction . . . . .	52
2.3.2	Preliminaries . . . . .	52
2.3.3	Detailed Calculation of Dispersion Curves . . . . .	54
2.4	Anisotropic and Inhomogeneous Plates . . . . .	55
2.4.1	Transverse Isotropy . . . . .	56
2.4.2	Stratified Media . . . . .	60
2.4.3	Plotting Dispersion Curves . . . . .	66
2.5	Propagation Normal to Fibres . . . . .	67

2.5.1	Material Properties . . . . .	67
2.5.2	Dispersion Curve . . . . .	71
2.6	Propagation Parallel to Fibres . . . . .	73
2.6.1	Dispersion Curve . . . . .	73
2.7	Cross Ply Composite . . . . .	75
2.7.1	Dispersion Curve . . . . .	75

# List of Figures

1.1	Triclinic Symmetry Point Groups . . . . .	10
1.2	Monoclinic Symmetry Point Groups . . . . .	11
1.3	Orthotropic Symmetry Point Groups . . . . .	12
1.4	Tetragonal Symmetry Point Groups . . . . .	13
1.5	Trigonal Symmetry Point Groups . . . . .	16
1.6	Hexagonal Symmetry Point Groups . . . . .	18
1.7	Slowness Curve for Isotropic Aluminium . . . . .	24
1.8	Slowness Curve for InAs, $\phi = 0$ . . . . .	25
1.9	Skew Curve for InAs, $\phi = 0$ . . . . .	26
1.10	Slowness Curve for InAs, $\phi = 45$ . . . . .	27
1.11	Skew Curve for InAs, $\phi = 45$ . . . . .	28
1.12	Slowness Curve for InAs, $\phi = 30$ . . . . .	29
1.13	Skew Curve for InAs, $\phi = 30$ . . . . .	30
1.14	Slowness Curve for Graphite Epoxy, $\phi = 0$ . . . . .	31
1.15	Skew Curve for Graphite Epoxy, $\phi = 0$ . . . . .	32
1.16	Slowness Curve for Graphite Epoxy, $\phi = 30$ . . . . .	33
1.17	Skew Curve for Graphite Epoxy, $\phi = 30$ . . . . .	34
1.18	Slowness Curve for Quartz, $\phi = 0$ , ( $X - Z$ Plane) . . . . .	35
1.19	Skew Curve for Quartz, $\phi = 0$ , ( $X - Z$ Plane) . . . . .	36
1.20	Slowness Curve for Quartz, $\phi = 90$ , ( $Y - Z$ Plane) . . . . .	37
1.21	Skew Curve for Quartz, $\phi = 90$ , ( $Y - Z$ Plane) . . . . .	38
1.22	Slowness Curve for Quartz, $\phi = 90$ , ( $X - Y$ Plane) . . . . .	39
1.23	Skew Curve for Quartz, $\phi = 90$ , ( $X - Y$ Plane) . . . . .	40
1.24	Slowness Curve for CdS, $\phi = 0$ , ( $X - Y$ Plane) . . . . .	41
1.25	Skew Curve for CdS, $\phi = 0$ , ( $X - Y$ Plane) . . . . .	42
1.26	Slowness Curve for CdS, $\phi = 90$ , ( $X - Z$ Plane) . . . . .	43
1.27	Skew Curve for CdS, $\phi = 90$ , ( $X - Z$ Plane) . . . . .	44
2.1	Schematic . . . . .	46
2.2	Velocity/frequency dispersion plot for aluminium. Solid lines are symmetric modes, dashed lines are antisymmetric modes. . . . .	55
2.3	Wavelength/Frequency Plot for $S_0$ Mode . . . . .	56

2.4	Schematic of propagation directions . . . . .	68
2.5	Slowness curves for propagation in the plane normal to the fibres	69
2.6	Slowness curves for propagation in a plane parallel to the fibres .	70
2.7	Velocity/frequency dispersion plot for unidirectional graphite fibre-reinforced epoxy, in plane of transverse isotropy. Solid lines are symmetric modes, dashed lines are antisymmetric modes. . . . .	72
2.8	Velocity/frequency dispersion plot for graphite fibre reinforced composite, in plane parallel to fibres. Solid lines are symmetric modes, dashed lines are antisymmetric modes. . . . .	74
2.9	Crossply plate geometry is of stacking sequence (a) $(90, 0, 90, 0, 90)_s$ , (b) $(0, 90, 0, 90, 0)_s$ . . . . .	78
2.10	Velocity/frequency dispersion plot for graphite fibre reinforced cross-ply composite as shown in Fig. 2.9(a). Solid lines are symmetric modes, dashed lines are antisymmetric modes. . . . .	79
2.11	Velocity/frequency dispersion plot for graphite fibre reinforced cross-ply composite as shown in Fig. 2.9(b). Solid lines are symmetric modes, dashed lines are antisymmetric modes. . . . .	80

# Chapter 1

## Bulk Waves

### 1.1 Basic Equations

The dynamic behaviour of a linear elastic generally anisotropic solid can be conveniently expressed using tensorial notation as shown below in equation (1.1), where indices  $i$  and  $j$  vary over 1,2,3. The usual tensor summation convention is assumed<sup>1</sup>

$$\frac{\partial \sigma'_{ij}}{\partial x'_j} = \rho' \frac{\partial^2 u'_i}{\partial t^2} \quad (1.1)$$

Equation (1.1), is written in the reference orthogonal coordinate system  $x'_i = (x'_1, x'_2, x'_3)$ . The constitutive relations, which show the interdependence of strain ( $\epsilon'_{kl}$ ) and stress ( $\sigma'_{i,j}$ ) can be given either in terms of stiffnesses ( $c'_{ijkl}$ )

$$\sigma'_{i,j} = c'_{ijkl} \epsilon'_{kl} \quad (1.2)$$

or inversely in terms of compliances ( $s'_{ijkl}$ ) as in equation (1.3).

$$\epsilon'_{i,j} = s'_{ijkl} \sigma'_{kl} \quad (1.3)$$

Finally, strain and displacement ( $u'_i$ ) are related as shown in equation (1.4).

$$\epsilon'_{k,l} = \frac{1}{2} \left( \frac{\partial u'_l}{\partial x'_k} + \frac{\partial u'_k}{\partial x'_l} \right). \quad (1.4)$$

In all of these equations, the presence of the prime indicates that the quantities are defined in the reference coordinate system.

Symmetry arguments allow some simplification of the quantities just intro-

---

<sup>1</sup> Summation over repeated indices:  $x_{i,j}y_j = x_{i,1}y_1 + x_{i,2}y_2 + x_{i,3}y_3$ .

duced. The strain and stress tensors are symmetric, i.e.  $\sigma'_{ij} = \sigma'_{ji}$  and  $\varepsilon'_{ij} = \varepsilon'_{ji}$ . Thus, the stiffness (and compliance tensors must have a corresponding degree of symmetry which leads to the simplifications shown in equation (1.5).

$$c'_{ijkl} = c'_{jikl} = c'_{ijlk} = c'_{jilk} \quad (1.5)$$

By energy considerations, as demonstrated in Nayfeh [1] and Auld [2], it can be shown that there is further symmetry in the stiffness and compliance tensor. The argument begins with a definition of strain energy density,  $U$ , and the use of the constitutive relation (1.2).

$$U = \frac{1}{2} \sigma'_{ij} \varepsilon'_{ij} = \frac{1}{2} c'_{ijkl} \varepsilon'_{kl} \varepsilon'_{ij} \quad (1.6)$$

Differentiating this expression gives the result

$$c'_{ijkl} = \frac{\partial^2 U}{\partial \varepsilon'_{ij} \partial \varepsilon'_{kl}}. \quad (1.7)$$

Interchanging the order of differentiation does not change this relation, and we conclude that

$$c'_{ijkl} = c'_{klij} \quad (1.8)$$

The simplifications introduced by (1.5) and (1.8) mean that rather than having  $3 \times 3 \times 3 \times 3 = 81$  independent values,  $c'_{ijkl}$  has at most 21 independent coefficients.

## 1.2 Reduced Notation

Often, when writing out expressions involving material stiffness properties, it is convenient to use a reduced notation which takes advantage of the symmetry present in the stiffness tensors describing even the most general elastic materials. This notation is a convenience, and is widely used in books and papers. In short, the contractions are as follows, where each pair of subscripts in the tensor equations is mapped to a single subscript in the reduced equations:

$$\begin{aligned} 1 &\iff 11, & 2 &\iff 22, & 3 &\iff 33 \\ 4 &\iff 23, & 5 &\iff 13, & 6 &\iff 12 \end{aligned} \quad (1.9)$$

To facilitate the use of this notation, engineering shear strain is introduced, defined as follows:

$$\gamma'_{12} = 2\varepsilon'_{12}, \quad \gamma'_{13} = 2\varepsilon'_{13}, \quad \gamma'_{23} = 2\varepsilon'_{23}, \quad (1.10)$$

We can now rewrite equation (1.2), using this new notation as shown in equation (1.11) (following the lead from Nayfeh [1], upper case  $C_{ij}$  is used to make the distinction from the full notation  $c_{ijkl}$  more apparent).

$$\begin{bmatrix} \sigma'_{11} \\ \sigma'_{22} \\ \sigma'_{33} \\ \sigma'_{23} \\ \sigma'_{13} \\ \sigma'_{12} \end{bmatrix} = \begin{bmatrix} C'_{11} & C'_{12} & C'_{13} & C'_{14} & C'_{15} & C'_{16} \\ C'_{12} & C'_{22} & C'_{23} & C'_{24} & C'_{25} & C'_{26} \\ C'_{13} & C'_{23} & C'_{33} & C'_{34} & C'_{35} & C'_{36} \\ C'_{14} & C'_{24} & C'_{34} & C'_{44} & C'_{45} & C'_{46} \\ C'_{15} & C'_{25} & C'_{35} & C'_{45} & C'_{55} & C'_{56} \\ C'_{16} & C'_{26} & C'_{36} & C'_{46} & C'_{56} & C'_{66} \end{bmatrix} \begin{bmatrix} \epsilon'_{11} \\ \epsilon'_{22} \\ \epsilon'_{33} \\ \gamma'_{23} \\ \gamma'_{13} \\ \gamma'_{12} \end{bmatrix} \quad (1.11)$$

### 1.3 Material Symmetry

Up to this point, we have been dealing with the most general relationships applying to linear elastic, generally anisotropic materials. Such materials are referred to as triclinic materials. Many real materials have inherent symmetries which can greatly simplify their behaviour. In this section, we will look at some of these materials.

It is important to introduce the concept of transformation tensors. Transformations are fundamental to the definition of tensors. In general, a fourth order tensor such as  $c'_{ijkl}$  transforms from the reference coordinate system  $x'_i$  to an alternative coordinate system  $x_i$  as follows

$$c_{mnop} = \beta_{mi}\beta_{nj}\beta_{ok}\beta_{pl}c'_{ijkl}. \quad (1.12)$$

Similarly, a second order tensor such as the stress tensor  $\sigma'_{ij}$  transforms as follows.

$$\sigma_{mn} = \beta_{mi}\beta_{nj}\sigma'_{ij}. \quad (1.13)$$

Finally, a first order tensor such as the displacement tensor  $u'_i$  transforms simply as

$$u_m = \beta_{mi}u'_i. \quad (1.14)$$

The transformation tensor  $\beta_{ij}$  has as elements the cosines of the angles between the  $x_i$  and the  $x'_j$  axes.

We will define our various symmetry classes in terms of transformation tensors (e.g. for a mirror reflection, or a three fold rotation). A symmetry condition means that the stiffness (or compliance) tensor must be invariant under such a transformation. This allows the formulation of equations which lead to simplifications in the stiffness tensor, either through the elimination of entries, or the establishment of relations between them. This is the method shown in the following treatment.

A slightly different, alternative approach, used by Lekhnitskii [3], is to look at

symmetry in terms of strain energy per unit volume,  $\bar{V}$ . Using the tensor summation convention,  $\bar{V}$  is shown in equation (1.15).

$$\bar{V} = \frac{1}{2} c_{ijkl} \sigma_{ij} \sigma_{kl} \quad (1.15)$$

Clearly, strain energy is independent of any particular coordinate system. If the material is symmetric under a coordinate transformation, then the terms  $c_{ijkl}$  of the stiffness tensor will also be invariant. The stresses  $\sigma_{ij}$  will transform to stresses  $\sigma'_{ij}$  in the new coordinate system. Applying these observations to equation (1.15) leads to the following result.

$$\frac{1}{2} c_{ijkl} \sigma_{ij} \sigma_{kl} = \frac{1}{2} c_{ijkl} \sigma'_{ij} \sigma'_{kl} \quad (1.16)$$

Given our earlier observations on the transformation of second order tensors (see equation (1.13)), we can easily substitute for the terms  $\sigma'_{ij}$  equivalent expressions in terms of the untransformed stresses, and the elements of the transformation matrix  $\beta_{ij}$ . Once this is done, coefficients for particular terms  $\sigma_{11}$ ,  $\sigma_{12}$ , ... are equated and simplifications become apparent.

The field of crystallography is a large one, and it has developed a rigorous way of classifying and identifying symmetry classes. I will not attempt a full examination of material symmetry. I will, however, go so far as to include point group diagrams for most of the symmetry classes discussed. On these diagrams, points are marked using either crosses or circles. A cross indicates that a point is above the plane of the page, a circle indicates a point below the page. Under the transformations defining the symmetry class, all points shown on the diagram must be equivalent. In the naming of the groups, a number such as 2 or 3 indicates a 2 or 3 fold rotation axis.  $m$  indicates a plane of mirror symmetry. If we write, for example,  $2/m$ ; this means that the plane of symmetry referred to by  $m$  is perpendicular to the axis referred to by 2.  $2m$  would mean that the plane of mirror symmetry was parallel with the 2-fold rotation axis. An overbar, indicates that an inversion is applied (e.g.  $\bar{2}$  indicates a 2-fold axis with inversion,  $\bar{1}$  is a simple inversion).

We will see that materials having different point groups may in fact be equivalent in terms of their stiffness tensor symmetry requirements.

It should be noted that Nayfeh's book [1] simplifies greatly the discussion of symmetry. He gives only a single example of each class (equivalent to discussing only one point group). These notes originally (and perhaps to some extent still) reflect this simplification, though I am attempting to add more detail. Auld [2], Fedorov [4], and various books on crystallography [5, 6, 7] provide more thorough treatments of the area.

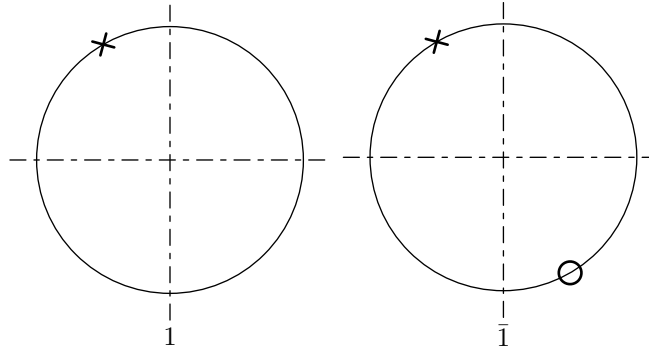


Figure 1.1: Triclinic Symmetry Point Groups

### 1.3.1 Triclinic Symmetry

It is worth noting that it is possible to introduce an inversion center without introducing any restrictions to the stiffness tensor. The transformation tensor for an inversion center is given as:

$$\beta_{ij} = \begin{bmatrix} -1 & 0 & 0 \\ 0 & -1 & 0 \\ 0 & 0 & -1 \end{bmatrix} \quad (1.17)$$

Now, since the stiffness tensor is even ordered (its order is 4), requiring identity under the application of  $\beta_{ij}$  to  $c_{ijkl}$  introduces no restrictions on the terms of  $c_{ijkl}$ . Similarly, in later discussion, any transformation tensors which differ only in terms of the application of an inversion center are equivalent in terms of their effects on the stiffness tensor.

It should also be noted that triclinic materials (and indeed all materials) are, of course, invariant under the identity operation.

### 1.3.2 Monoclinic Symmetry

Monoclinic materials are materials having, for example, one plane of mirror symmetry. Other examples can be seen in figure 1.19. Considering the mirror symmetry case, let us say that this plane coincides with the  $x'_1 - x'_2$  plane. This symmetry condition requires that the material be invariant under the transformation  $\beta_{ij}$  defined by equation (1.18).

$$\beta_{ij} = \begin{bmatrix} 1 & 0 & 0 \\ 0 & 1 & 0 \\ 0 & 0 & -1 \end{bmatrix} \quad (1.18)$$

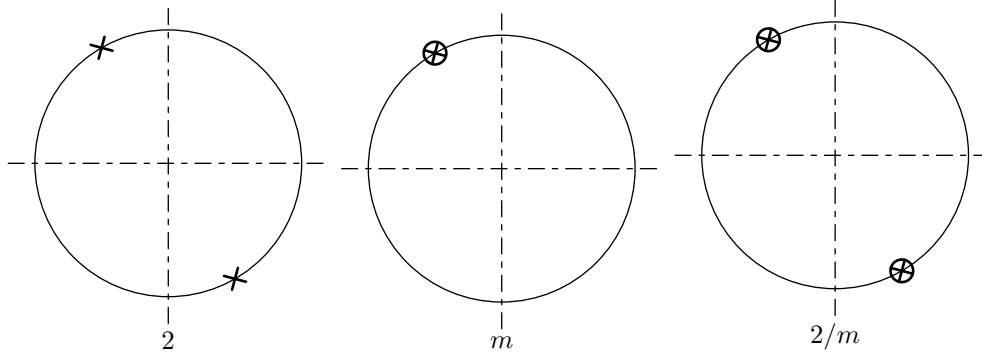


Figure 1.2: Monoclinic Symmetry Point Groups

Consider the formation of the term  $c_{2312}$ . Clearly  $c_{2312} = \beta_{2i}\beta_{3i}\beta_{1i}\beta_{2i}c'_{ijkl}$ . Now, looking at equation (1.18), it is clear that the terms  $\beta_{ij} = 0$  for  $i \neq j$ . Thus we get  $c_{2312} = \beta_{22}\beta_{33}\beta_{11}\beta_{22}c'_{2312} = -c'_{2312}$ . However, we require that  $c_{2312} = c'_{2312}$ , which leads to the conclusion  $c'_{2312} = 0$ . Other elements of  $c'_{ijkl}$  which vanish are  $c'_{1123}$ ,  $c'_{2223}$ ,  $c'_{3323}$ ,  $c'_{1113}$ ,  $c'_{2213}$ ,  $c'_{3313}$  and  $c'_{1312}$ . These are all the unique terms with an uneven number of 3's in their subscript. With these 8 terms removed, we are left with 13 unique coefficients (compared with 21 for the more general triclinic material). The form of the reduced stiffness matrix for monoclinic materials is shown in equation (1.19).

$$\begin{bmatrix} \sigma'_{11} \\ \sigma'_{22} \\ \sigma'_{33} \\ \sigma'_{23} \\ \sigma'_{13} \\ \sigma'_{12} \end{bmatrix} = \begin{bmatrix} C'_{11} & C'_{12} & C'_{13} & 0 & 0 & C'_{16} \\ C'_{12} & C'_{22} & C'_{23} & 0 & 0 & C'_{26} \\ C'_{13} & C'_{23} & C'_{33} & 0 & 0 & C'_{36} \\ 0 & 0 & 0 & C'_{44} & C'_{45} & 0 \\ 0 & 0 & 0 & C'_{45} & C'_{55} & 0 \\ C'_{16} & C'_{26} & C'_{36} & 0 & 0 & C'_{66} \end{bmatrix} \begin{bmatrix} \epsilon'_{11} \\ \epsilon'_{22} \\ \epsilon'_{33} \\ \gamma'_{23} \\ \gamma'_{13} \\ \gamma'_{12} \end{bmatrix} \quad (1.19)$$

### 1.3.3 Orthotropic Symmetry

If we introduce a second plane of symmetry, say the  $x'_1 - x'_3$  plane, we get an orthotropic material. As well as being invariant under the transformation tensor (1.18), this material is also invariant under the transformation tensor (1.20).

$$\beta_{ij} = \begin{bmatrix} 1 & 0 & 0 \\ 0 & -1 & 0 \\ 0 & 0 & 1 \end{bmatrix} \quad (1.20)$$

Unique elements of  $c'_{ijkl}$  which vanish under this invariance condition are  $c'_{1112}$ ,  $c'_{2212}$ ,  $c'_{3312}$  and  $c'_{1323}$  (elements with even numbers of 2's). These simplifications leave us with  $13 - 4 = 9$  independent coefficients. Since we have two orthogonal planes of symmetry, introducing a third plane will have no further effect on the stiffness tensor<sup>2</sup>. The form of the reduced stiffness matrix for orthotropic mate-

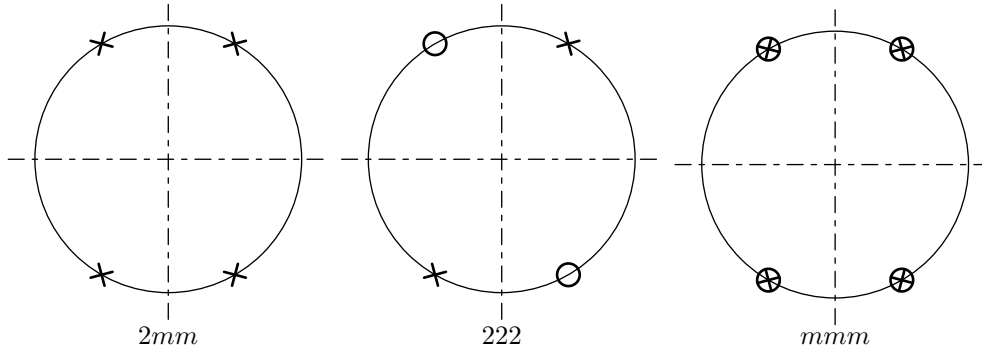


Figure 1.3: Orthotropic Symmetry Point Groups

rials is shown in equation (1.21). The point diagrams of the symmetry classes satisfied by this equation are shown in figure 1.3.

$$\begin{bmatrix} \sigma'_{11} \\ \sigma'_{22} \\ \sigma'_{33} \\ \sigma'_{23} \\ \sigma'_{13} \\ \sigma'_{12} \end{bmatrix} = \begin{bmatrix} C'_{11} & C'_{12} & C'_{13} & 0 & 0 & 0 \\ C'_{12} & C'_{22} & C'_{23} & 0 & 0 & 0 \\ C'_{13} & C'_{23} & C'_{33} & 0 & 0 & 0 \\ 0 & 0 & 0 & C'_{44} & 0 & 0 \\ 0 & 0 & 0 & 0 & C'_{55} & 0 \\ 0 & 0 & 0 & 0 & 0 & C'_{66} \end{bmatrix} \begin{bmatrix} \epsilon'_{11} \\ \epsilon'_{22} \\ \epsilon'_{33} \\ \gamma'_{23} \\ \gamma'_{13} \\ \gamma'_{12} \end{bmatrix} \quad (1.21)$$

### 1.3.4 Tetragonal Symmetry

In the next symmetry case, we introduce the concept of transformation by rotation. For the case of a counterclockwise rotation of an angle  $\phi$  about the  $x'_3$  axis, the

<sup>2</sup> Nayfeh [1] incorrectly states that if we have two perpendicular planes of mirror symmetry, then any plane normal to them must also be a plane of mirror symmetry. Working through the elementary calculations, we see that combining (1.18) and (1.20) does not produce the transformation matrix of the third plane of symmetry, but differs from it by a factor of  $-1$  (it is equivalent to a two-fold rotation axis aligned along the intersection of the two mirror-planes). We have already seen (§1.3.1) that an inversion imposes no extra conditions on the stiffness matrix. Thus, Nayfeh is correct in ignoring the effect of a third plane of mirror symmetry on the stiffness tensor.

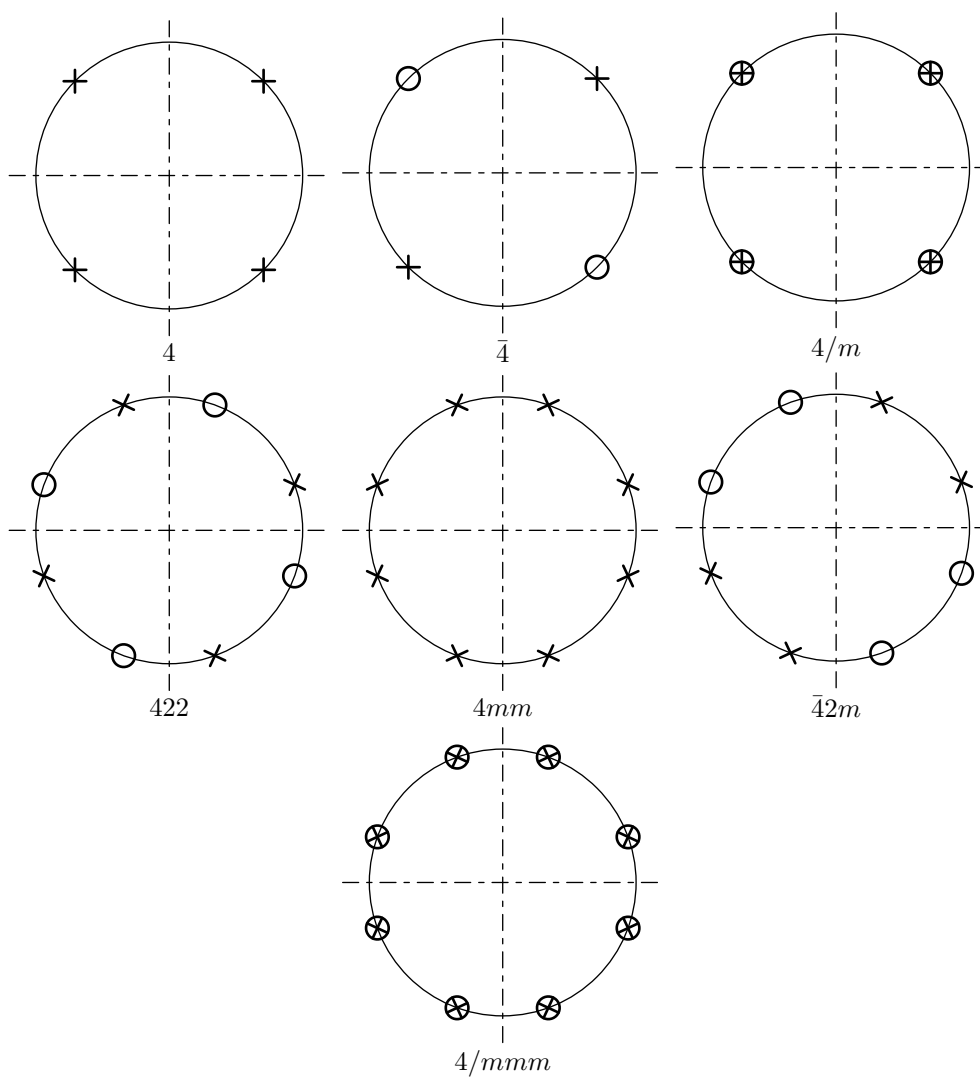


Figure 1.4: Tetragonal Symmetry Point Groups

transformation matrix  $\beta_{ij}$  is given as

$$\beta_{ij} = \begin{bmatrix} \cos \phi & \sin \phi & 0 \\ -\sin \phi & \cos \phi & 0 \\ 0 & 0 & 1 \end{bmatrix}. \quad (1.22)$$

Fedorov [4] describes the tetragonal symmetry class. In this case, we say that the material properties are invariant under rotations of  $\phi = \pi/2$  about axis  $x'_3$ . These systems have 6 significant elastic moduli<sup>3</sup> The form of the reduced stiffness matrix for tetragonal materials is shown in equation (1.23).

$$\begin{bmatrix} \sigma'_{11} \\ \sigma'_{22} \\ \sigma'_{33} \\ \sigma'_{23} \\ \sigma'_{13} \\ \sigma'_{12} \end{bmatrix} = \begin{bmatrix} C'_{11} & C'_{12} & C'_{13} & 0 & 0 & 0 \\ C'_{12} & C'_{11} & C'_{13} & 0 & 0 & 0 \\ C'_{13} & C'_{13} & C'_{33} & 0 & 0 & 0 \\ 0 & 0 & 0 & C'_{44} & 0 & 0 \\ 0 & 0 & 0 & 0 & C'_{44} & 0 \\ 0 & 0 & 0 & 0 & 0 & C'_{66} \end{bmatrix} \begin{bmatrix} \epsilon'_{11} \\ \epsilon'_{22} \\ \epsilon'_{33} \\ \gamma'_{23} \\ \gamma'_{13} \\ \gamma'_{12} \end{bmatrix} \quad (1.23)$$

The matrix given in (1.23) is taken from Fedorov's work [4], and applies to all tetragonal materials. Auld [2] (and some Russian workers cited by Fedorov) divide the tetragonal (and trigonal, see below) systems into subclasses with either 7 or 6 independent moduli. The classes with 6 moduli have the matrix as shown in (1.23), while those with 7 have a matrix in the form of (1.24) below.

$$\begin{bmatrix} \sigma'_{11} \\ \sigma'_{22} \\ \sigma'_{33} \\ \sigma'_{23} \\ \sigma'_{13} \\ \sigma'_{12} \end{bmatrix} = \begin{bmatrix} C'_{11} & C'_{12} & C'_{13} & 0 & 0 & C'_{16} \\ C'_{12} & C'_{12} & C'_{13} & 0 & 0 & -C'_{16} \\ C'_{13} & C'_{13} & C'_{33} & 0 & 0 & 0 \\ 0 & 0 & 0 & C'_{44} & 0 & 0 \\ 0 & 0 & 0 & 0 & C'_{44} & 0 \\ C'_{16} & -C'_{16} & 0 & 0 & 0 & C'_{66} \end{bmatrix} \begin{bmatrix} \epsilon'_{11} \\ \epsilon'_{22} \\ \epsilon'_{33} \\ \gamma'_{23} \\ \gamma'_{13} \\ \gamma'_{12} \end{bmatrix} \quad (1.24)$$

The classes with 7 moduli are  $4, \bar{4}$  and  $4/m$ . Those with 6 are  $4mm, 422, \bar{4}2m$  and  $4/mmm$ . Fedorov asserts that the distinction is artificial, and that correct choice of axes reduces all tetragonal (and trigonal) systems to 6 independent significant

---

<sup>3</sup> Fedorov quotes different numbers of independent elastic moduli to Nayfeh, and also to Auld. For example, in the case of monoclinic crystal he gives the number of 12, as opposed to 13 in Nayfeh's work. As far as I understand, this discrepancy is because Fedorov uses the 13<sup>th</sup> number to fix the orientation of the coordinate system. Thus, for the orthorhombic/orthotropic system, Nayfeh and Fedorov agree on the number of 9, as the two perpendicular planes are sufficient to fix the orientation of the coordinate system. I should look into this in more detail, and maybe browse through a book on crystallography (Fedorov alludes to far more detail on symmetry classes than Nayfeh does).

moduli. It will be noted that the classes with the larger number of moduli are those which inherently fix only one direction (principally the axis about which the rotations occur), while the classes with 6 moduli are those which inherently fix all coordinate directions (axis of rotation, and normal to a mirror plane, for example). See also the footnote for a couple of notes. I will go through this in more detail in the future. The point groups for all of these classes are shown in figure 1.4.

### 1.3.5 Trigonal Symmetry

Materials with trigonal symmetry have a trigonal axis, which we will assume to coincide with  $x'_3$ . This means that the material is invariant under rotations of  $\phi = 2\pi/3$  about the  $x'_3$  axis. According to Fedorov [4], in this case there are 6 significant moduli (see footnote in §1.3.4). The form of the reduced stiffness matrix for trigonal materials is shown in equation (1.25).

$$\begin{bmatrix} \sigma'_{11} \\ \sigma'_{22} \\ \sigma'_{33} \\ \sigma'_{23} \\ \sigma'_{13} \\ \sigma'_{12} \end{bmatrix} = \begin{bmatrix} C'_{11} & C'_{12} & C'_{13} & C'_{14} & -C'_{25} & 0 \\ C'_{12} & C'_{11} & C'_{13} & -C'_{14} & C'_{25} & 0 \\ C'_{13} & C'_{13} & C'_{33} & 0 & 0 & 0 \\ C'_{14} & -C'_{14} & 0 & C'_{44} & 0 & C'_{25} \\ -C'_{25} & C'_{25} & 0 & 0 & C'_{44} & C'_{14} \\ 0 & 0 & 0 & C'_{25} & C'_{14} & \frac{1}{2}(C'_{11} - C'_{12}) \end{bmatrix} \begin{bmatrix} \epsilon'_{11} \\ \epsilon'_{22} \\ \epsilon'_{33} \\ \gamma'_{23} \\ \gamma'_{13} \\ \gamma'_{12} \end{bmatrix} \quad (1.25)$$

Fedorov shows that equation (1.25) may be simplified by correct choice of coordinate system, to give the form:

$$\begin{bmatrix} \sigma'_{11} \\ \sigma'_{22} \\ \sigma'_{33} \\ \sigma'_{23} \\ \sigma'_{13} \\ \sigma'_{12} \end{bmatrix} = \begin{bmatrix} C'_{11} & C'_{12} & C'_{13} & C'_{14} & 0 & 0 \\ C'_{12} & C'_{11} & C'_{13} & -C'_{14} & 0 & 0 \\ C'_{13} & C'_{13} & C'_{33} & 0 & 0 & 0 \\ C'_{14} & -C'_{14} & 0 & C'_{44} & 0 & 0 \\ 0 & 0 & 0 & 0 & C'_{44} & C'_{14} \\ 0 & 0 & 0 & 0 & C'_{14} & \frac{1}{2}(C'_{11} - C'_{12}) \end{bmatrix} \begin{bmatrix} \epsilon'_{11} \\ \epsilon'_{22} \\ \epsilon'_{33} \\ \gamma'_{23} \\ \gamma'_{13} \\ \gamma'_{12} \end{bmatrix} \quad (1.26)$$

As mentioned before in section 1.3.4, Fedorov [4] and Auld [2] differ on the number of independent moduli. Fedorov asserts it is 6 for all trigonal classes. Auld argues that it is 7 for classes 3 and  $\bar{3}$ , which have the stiffness matrix as shown in (1.25). Auld says that there are 6 significant constants for classes 32,  $3m$  and  $\bar{3}m$ . Similar arguments may be made as in the case of tetragonal systems 1.3.4. See also footnotes. More detail required on this topic. The point diagrams for all classes are shown in figure 1.5.

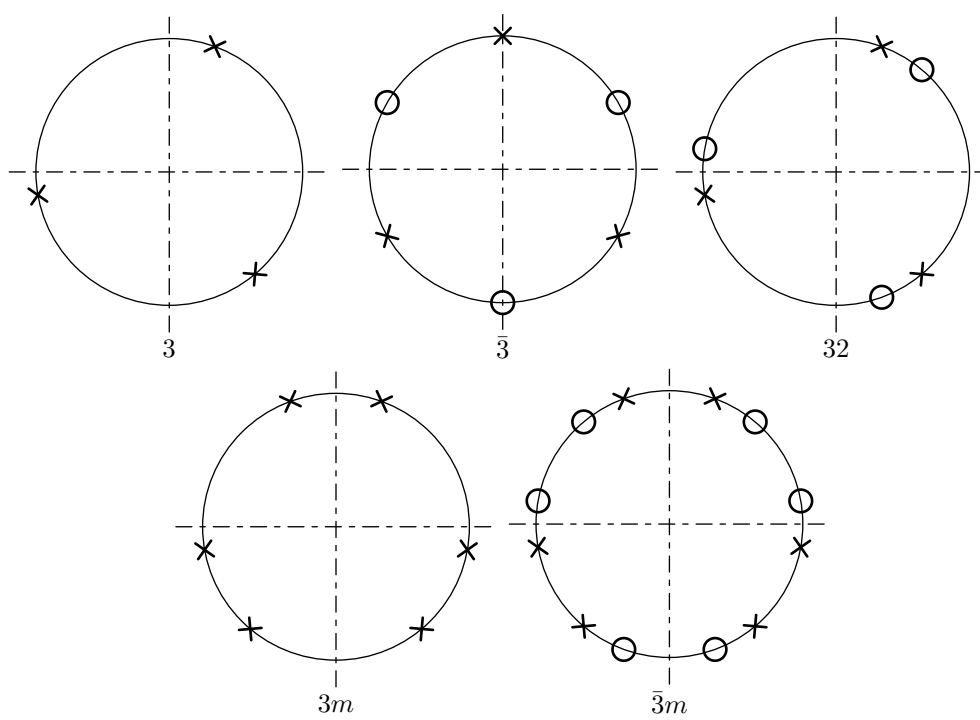


Figure 1.5: Trigonal Symmetry Point Groups

### 1.3.6 Transversely Isotropic Symmetry

To obtain properties for transversely isotropic materials, we can apply the rotation transformation (1.22) to the properties for an orthotropic material (see section 1.3.3). It is possible to write out expressions for each of the terms in the new stiffness tensor  $c_{ijkl}$ . Full details can be found in Nayfeh's book [1], and can also be found in the computer code accompanying this document. A couple of samples are presented here:

$$c_{1111} = c'_{1111} \cos^4 \phi + c'_{2222} \sin^4 \phi + 2(c'_{1122} + 2c'_{1212}) \sin^2 \phi \cos^2 \phi \quad (1.27)$$

$$c_{2222} = c'_{1111} \sin^4 \phi + c'_{2222} \cos^4 \phi + 2(c'_{1122} + 2c'_{1212}) \sin^2 \phi \cos^2 \phi \quad (1.28)$$

$$c_{2212} = (c'_{1111} - c'_{1122} - 2c'_{1212}) \cos \phi \sin^3 \phi + (c'_{1122} - c'_{2222} + 2c'_{1212}) \sin \phi \cos^3 \phi \quad (1.29)$$

Clearly from (1.27) and (1.28), if we require the material properties to be invariant for  $\phi = \pi/2$ , it is necessary for  $c'_{1111}$  and  $c'_{2222}$  to be identical. The full set of restrictions thus imposed are:

$$\begin{aligned} c'_{1111} &= c'_{2222} \\ c'_{2233} &= c'_{1133} \\ c'_{1313} &= c'_{2323} \end{aligned} \quad (1.30)$$

Further requiring invariance under general rotations about the  $x'_3$  axis, leads to additional restrictions. Consider equation (1.29). Under the invariance condition, we require  $c_{2212} = c'_{2212}$ . However, for an orthotropic material,  $c'_{2212} = 0$ . This means that the right hand side of (1.29) equals zero. This, along with (1.30) gives the relation:

$$c'_{1111} - c'_{1122} = 2c'_{1212}. \quad (1.31)$$

Thus, there are  $9 - 4 = 5$  independent coefficients in the stiffness tensor. The form of the reduced stiffness matrix for transversely isotropic materials is shown in equation (1.32). It should be noted that this appears to be identical to the matrix supplied by Fedorov [4] for the case of a hexagonal crystal. He forms the hexagonal case by noting that it is equivalent to the simultaneous presence of identically direct twofold and threefold axes. He forms the matrix  $C_{ij}$  for the hexagonal case by combining the properties of these two cases (equations (1.19) and (1.25)). The

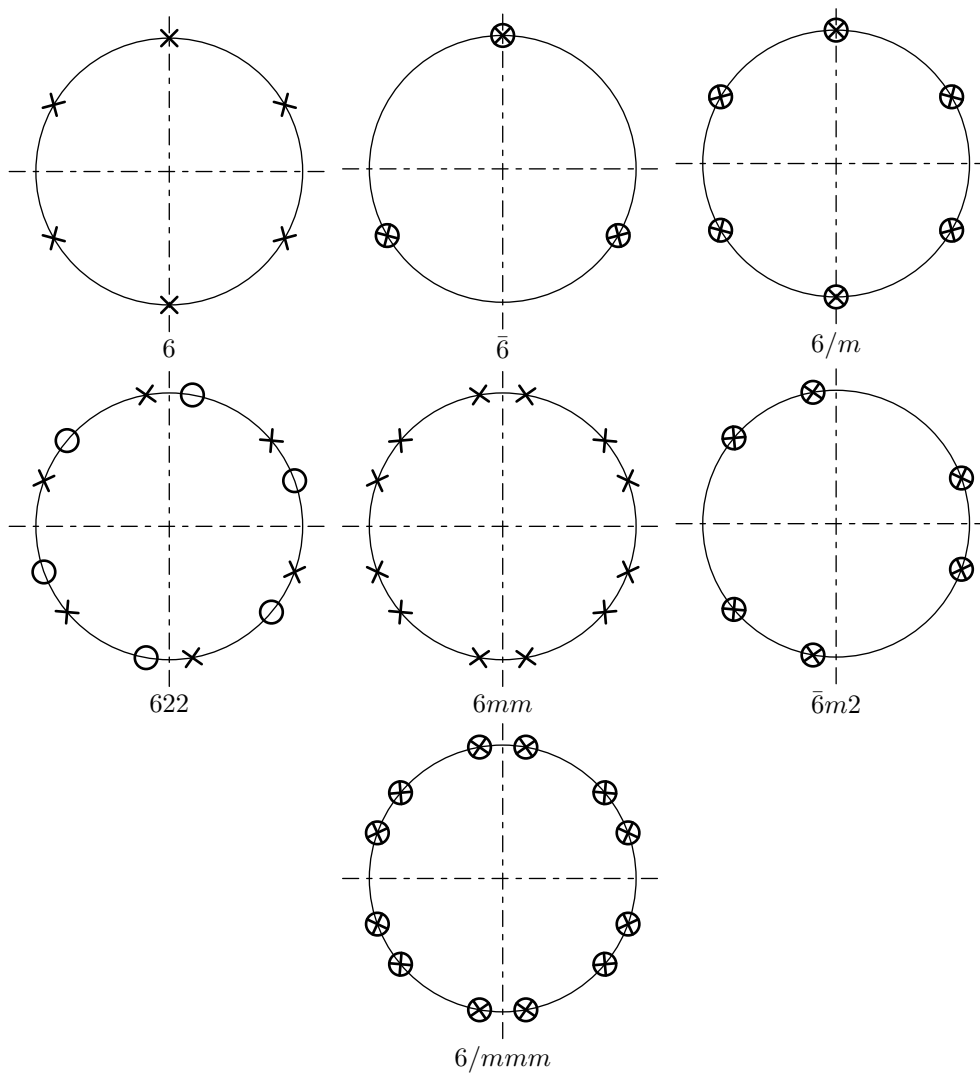


Figure 1.6: Hexagonal Symmetry Point Groups

point groups for the hexagonal symmetry case are shown in figure 1.6.

$$\begin{bmatrix} \sigma'_{11} \\ \sigma'_{22} \\ \sigma'_{33} \\ \sigma'_{23} \\ \sigma'_{13} \\ \sigma'_{12} \end{bmatrix} = \begin{bmatrix} C'_{11} & C'_{12} & C'_{13} & 0 & 0 & 0 \\ C'_{12} & C'_{11} & C'_{13} & 0 & 0 & 0 \\ C'_{13} & C'_{13} & C'_{33} & 0 & 0 & 0 \\ 0 & 0 & 0 & C'_{55} & 0 & 0 \\ 0 & 0 & 0 & 0 & C'_{55} & 0 \\ 0 & 0 & 0 & 0 & 0 & \frac{1}{2}(C'_{11} - C'_{12}) \end{bmatrix} \begin{bmatrix} \epsilon'_{11} \\ \epsilon'_{22} \\ \epsilon'_{33} \\ \gamma'_{23} \\ \gamma'_{13} \\ \gamma'_{12} \end{bmatrix} \quad (1.32)$$

### 1.3.7 Cubic Symmetry

To define cubic symmetry, we start from the orthotropic case (§1.3.3), and again apply rotations, both by angle  $\phi$  about the  $x'_3$  axis (as in §1.3.6) and by angle  $\gamma$  about the  $x'_2$  axis. We require that the material is invariant for rotations  $\phi = \pi/2$  and  $\gamma = \pi/2$ . This means that the coordinates  $x'_1$ ,  $x'_2$  and  $x'_3$  are completely interchangeable. This reduces by 6 the number of independent stiffness coefficients (compared with the orthotropic case) to give  $9 - 6 = 3$  independent coefficients. The form of the reduced stiffness matrix for cubic isotropic materials is shown in equation (1.33).

$$\begin{bmatrix} \sigma'_{11} \\ \sigma'_{22} \\ \sigma'_{33} \\ \sigma'_{23} \\ \sigma'_{13} \\ \sigma'_{12} \end{bmatrix} = \begin{bmatrix} C'_{11} & C'_{12} & C'_{12} & 0 & 0 & 0 \\ C'_{12} & C'_{11} & C'_{12} & 0 & 0 & 0 \\ C'_{12} & C'_{12} & C'_{11} & 0 & 0 & 0 \\ 0 & 0 & 0 & C'_{66} & 0 & 0 \\ 0 & 0 & 0 & 0 & C'_{66} & 0 \\ 0 & 0 & 0 & 0 & 0 & C'_{66} \end{bmatrix} \begin{bmatrix} \epsilon'_{11} \\ \epsilon'_{22} \\ \epsilon'_{33} \\ \gamma'_{23} \\ \gamma'_{13} \\ \gamma'_{12} \end{bmatrix} \quad (1.33)$$

### 1.3.8 Isotropic Symmetry

Finally, the greatest degree of symmetry possible is isotropic symmetry. In this case, the material is invariant under rotation by arbitrary angles  $\gamma$  and  $\phi$ . In this case, there are only two independent stiffness constants. The form of the reduced stiffness matrix for cubic isotropic materials is shown in equation (1.34) (stress and strain terms are omitted for clarity). Point group diagrams are superfluous for this case as every point is equivalent to every other point.

$$\begin{bmatrix} C'_{11} & C'_{12} & C'_{12} & 0 & 0 & 0 \\ C'_{12} & C'_{11} & C'_{12} & 0 & 0 & 0 \\ C'_{12} & C'_{12} & C'_{11} & 0 & 0 & 0 \\ 0 & 0 & 0 & \frac{1}{2}(C'_{11} - C'_{12}) & 0 & 0 \\ 0 & 0 & 0 & 0 & \frac{1}{2}(C'_{11} - C'_{12}) & 0 \\ 0 & 0 & 0 & 0 & 0 & \frac{1}{2}(C'_{11} - C'_{12}) \end{bmatrix} \quad (1.34)$$

The two existing constants can be represented in various ways. One commonly used form of elastic constants are the Lamé constants. These are defined in terms of elements of  $C_{ij}$  as follows [2]:

$$\begin{aligned}\lambda &= C_{12} \\ \mu &= C_{44} = \frac{1}{2}(C_{11} - C_{12})\end{aligned}\quad (1.35)$$

Conversely, the terms of the tensor  $c_{ijkl}$  can be neatly expressed in terms of Lamé constants and Dirac deltas [8]:

$$c_{ijkl} = \lambda \delta_{ij} \delta_{kl} + \mu (\delta_{ik} \delta_{jl} + \delta_{il} \delta_{jk}) \quad (1.36)$$

In engineering work, another commonly used pair of elastic properties are Young's modulus and Poisson's ratio. The definitions of Young's modulus and Poisson's ratio, along with expressions for them in terms of elements of  $C_{ij}$  are given in Equations (1.37) and (1.38) respectively. The directions used are of course arbitrary since any orthogonal coordinate system can be used equivalently.

$$E = \frac{\sigma_{11}}{\epsilon_{11}} = C_{11} - \frac{2C_{12}^2}{C_{11} + C_{12}} \quad (1.37)$$

$$\nu = -\frac{\epsilon_{33}}{\epsilon_{11}} = -\frac{\epsilon_{22}}{\epsilon_{11}} = \frac{1}{C_{11}/C_{12} + 1} \quad (1.38)$$

## 1.4 Bulk Waves

### 1.4.1 Bulk Waves Background

In general, for wave propagation in a direction  $\vec{n}$ , three types of waves are possible. These are associated with the directions of the three particle displacement vectors  $\vec{u}^{(k)}$  ( $k = 1, 2, 3$ ). These can be referred to as having different polarisations. Pure modes can be defined in different ways, but Nayfeh [1] and Auld [2] define them as modes where either  $\vec{u} \perp \vec{n}$  or  $\vec{u} \parallel \vec{n}$ . Where  $\vec{u} \perp \vec{n}$ , we say that the mode is longitudinal. Where  $\vec{u} \parallel \vec{n}$ , we can say that the mode is shear. In cases where the modes are not pure, they are described as quasi-longitudinal or quasi-shear, depending on which they are closest to.

Combining the momentum equation (1.1) and the stress-strain relation (1.2) and the strain-displacement relationship (1.4), gives the following result:

$$\rho \frac{\partial^2 u_i}{\partial t^2} = \frac{1}{2} c_{ijkl} \frac{\partial}{\partial x_j} \left( \frac{\partial u_l}{\partial x_k} + \frac{\partial u_k}{\partial x_l} \right) \quad (1.39)$$

By symmetry arguments ( $k$  and  $l$  are interchangeable) we can simplify (1.39) to get

$$\rho \frac{\partial^2 u_i}{\partial t^2} = c_{ijkl} \frac{\partial^2 u_l}{\partial x_k \partial x_j} \quad (1.40)$$

We look for solutions,  $u_i$  of the following form, in terms of  $\zeta$  the bulk wavenumber,  $\vec{U}$  the displacement amplitude vector (which defines polarisation), and  $\vec{n}$  the propagation direction unit vector:

$$u_i = U_i e^{j(\zeta n_j x_j - \omega t)} \quad (1.41)$$

Substituting (1.41) into (1.40), and introducing  $\lambda_{ijkl} = c_{ijkl}/\rho$ , gives the following:

$$\omega^2 U_i = \frac{c_{ijkl}}{\rho} \zeta^2 n_k n_j U_l \Leftrightarrow \omega^2 U_i = \lambda_{ijkl} \zeta^2 n_k n_j U_l \quad (1.42)$$

Now, we introduce the phase velocity,  $v$ , defined as follows:

$$v = \frac{\omega}{\zeta} \quad (1.43)$$

Using  $v$ , equation (1.42) can be rewritten as follows:

$$\begin{aligned} (\lambda_{ijkl} n_k n_j - v^2 \delta_{il}) U_l &= 0 \\ \Leftrightarrow (\Lambda_{il} - v^2 \delta_{il}) U_l &= 0 \end{aligned} \quad (1.44)$$

where  $\Lambda_{il} = \lambda_{ijkl} n_k n_j$ . Clearly (1.44) represents an eigenvalue problem, where the phase velocities  $v$  are the eigenvalues, and the  $U_l$  vectors (polarisation vectors) are the eigenvectors. In general, there will be three phase velocities, accompanied by three polarisation vectors. These phase velocities and polarisations define a single (quasi)longitudinal and two (quasi)shear modes. Explicitly, the eigenvalue problem is as follows

$$\begin{pmatrix} \Lambda_{11} - v^2 & \Lambda_{12} & \Lambda_{13} \\ \Lambda_{12} & \Lambda_{22} - v^2 & \Lambda_{23} \\ \Lambda_{13} & \Lambda_{23} & \Lambda_{33} - v^2 \end{pmatrix} \begin{Bmatrix} U_1 \\ U_2 \\ U_3 \end{Bmatrix} = 0 \quad (1.45)$$

An important concept to introduce at this stage is the *slowness curve*. A slowness curve is a plot of the inverse of velocity (units are therefore seconds/metre or equivalent). Typically, a slowness curve is produced by choosing a plane in the material of interest, and then calculating the different phase velocities for a selection of propagation directions. Slowness is then plotted as a function of propagation direction in a polar plot. Slowness curves feature in most texts deal-

ing with wave propagation in solids. Slowness curves can be combined to obtain a slowness surface, which would completely characterise the phase velocities of the possible modes in a given material. However, there are obvious difficulties in printing or displaying such surfaces.

Another concept which is introduced is the *skew curve*. This is a plot which I have only seen in Nayfeh's work [1]. As was mentioned earlier (page 20), pure modes are defined as being modes which are either normal to or parallel with the direction of propagation. Skew is a measure of how far any particular mode deviates from this ideal. If the mode is pure, skew will be zero. For other modes, the skew is the angle between the polarisation vector and the direction of propagation (for quasi-longitudinal modes) or the normal to the direction of propagation (for quasi-shear modes).

## 1.4.2 Computation of Slowness and Skew Curves Background

At this point, we are ready to calculate slowness curves for a wide range of materials. All that is required are the entries from the stiffness tensor  $c_{ijkl}$ , or equivalently the entries of the reduced stiffness matrix  $C_{ij}$ .

We map out the slowness data by considering planes parallel to the  $x_3$  axis (which without loss of generality, can coincide with the  $x'_3$  axis). Given a set of material properties  $c'_{ijkl}$ , expressed in the coordinate system  $(x'_1, x'_2, x'_3)$ , we can transform it to  $c_{ijkl}$  expressed in the coordinate system  $(x_1, x_2, x_3)$  by rotating about the  $x'_3$  axis. In this way, we can arrange that the coordinates of any direction of propagation,  $\vec{n}$  are of the form

$$\vec{n} = \begin{Bmatrix} \cos \theta \\ 0 \\ \sin \theta \end{Bmatrix} \quad \text{where} \quad 0 \leq \theta \leq 2\pi \quad (1.46)$$

when expressed in the transformed coordinate system. Once the transformed stiffness matrix or tensor is obtained, the angle  $\theta$  is varied in the range  $0 \leq \theta \leq 2\pi$ , giving different propagation direction vectors,  $\vec{n}$ . For each  $\vec{n}$ ,  $\Lambda_{ij}$  from equation (1.45) is obtained. The eigenvalues and eigenvectors of  $\Lambda_{ij}$  are found. The entire slowness surface can be determined by applying different rotations about  $x_3$  and repeating the process.

An issue that caused me some difficulty when implementing this code was the sorting of the modes (i.e. which eigenvector/eigenvalue pair corresponds to longitudinal mode, which corresponds to the "fast shear" mode and which corresponds to the "slow shear" mode). Sorting by phase velocity gives correct results in particular cases, but for some materials the slowness curves cross each other (we will see this shortly). Nayfeh [1] indicates that the modes can be identified by looking

at the dot and cross products of their eigenvectors with the propagation direction  $\vec{n}$ . This immediately identifies the longitudinal mode, which will generally make a relatively small angle with the propagation direction. The two remaining shear modes can then be sorted by how close they come to being normal to the propagation direction. For some cases this is sufficient to sort the modes. However for other more complicated materials, this leads to “curve-jumping”. An alternative tried was to sort the shear modes by how close they came to lying along the  $x_2$  axis (i.e. to being perpendicular to the plane containing the  $x_3$  axis and the propagation directions). Again, this works for some materials, but at particular points the modes swap over leading to discontinuities in the curves.

The solution I settled on when sorting the modes is as follows. For the first propagation direction tested, take the dot product of each polarisation vector with the propagation direction. The vector giving the largest number (smallest angle) is designated as the quasi-longitudinal mode. Then take the dot product of the remaining two vectors with the vector  $(0, 1, 0)$ . The mode giving the largest dot-product is designated as the first shear mode. The remaining mode is the second shear mode. For subsequent propagation directions  $\vec{n}$ , classify the resulting eigenvectors by how close they come to the previous longitudinal or shear modes (again using dot products). This works as long as each  $\vec{n}$  is relatively close to the previous one (i.e. as long as the increments in  $\theta$  are relatively small). In this way, the new vector closest to our last longitudinal vector is the new longitudinal mode. The new vector closest to the previous first shear mode vector is the new first shear mode. The remaining vector is the new second shear mode.

### 1.4.3 Examples of Slowness and Skew Curves

In this section I will present some sample slowness and skew curves calculated with the Python code I have written. Material properties used will also be presented here. The examples chosen are the same as the ones used by Nayfeh, so that I could more easily verify their correctness.

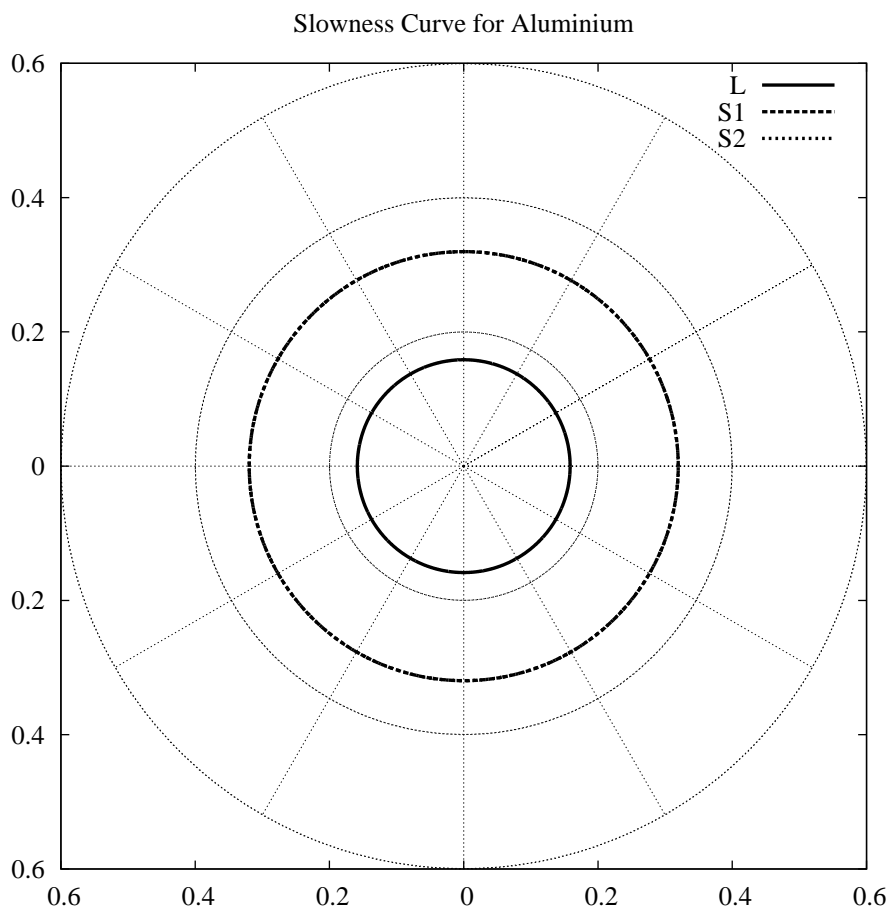
#### Aluminium

Aluminium is an isotropic material (this is not true in all cases, for example rolled aluminium can have directionality in material properties), and has very simple slowness and skew curves. The propagation velocities are the same for all directions. Skew is zero for all directions (all modes are pure modes). Additionally, the two shear modes present are degenerate (they have the same velocity). The slowness curve is shown in figure 1.7. The material properties are shown in equa-

tion 1.47.

$$\begin{bmatrix} 107.50 & 54.59 & 54.59 & 0.00 & 0.00 & 0.00 \\ 54.59 & 107.50 & 54.59 & 0.00 & 0.00 & 0.00 \\ 54.59 & 54.59 & 107.50 & 0.00 & 0.00 & 0.00 \\ 0.00 & 0.00 & 0.00 & 26.45 & 0.00 & 0.00 \\ 0.00 & 0.00 & 0.00 & 0.00 & 26.45 & 0.00 \\ 0.00 & 0.00 & 0.00 & 0.00 & 0.00 & 26.45 \end{bmatrix} \quad (1.47)$$

Figure 1.7: Slowness Curve for Isotropic Aluminium



**InAs**

InAs is a cubic material. Its reduced stiffness matrix is given below for coordinate axes coinciding with cubic axes (i.e. in its simplest form).

$$\begin{bmatrix} 83.29 & 45.26 & 45.26 & 0.0 & 0.0 & 0.0 \\ 45.26 & 83.29 & 45.26 & 0.0 & 0.0 & 0.0 \\ 45.26 & 45.26 & 83.29 & 0.0 & 0.0 & 0.0 \\ 0.0 & 0.0 & 0.0 & 39.59 & 0.0 & 0.0 \\ 0.0 & 0.0 & 0.0 & 0.0 & 39.59 & 0.0 \\ 0.0 & 0.0 & 0.0 & 0.0 & 0.0 & 39.59 \end{bmatrix} \quad (1.48)$$

This gives the slowness and skew curves as shown below in figures 1.8 and 1.9.

Figure 1.8: Slowness Curve for InAs,  $\phi = 0$

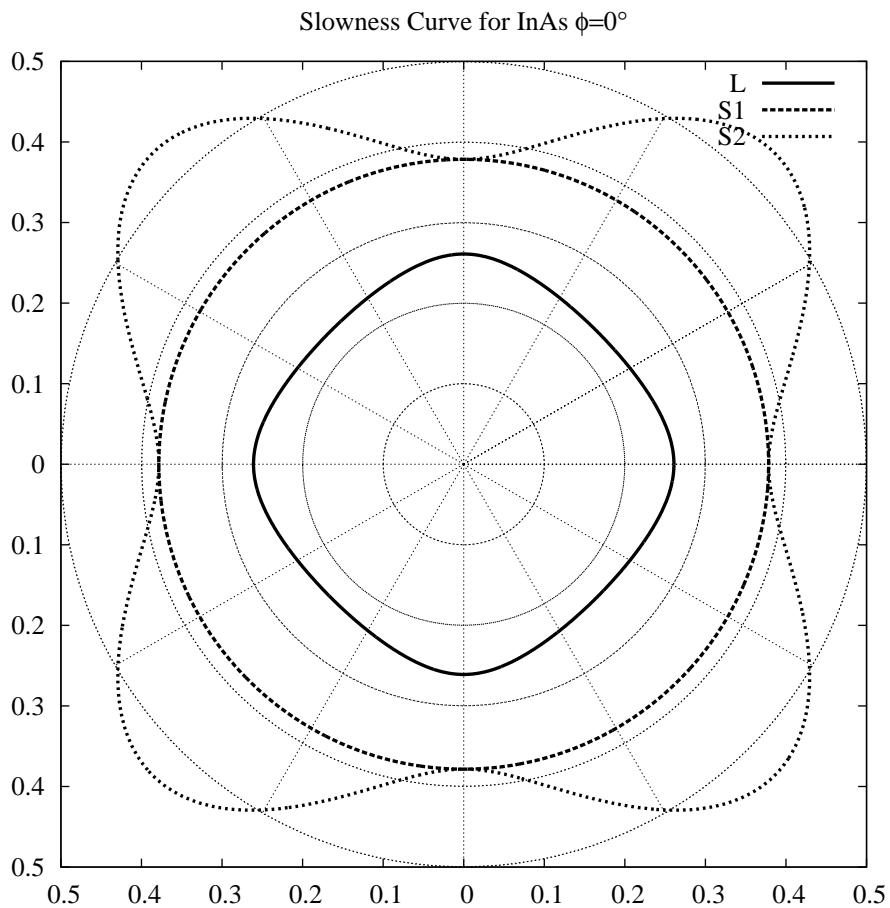
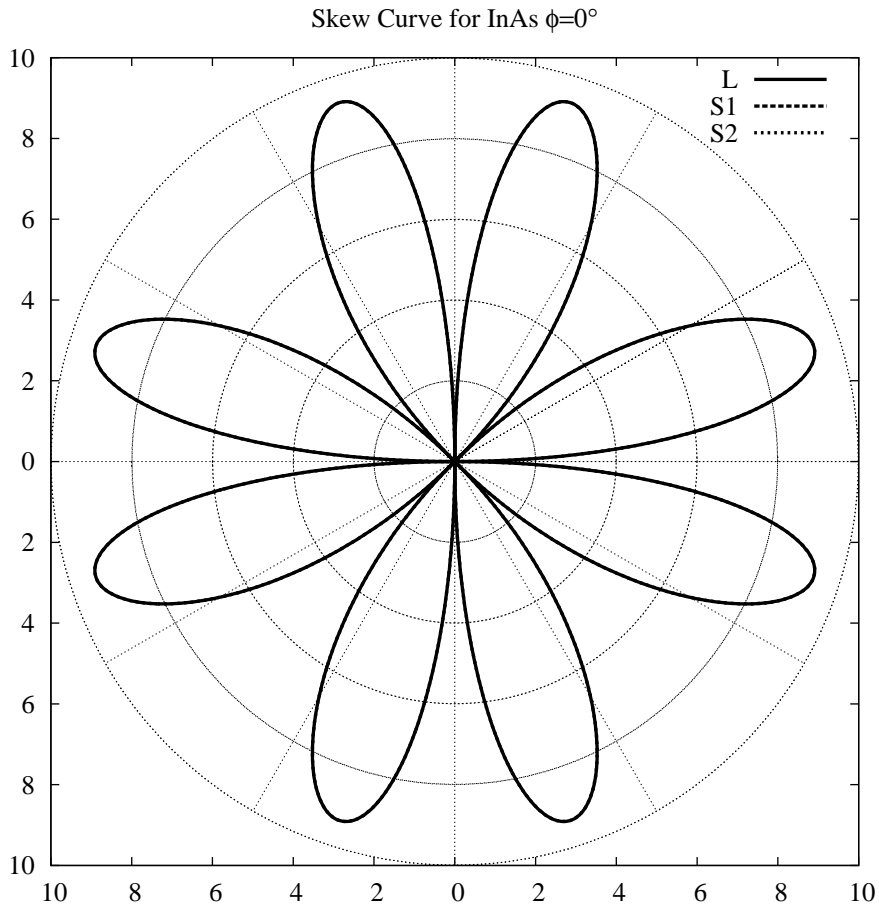


Figure 1.9: Skew Curve for InAs,  $\phi = 0$



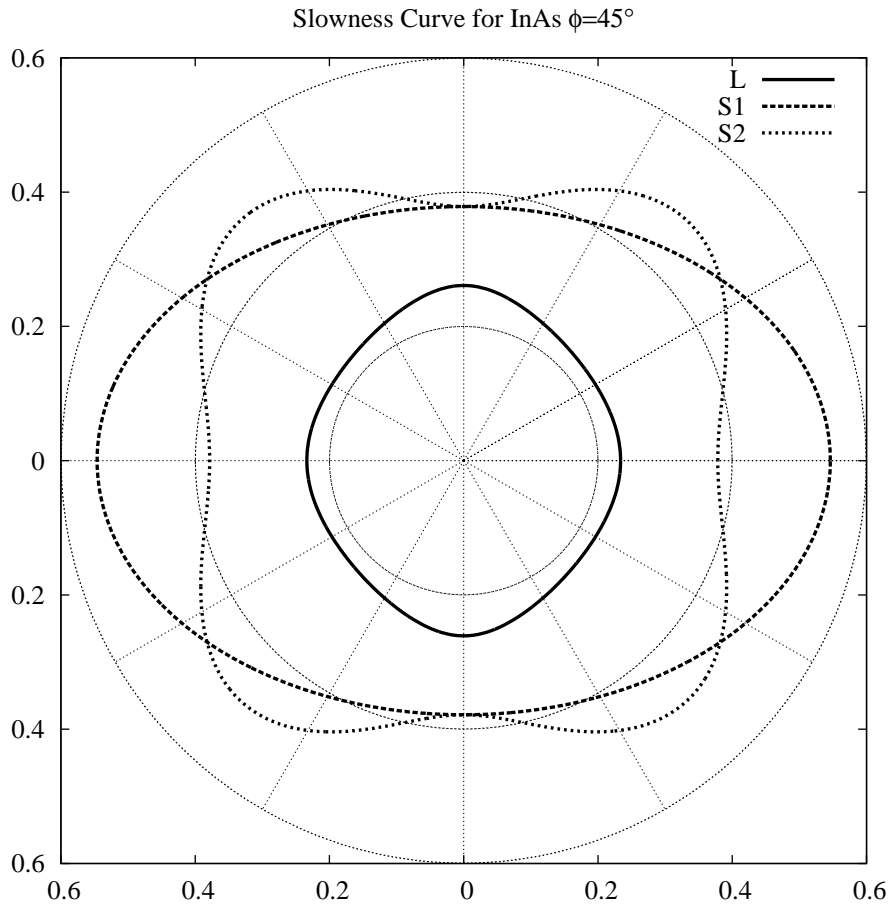
Rotating by an angle of 45 gives the reduced stiffness matrix shown in (1.49).

$$\begin{bmatrix} 103.86 & 24.68 & 45.26 & 0.0 & 0.0 & 0.0 \\ 24.68 & 103.86 & 45.26 & 0.0 & 0.0 & 0.0 \\ 45.26 & 45.26 & 83.29 & 0.0 & 0.0 & 0.0 \\ 0.0 & 0.0 & 0.0 & 39.59 & 0.0 & 0.0 \\ 0.0 & 0.0 & 0.0 & 0.0 & 39.59 & 0.0 \\ 0.0 & 0.0 & 0.0 & 0.0 & 0.0 & 19.01 \end{bmatrix} \quad (1.49)$$

Computation of the slowness and skew curves is straightforward. They are plotted in figures 1.10 and 1.11 respectively.

Rotating by an angle of 30 degrees (relative to the *original* orientation repre-

Figure 1.10: Slowness Curve for InAs,  $\phi = 45^\circ$

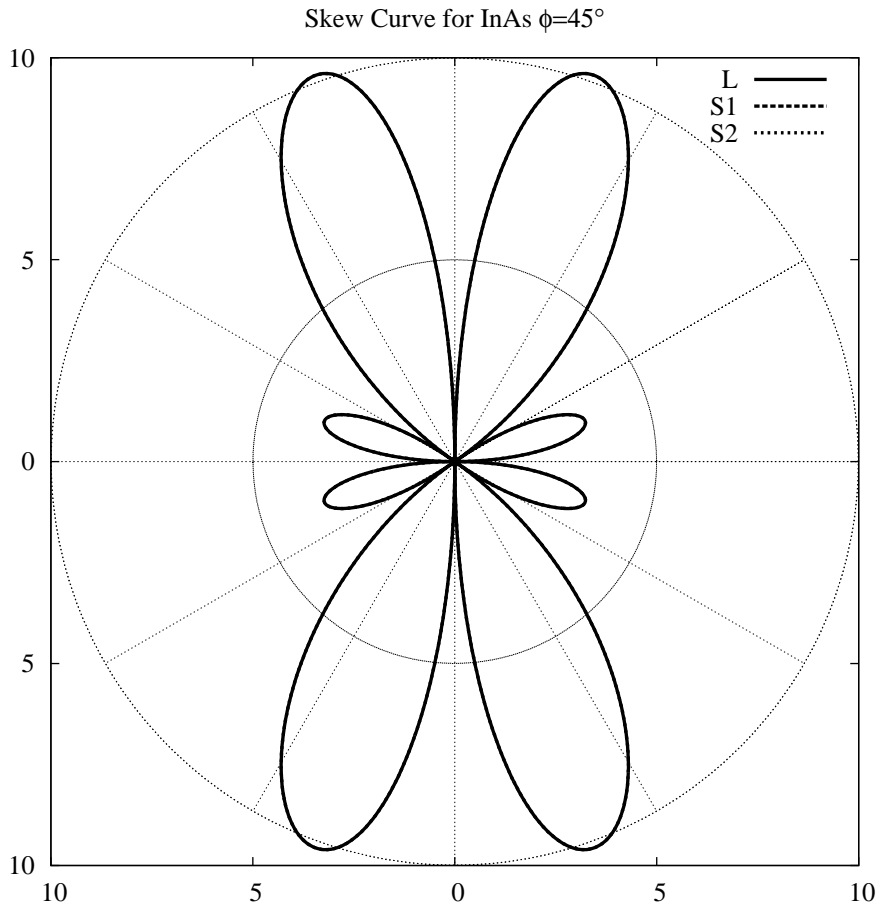


sented by (1.48)) gives the reduced stiffness matrix of (1.50).

$$\begin{bmatrix}
 98.72 & 29.83 & 45.26 & 0.00 & 0.00 & -8.91 \\
 29.83 & 98.72 & 45.26 & 0.00 & 0.00 & 8.91 \\
 45.26 & 45.26 & 83.29 & 0.00 & 0.00 & 0.00 \\
 0.00 & 0.00 & 0.00 & 39.59 & 0.00 & 0.00 \\
 0.00 & 0.00 & 0.00 & 0.00 & 39.59 & 0.00 \\
 -8.91 & 8.91 & 0.00 & 0.00 & 0.00 & 24.16
 \end{bmatrix} \quad (1.50)$$

The computed slowness and skew curves are shown in figures 1.12 and 1.13 respectively.

Figure 1.11: Skew Curve for InAs,  $\phi = 45^\circ$



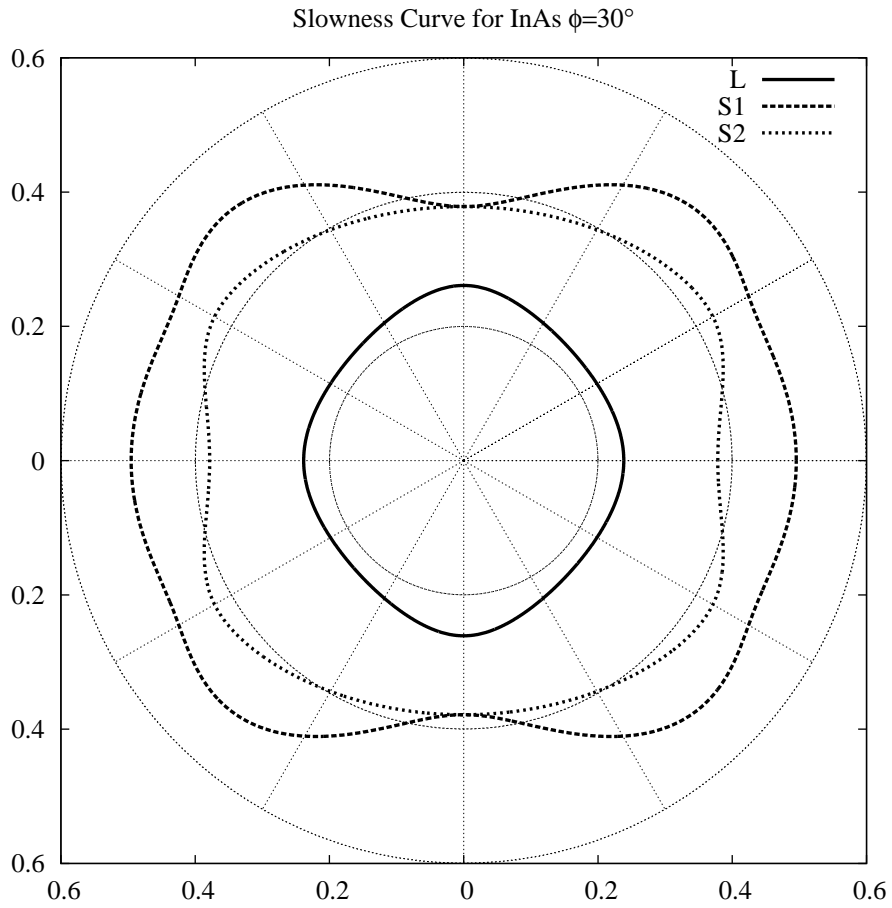
### Graphite-Epoxy (65%-35%)

First, it should be noted that these curves differ significantly from those given by Nayfeh. There is at least one error in the material properties provided by Nayfeh<sup>4</sup> Graphite-epoxy slowness and skew curves are shown in figures 1.14 and 1.15

<sup>4</sup> If I remember correctly, the Graphite-Epoxy  $\phi = 30$  data cannot be obtained from the  $\phi = 0$  data through transformation relations. Rather, it differs in a couple of terms by a factor of -1. The material properties given here are taken directly from the ones provided by Nayfeh, errors and all, though I may correct them in the future when I know which data are correct. I will soon begin reproducing figures from Auld for further validation of this code.

Note on Tue Jun 18 15:50:35 IST 2002: I have done this for quartz, a trigonal material, in § 1.4.3.

Figure 1.12: Slowness Curve for InAs,  $\phi = 30$

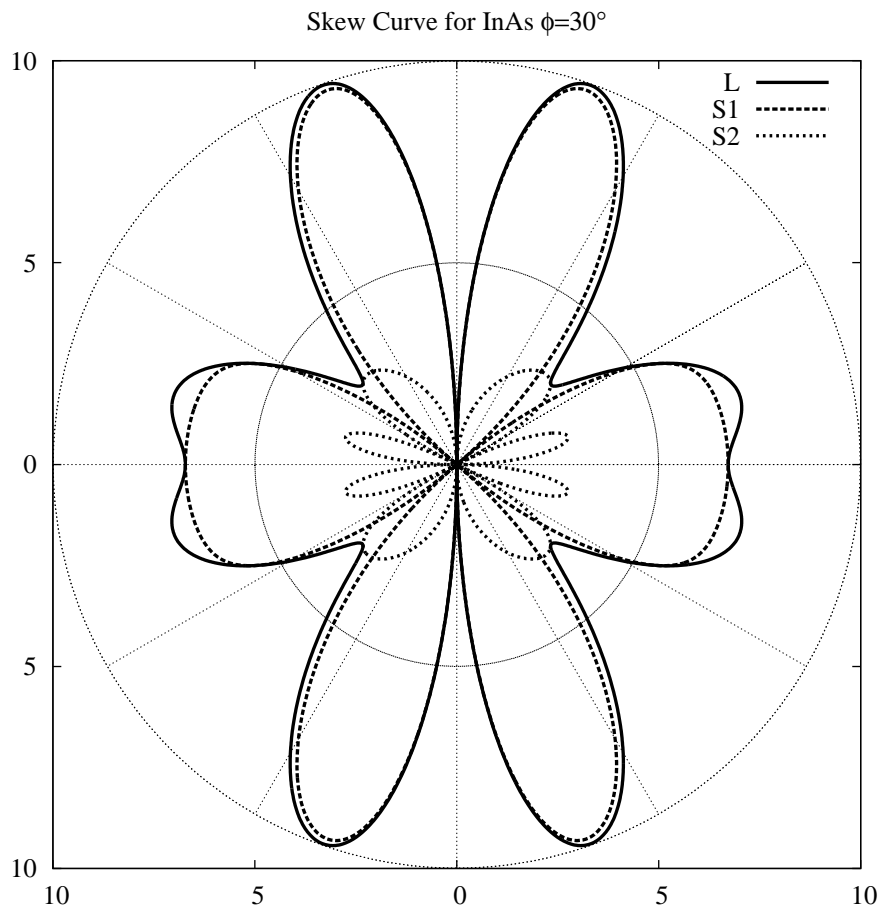


respectively. The matrix of stiffness constants is shown in equation (1.51).

$$\begin{bmatrix}
 155.43 & 3.72 & 3.72 & 0.00 & 0.00 & 0.00 \\
 3.72 & 16.34 & 4.96 & 0.00 & 0.00 & 0.00 \\
 3.72 & 4.96 & 16.34 & 0.00 & 0.00 & 0.00 \\
 0.00 & 0.00 & 0.00 & 3.37 & 0.00 & 0.00 \\
 0.00 & 0.00 & 0.00 & 0.00 & 7.48 & 0.00 \\
 0.00 & 0.00 & 0.00 & 0.00 & 0.00 & 7.48
 \end{bmatrix} \quad (1.51)$$

Corresponding slowness and skew curves for graphite-epoxy after a 30 degrees rotation are shown in figures 1.16 and 1.17. The matrix of material properties

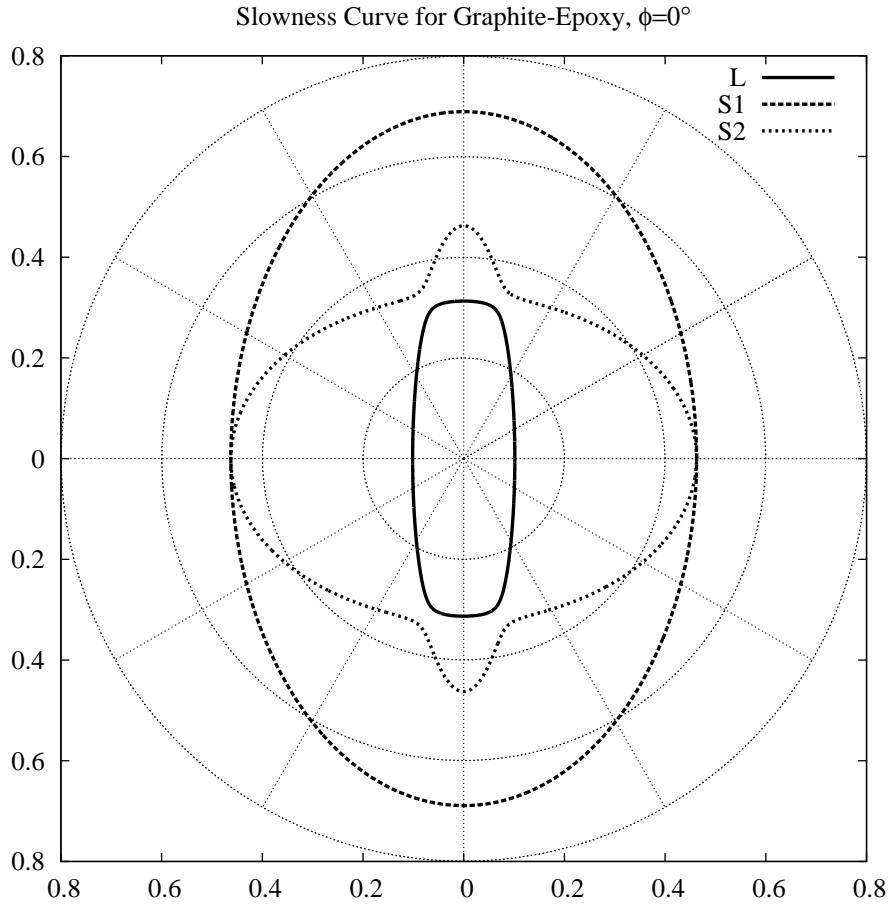
Figure 1.13: Skew Curve for InAs,  $\phi = 30^\circ$



following this transformation are show in (1.52).

$$\begin{bmatrix}
 95.46 & 28.93 & 4.03 & 0.00 & 0.00 & 44.67 \\
 28.93 & 25.91 & 4.65 & 0.00 & 0.00 & 15.56 \\
 4.03 & 4.65 & 16.34 & 0.00 & 0.00 & 0.54 \\
 0.00 & 0.00 & 0.00 & 4.40 & -1.78 & 0.00 \\
 0.00 & 0.00 & 0.00 & -1.78 & 6.45 & 0.00 \\
 44.67 & 15.56 & 0.54 & 0.00 & 0.00 & 32.68
 \end{bmatrix} \tag{1.52}$$

Figure 1.14: Slowness Curve for Graphite Epoxy,  $\phi = 0$



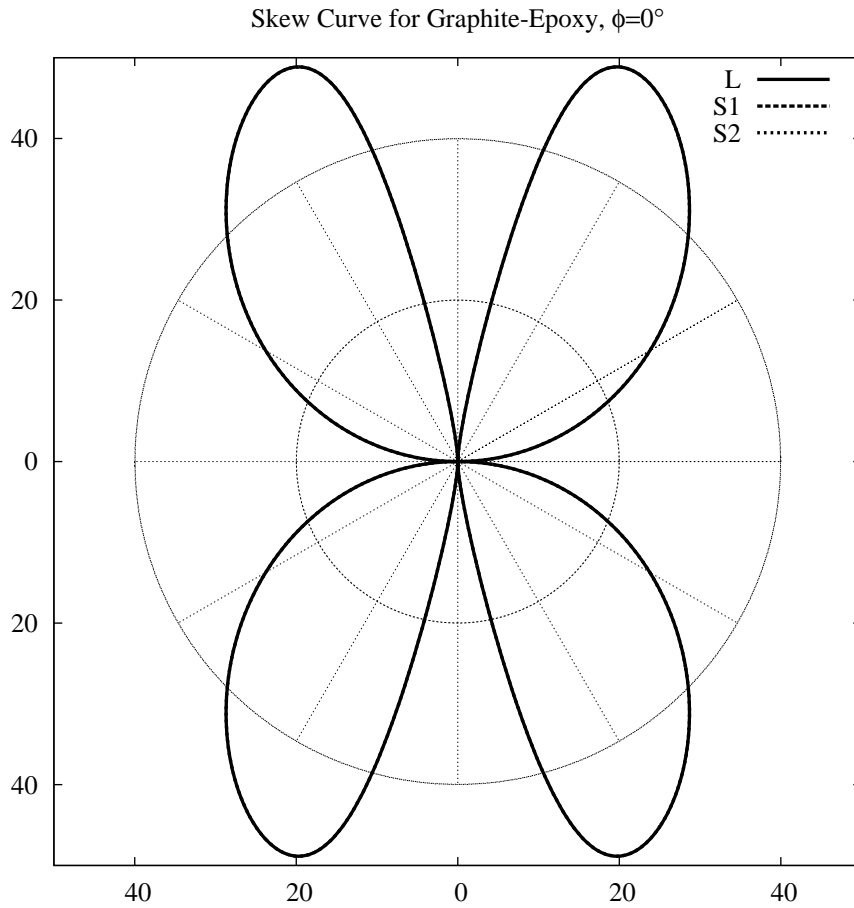
### Quartz

First, it must be noted that in this discussion, the piezoelectric properties are neglected. The material properties given by Auld are as follows

$$\begin{aligned}
 c_{11} &= 8.674 \times 10^{10} \text{N/m}^2 & c_{12} &= 0.699 \times 10^{10} \text{N/m}^2 \\
 c_{33} &= 10.72 \times 10^{10} \text{N/m}^2 & c_{13} &= 0.699 \times 10^{10} \text{N/m}^2 \\
 c_{44} &= 5.794 \times 10^{10} \text{N/m}^2 & c_{14} &= -1.791 \times 10^{10} \text{N/m}^2
 \end{aligned}$$

Since quartz is a trigonal material, the remainder of the stiffness matrix can be determined by substituting into (1.26). Solving the eigenvalue problem for the slowness and skew of the different polarisations gives the results shown in figures

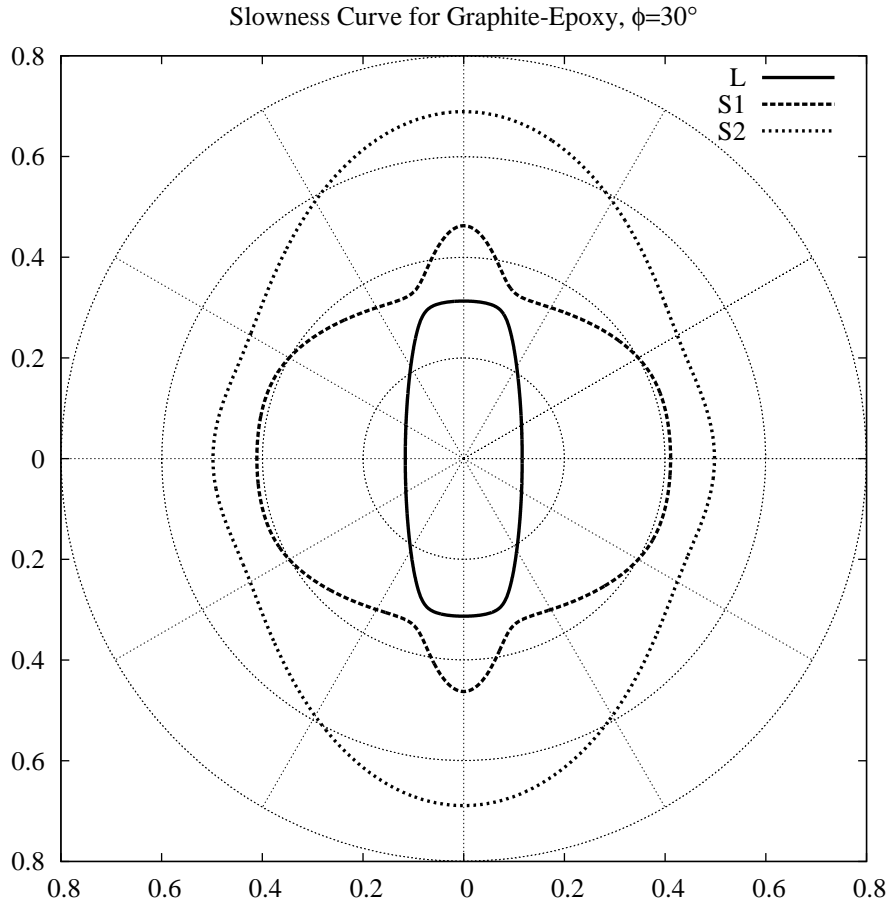
Figure 1.15: Skew Curve for Graphite Epoxy,  $\phi = 0$



1.18 and 1.19. Applying a rotation of  $\pi/2$  about the  $Z$  axis, gives the slowness and skew curves shown in figures 1.20 and 1.21.

We now look at propagation in the plane perpendicular to the  $Z$  axis. This means that we rotate the coordinates from the first system by  $\pi/2$  about the  $X$  axis, or equivalently rotate the coordinates from the second system by  $\pi/2$  about the  $Y$  axis. The resulting slowness and skew curves are shown in figures 1.22 and 1.23.

Figure 1.16: Slowness Curve for Graphite Epoxy,  $\phi = 30$



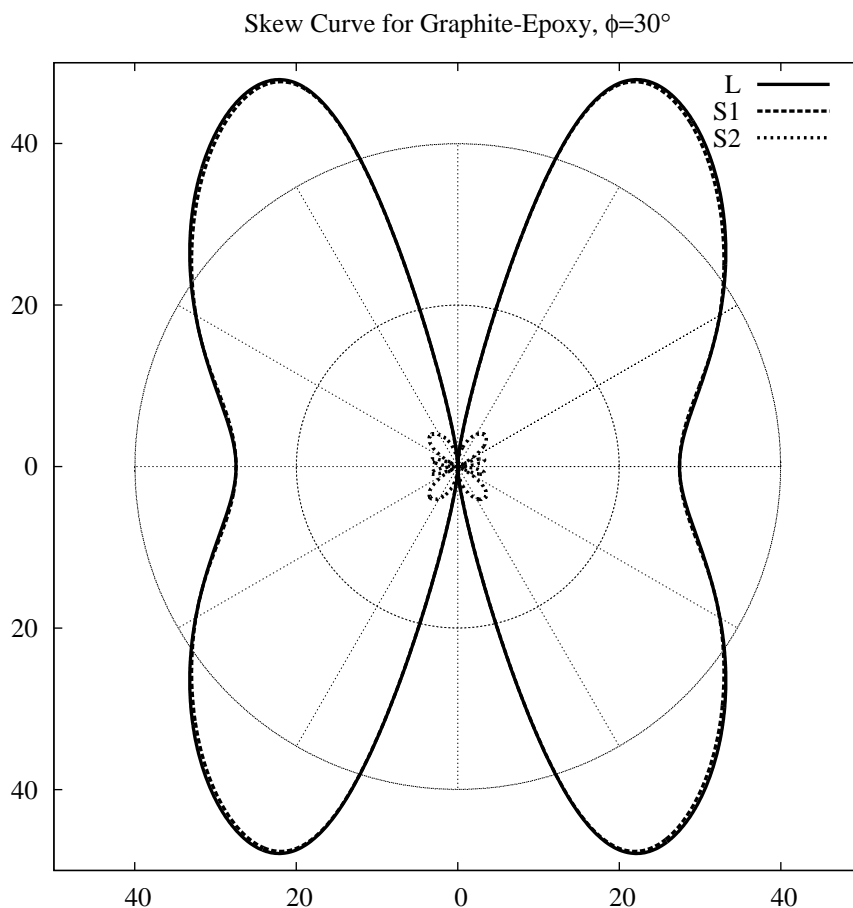
### Cadmium Sulfide

Piezoelectric properties are neglected in this case. The material properties given by Auld are as follows

$$\begin{aligned}
 c_{11} &= 9.07 \times 10^{10} \text{N/m}^2 & c_{12} &= 5.81 \times 10^{10} \text{N/m}^2 \\
 c_{33} &= 9.38 \times 10^{10} \text{N/m}^2 & c_{13} &= 5.10 \times 10^{10} \text{N/m}^2 \\
 c_{44} &= 1.504 \times 10^{10} \text{N/m}^2 & &
 \end{aligned}$$

Since cadmium sulfide is a hexagonal material, the remainder of the stiffness matrix can be determined by substituting into (1.32). Solving the eigenvalue problem for the slowness and skew of the different polarisations gives the results shown in

Figure 1.17: Skew Curve for Graphite Epoxy,  $\phi = 30$



figures 1.24 and 1.25. This is for propagation in the plane normal to the axis of symmetry. Rotating the coordinate system by  $\pi/2$  and again solving the eigenvalue problem gives the results for a plane parallel to the axis of symmetry. These results are shown in figures 1.26 and 1.27.

Figure 1.18: Slowness Curve for Quartz,  $\phi = 0$ , ( $X - Z$  Plane)

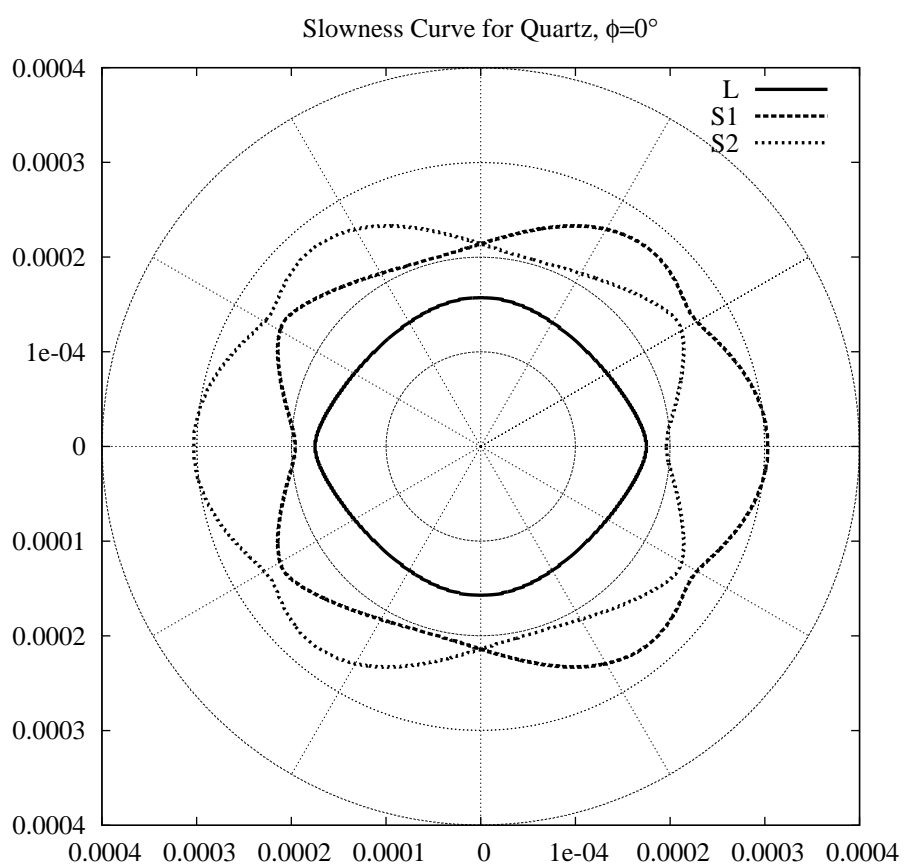


Figure 1.19: Skew Curve for Quartz,  $\phi = 0$ , ( $X - Z$  Plane)

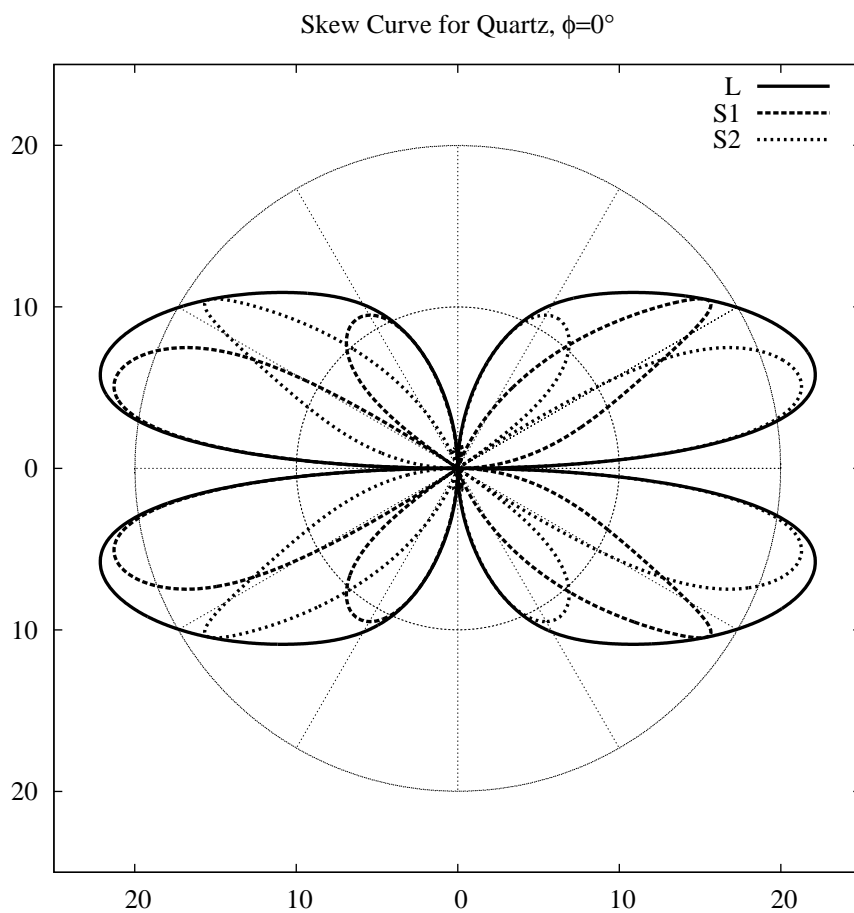


Figure 1.20: Slowness Curve for Quartz,  $\phi = 90^\circ$ , ( $Y - Z$  Plane)

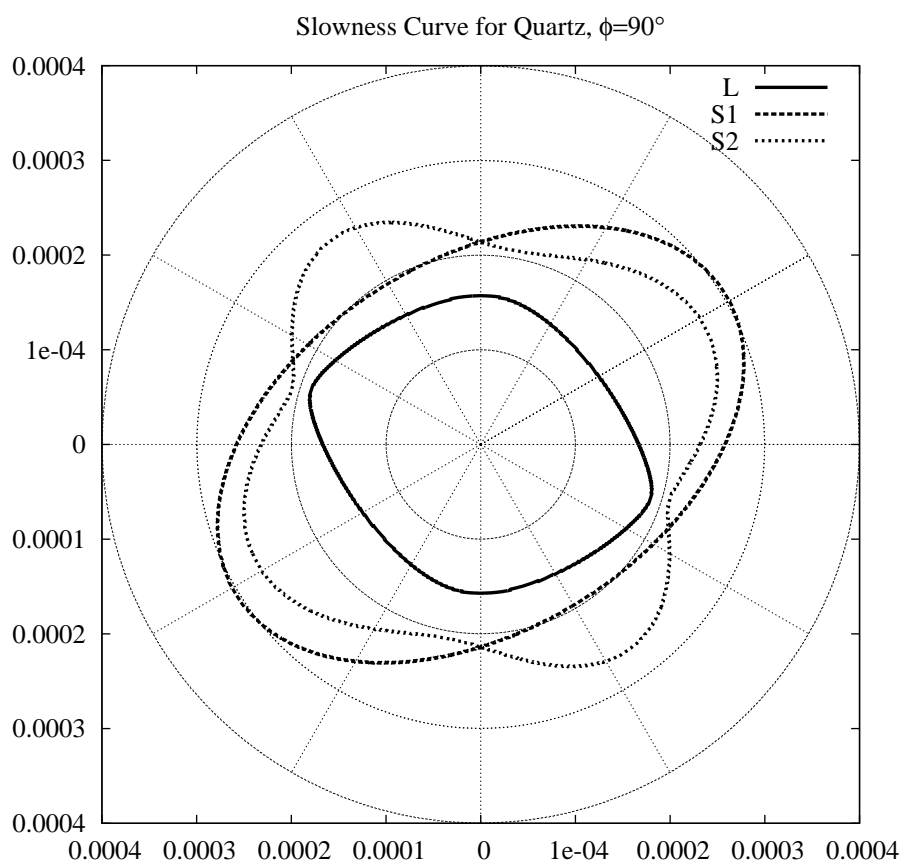


Figure 1.21: Skew Curve for Quartz,  $\phi = 90$ , ( $Y - Z$  Plane)

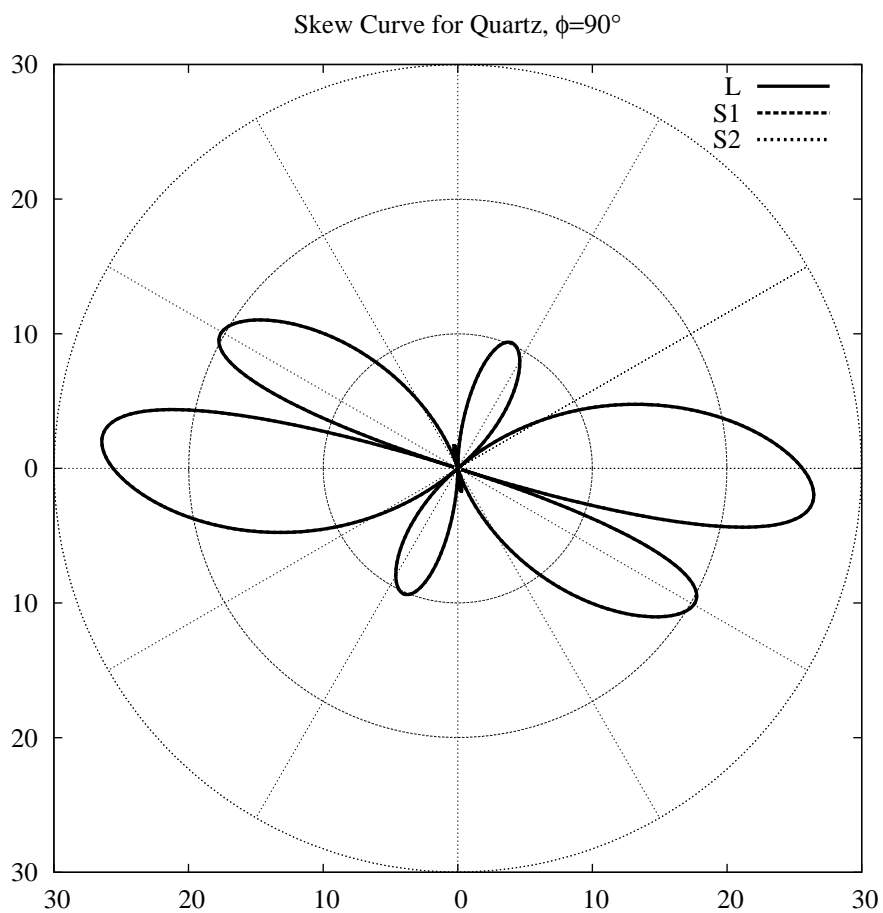


Figure 1.22: Slowness Curve for Quartz,  $\phi = 90^\circ$ , ( $X - Y$  Plane)

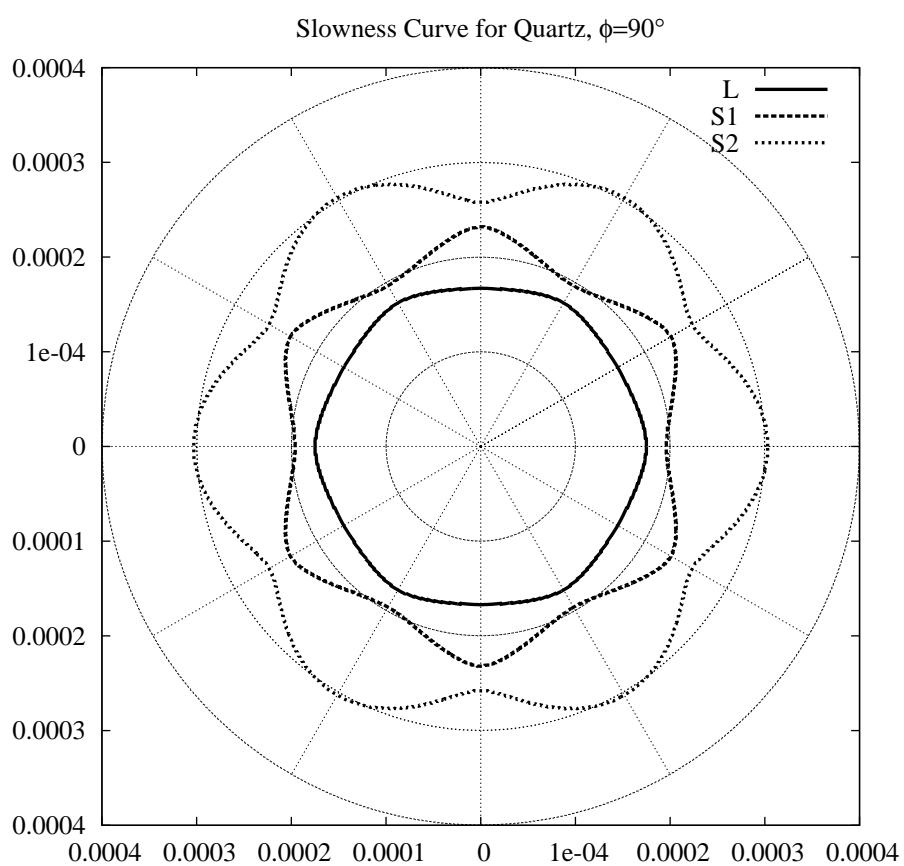


Figure 1.23: Skew Curve for Quartz,  $\phi = 90$ , ( $X - Y$  Plane)

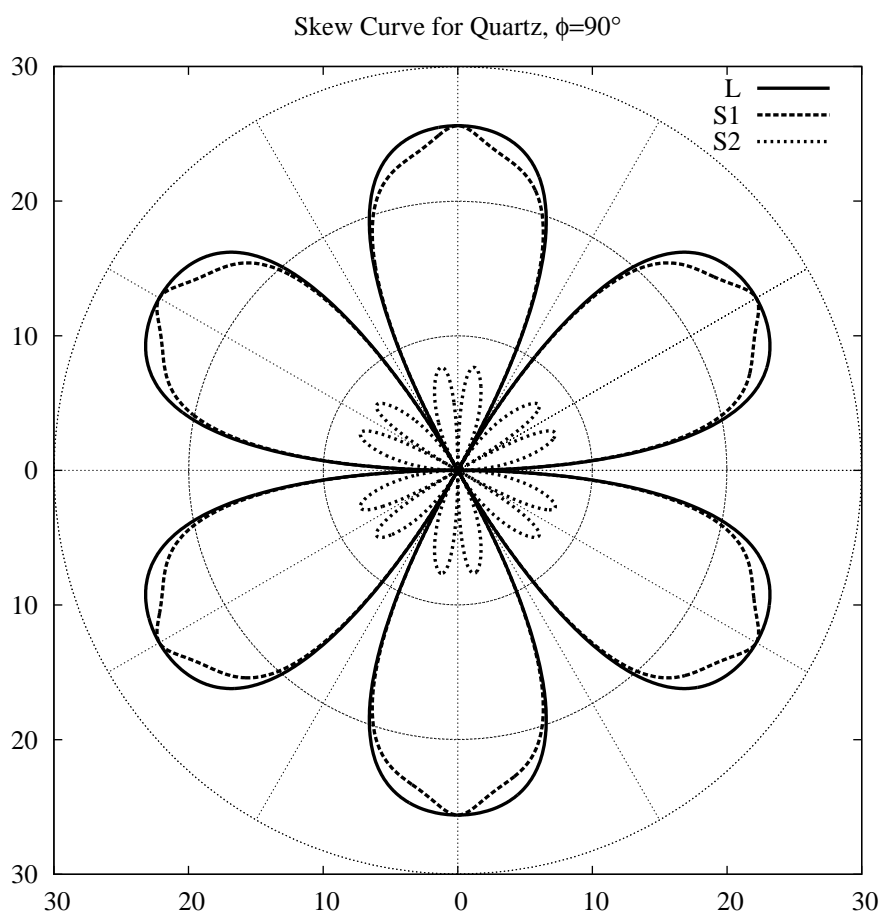


Figure 1.24: Slowness Curve for CdS,  $\phi = 0$ , ( $X - Y$  Plane)

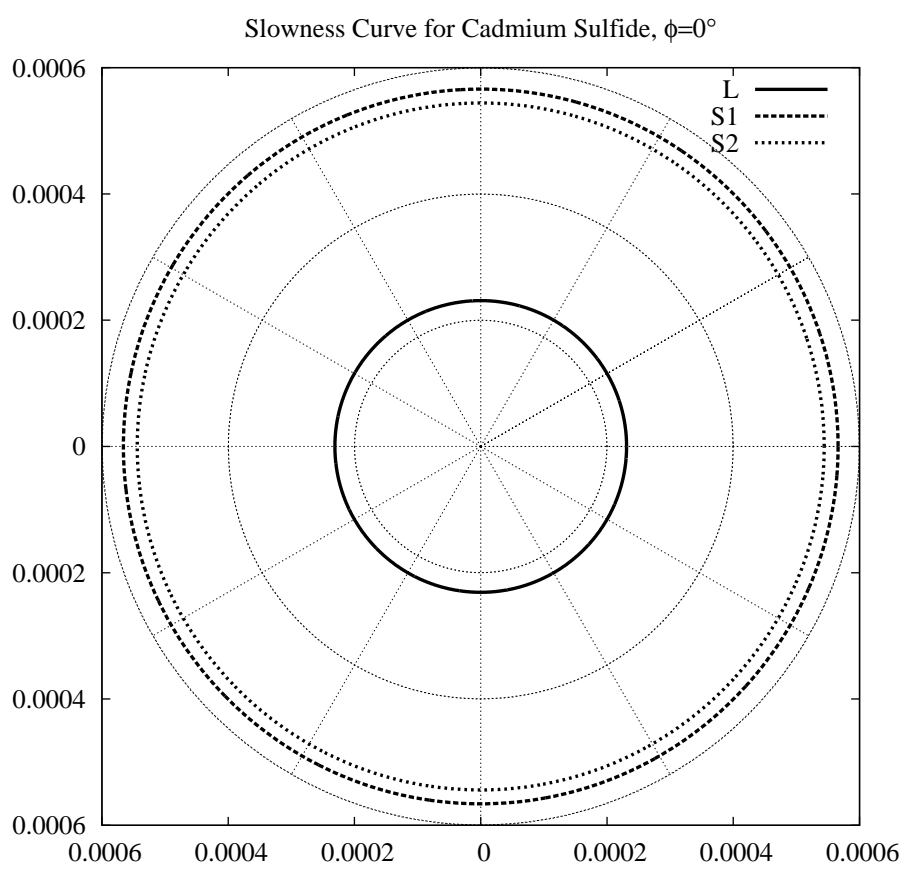


Figure 1.25: Skew Curve for CdS,  $\phi = 0$ , ( $X - Y$  Plane)

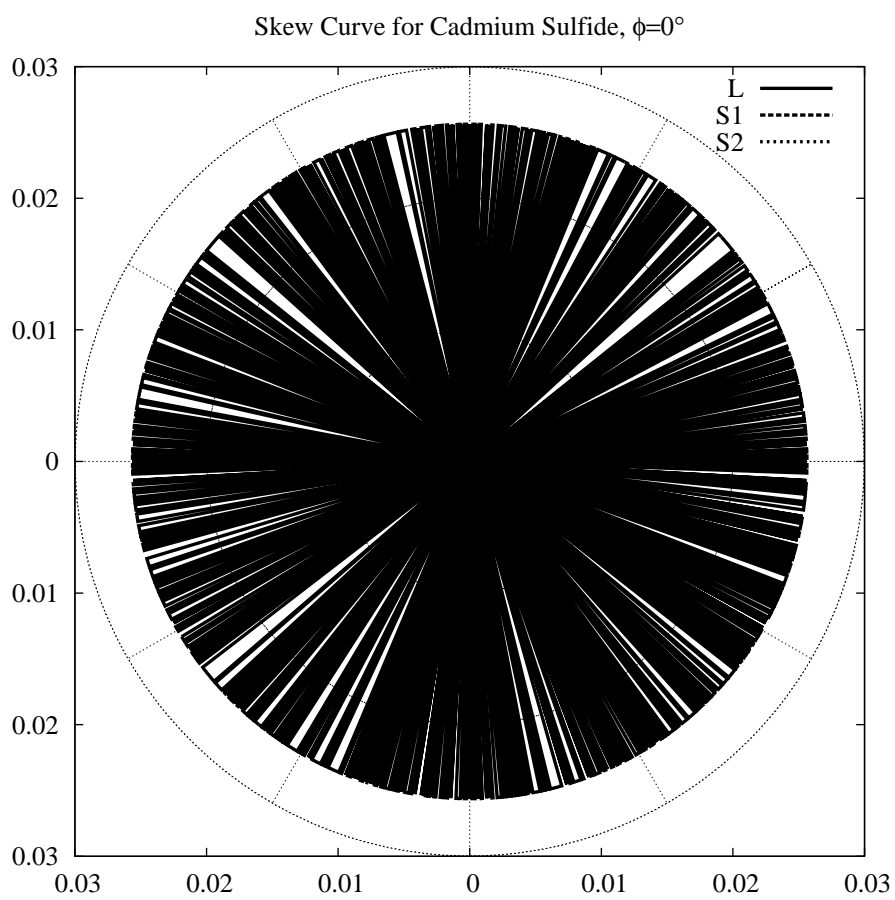


Figure 1.26: Slowness Curve for CdS,  $\phi = 90^\circ$ , ( $X - Z$  Plane)

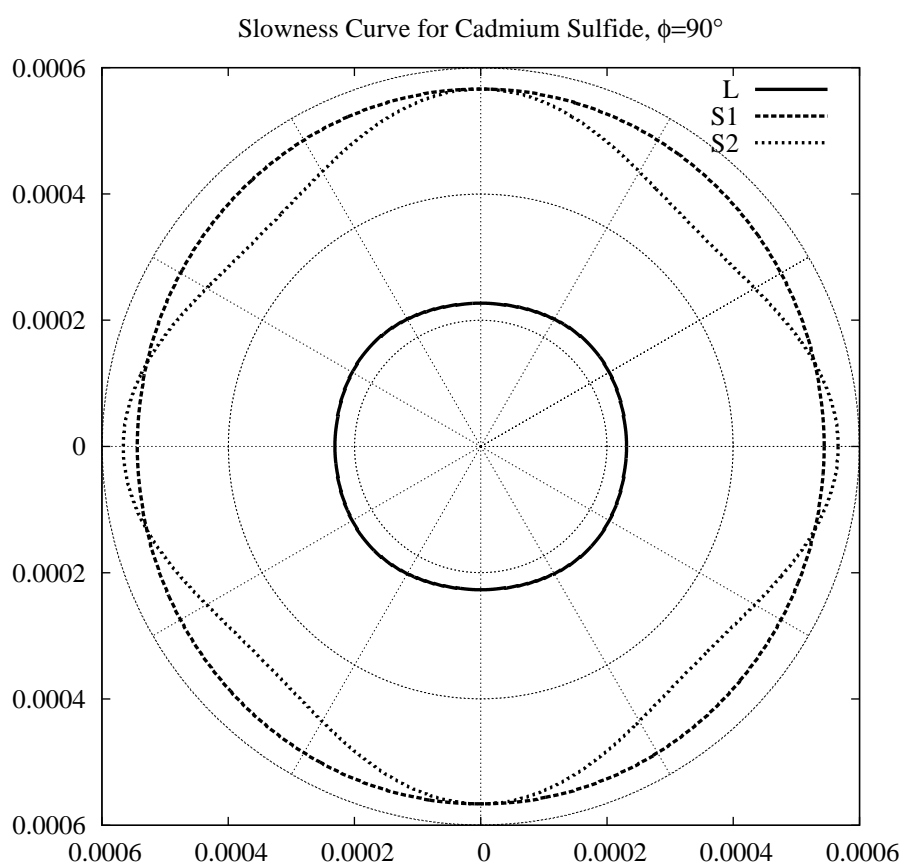
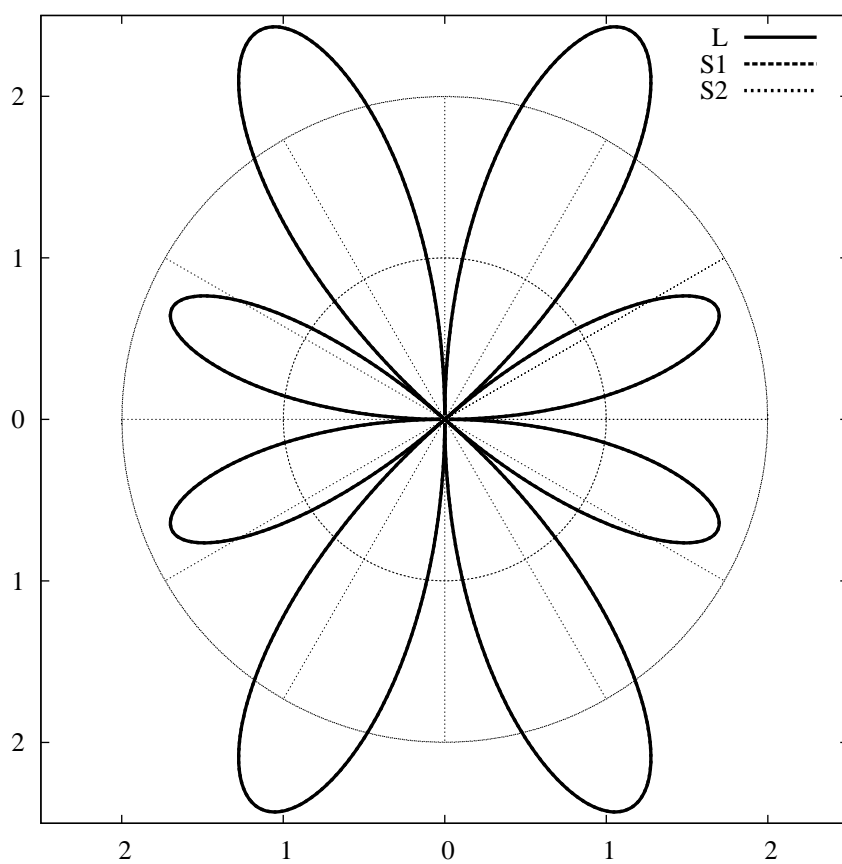


Figure 1.27: Skew Curve for CdS,  $\phi = 90^\circ$ , ( $X - Z$  Plane)

Skew Curve for Cadmium Sulfide,  $\phi=90^\circ$



# Chapter 2

## Guided Waves in Plates

### 2.1 Introduction

My aim in this section of the document is to summarise some information on elastic wave propagation in plates. Such waves, when propagating in infinite plates of isotropic homogeneous linearly elastic media, are known as Lamb waves. In this document, I will also discuss wave propagation in anisotropic and inhomogeneous (layered) media. Although strictly speaking such guided waves are not Lamb waves, I will use the term to describe such propagating guided modes. To follow this discussion, it is important to have a basic understanding of propagating bulk waves in isotropic and anisotropic media.

### 2.2 Lamb Waves

Lamb waves are defined as the waves propagating in a plate of isotropic material, where the particle displacements are polarised in a plane parallel to both a normal to the plate's free surfaces, and to the direction of propagation (we would call this plane the *sagittal plane*, illustrated in Fig. 2.1). A second form of propagating wave which can propagate in a free plate of isotropic material is the shear-horizontal (or *SH*) wave, where particle displacements are *normal* both to the direction of propagation and to the plate normal. The equations describing the behaviour of Lamb waves are obtained by starting with the basic equations governing an elastic solid, as described in section 1.1, and then applying boundary conditions corresponding to the free surfaces of the plate. This was first studied by Lord-Rayleigh [9], and by Lamb [10], though a full study of the details of dispersion behaviour was not completed until decades later. A seminal and illuminating discussion of the details of Lamb wave propagation is to be found in work by Mindlin [11].

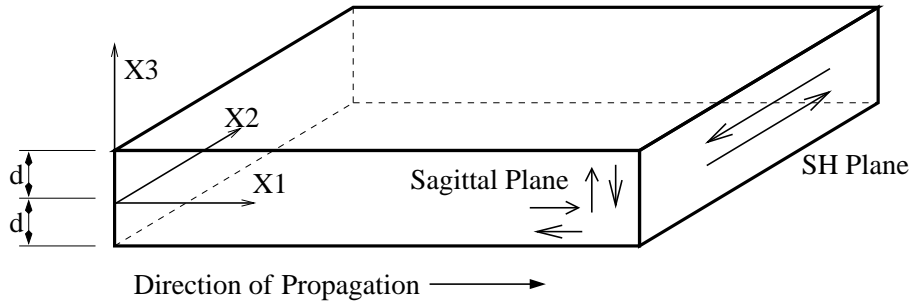


Figure 2.1: Schematic

A brief derivation of the Lamb wave dispersion relations will be presented here. This will be facilitated by the use of a dimensionless notation, in particular a dimensionless frequency. The dispersion relations obtained will be solved in order to provide dispersion data for the materials which will be modelled later.

### 2.2.1 Lamb Waves in Aluminium Plate

The starting point in this section is the dynamic equation for a linear elastic solid, Equation (1.1). A more convenient form to begin with is shown in Equation (2.1) [12], which uses the Lamé constants mentioned in Section 1.3.8.

$$\rho \frac{\partial^2 u_i}{\partial t^2} = (\lambda + \mu) \frac{\partial \theta}{\partial x_i} + \mu \nabla^2 u_i \quad (2.1)$$

$\theta$  represents the divergence or dilation, and is defined in Equation (2.2) where the summation has been written explicitly for clarity. If the wave is decomposed into rotational and irrotational potentials, then the dilation represents the irrotational component.

$$\theta = \frac{\partial u_1}{\partial x_1} + \frac{\partial u_2}{\partial x_2} + \frac{\partial u_3}{\partial x_3} \quad (2.2)$$

Before going any further, it is useful at this point to introduce a dimensionless notation which allows some useful simplification of the current analysis. If certain simplifications are made regarding material properties, then a dimensionless treatment of the equations described so far makes it possible to express the equations in a more compact form as shown below. First, the simplification is made that Poisson's ratio is equal to a third,  $\nu = 1/3$ . This is approximately the case for aluminium. This simplification is expressed in terms of Lamé's constants in equation (2.3).

$$\lambda = 2\mu \quad (2.3)$$

The removal of dimensionality is done in the following way. Lengths (such as  $x_i$  and  $u_i$ ) are expressed in terms of the plate half-thickness,  $d$  (see Fig. 2.1). Time is scaled by a time scaling factor,  $\eta$ , which will be defined in terms of bulk wave speeds in the material and the half-thickness of the plate.  $\eta$  is thus a function of the material properties of the plate, as well as the scale of the plate. The new dimensionless quantities are distinguished from their dimensioned counterparts by the use of upper case. Equation (2.4) illustrates the transformation.

$$X_1 = \frac{x_1}{d} \quad , \quad X_3 = \frac{x_3}{d} \quad , \quad T = t\eta \quad , \quad \bar{c}_{(t,l)} = \frac{c_{(t,l)}}{\eta d} \quad , \quad \Omega = \frac{\omega}{\eta} \quad (2.4)$$

Note that in Equation (2.4),  $c_t$  and  $c_l$  are the transverse (shear) and longitudinal bulk wavespeeds. Confusion with earlier terms  $c_{ijkl}$  from the stiffness tensor is avoided since the meaning should be clear in context, and also due to the number of subscripts. If we now express Equation (2.1) using this new notation, and applying Equation (2.3) we get the expression shown in Equation (2.5).

$$\frac{\rho d^2 \eta^2}{\mu} \frac{\partial^2 U_i}{\partial T^2} = 3 \frac{\partial \theta}{\partial X_i} + \nabla^2 U_i \quad (2.5)$$

We have not yet defined the time scaling factor  $\eta$ , so for convenience we will pick it such that

$$\eta^2 = \frac{\mu}{\rho d^2} \equiv \frac{c_t^2}{d^2} \quad \Leftrightarrow \quad \rho d^2 \eta^2 = \mu \quad (2.6)$$

Thus, Equation (2.5) simplifies to give

$$\frac{\partial^2 U_i}{\partial T^2} = 3 \frac{\partial \theta}{\partial X_i} + \nabla^2 U_i. \quad (2.7)$$

Since the dependence on time is of the form  $e^{i\Omega T}$ , Equation (2.7) is equivalent to Equation (2.8).

$$(\nabla^2 + \Omega^2) U_i = -3 \frac{\partial \theta}{\partial X_i} \quad (2.8)$$

If for each  $i = 1, 2, 3$ , (2.8) is differentiated with respect to  $X_i$ , and the resulting three equations are summed, we obtain the expression in  $\theta$  shown in Equation (2.9).

$$\left( \nabla^2 + \frac{\Omega^2}{4} \right) \theta = 0 \quad (2.9)$$

A solution of Equation (2.8) is given by

$$U_i = -\frac{4}{\Omega^2} \frac{\partial \theta}{\partial X_i} + \alpha_i \quad (2.10)$$

The complementary solution terms  $\alpha_i$  satisfy the relations

$$(\nabla^2 + \Omega^2) \alpha_i = 0 \quad (2.11)$$

$$\frac{\partial \alpha_1}{\partial X_1} + \frac{\partial \alpha_2}{\partial X_2} + \frac{\partial \alpha_3}{\partial X_3} = 0 \quad (2.12)$$

$\alpha_i$  is expressed in terms of a potential  $\chi$

$$\alpha_1 = \frac{\partial \chi}{\partial X_3} \quad \text{and} \quad \alpha_3 = \frac{-\partial \chi}{\partial X_1} \quad (2.13)$$

Where  $\chi$  is a function of  $X_1$  and  $X_3$  which satisfies

$$(\nabla^2 + \Omega^2) \chi = 0 \quad (2.14)$$

The solutions for the two potentials  $\chi$  and  $\theta$  are respectively:

$$\chi = (A \sinh SX_3 + B \cosh SX_3) e^{iFX_1 - i\Omega T} \quad (2.15)$$

$$\theta = (C \cosh QX_3 + D \sinh QX_3) e^{iFX_1 - i\Omega T} \quad (2.16)$$

where

$$Q^2 = F^2 - \Omega^2/4 \quad (2.17)$$

$$S^2 = F^2 - \Omega^2 \quad (2.18)$$

Finally, the dimensionless displacements  $U_1$  and  $U_2$  can be expressed in terms of the potentials  $\phi^1$  and  $\chi$  as follows:

$$U_1 = \frac{-\partial \phi}{\partial X_1} + \frac{\partial \chi}{\partial X_3} \quad \text{and} \quad U_3 = \frac{-\partial \phi}{\partial X_3} + \frac{-\partial \chi}{\partial X_1} \quad (2.19)$$

## 2.2.2 Boundary Conditions

Up to this point, no mention has been made of boundary conditions, or of the geometry of the elastic space being studied. Everything mentioned in the previous discussion is valid for any isotropic linear-elastic solid. The only restriction introduced so far has been to limit our study to plane waves, and to align our coordinate system such that the  $x_1$  axis points in the direction of propagation. The waves which we have defined are basic longitudinal and shear waves, which are fundamentally characterised in equations (2.9) and (2.14) respectively.

The boundary conditions which must be satisfied by the waves in the plate are

---

<sup>1</sup> $\phi$  is formed by absorbing the  $4/\Omega^2$  in Equation (2.10) into the  $\theta$  term.

the result of the traction free condition on the top and bottom surfaces of the plate.

$$\left. \begin{array}{l} \sigma_{33} = 0 \\ \sigma_{13} = \sigma_{31} = 0 \end{array} \right\} \quad x_3 = \pm d \iff X_3 = \pm 1 \quad (2.20)$$

These boundary conditions can be expanded using the constitutive equation of an isotropic material (1.34), and the definitions of the Lamé constants (1.35) to give the expressions in Equations (2.21) and (2.22) (again, for  $X_3 = \pm 1$ ).

$$\lambda \left( \frac{\partial U_1}{\partial X_1} + \frac{\partial U_2}{\partial X_2} + \frac{\partial U_3}{\partial X_3} \right) + 2\mu \frac{\partial U_3}{\partial X_3} = 0 \quad (2.21)$$

$$\mu \left( \frac{\partial U_1}{\partial X_3} + \frac{\partial U_3}{\partial X_1} \right) = 0 \quad (2.22)$$

We have already, in Equation (2.19), expressed the displacements  $U_1$  and  $U_3$  in terms of potentials  $\phi$  and  $\chi$ . Also, in Equations (2.15) and (2.16), these potentials have been expressed in terms of the coordinate  $X_3$  and constants. Substituting from these expressions into the shear stress boundary condition (2.22), and ignoring the  $\mu$  term, gives the following condition:

$$\frac{\partial^2 \chi}{\partial X_3^2} - \frac{2\partial^2 \phi}{\partial X_3 \partial X_1} - \frac{\partial^2 \chi}{\partial X_1^2} = 0 \quad \text{for } X_3 = \pm 1 \quad (2.23)$$

Then substitute for the potentials from Equations (2.15) and (2.16), the following expressions are obtained for  $X = \pm 1$  respectively (common  $\exp iFX_1 - i\Omega T$  terms omitted here and in subsequent expressions for neatness).

$$(F^2 + S^2) (A \sinh S + B \cosh S) - 2iFQ (C \sinh Q + D \cosh Q) = 0 \quad (2.24)$$

$$(F^2 + S^2) (-A \sinh S + B \cosh S) - 2iFQ (-C \sinh Q + D \cosh Q) = 0 \quad (2.25)$$

Recalling Equation (2.3), the normal stress condition of Equation (2.21) gives the following result:

$$-\frac{2\partial^2 \phi}{\partial X_3^2} - \frac{\partial^2 \chi}{\partial X_3 \partial X_1} + \frac{\partial^2 \phi}{\partial X_1^2} = 0 \quad \text{for } X_3 = \pm 1 \quad (2.26)$$

And when the expressions for the potentials  $\phi$  and  $\chi$  from (2.15) and (2.16) have been substituted in, the following expressions are obtained for  $X = \pm 1$  respec-

tively.

$$(F^2 + S^2) (C \cosh Q + D \sinh Q) + 2iFS (A \cosh S + B \sinh S) = 0 \quad (2.27)$$

$$(F^2 + S^2) (C \cosh Q - D \sinh Q) + 2iFS (A \cosh S - B \sinh S) = 0 \quad (2.28)$$

It should be noted that it is possible to separate the potentials  $\chi$  and  $\phi$  (and hence displacements and stresses) into symmetric and non symmetric wave components. This occurs naturally in each pair of boundary condition equations above, which can be added or subtracted to give the boundary conditions for symmetric or asymmetric waves. These separated boundary conditions are shown in Equations (2.29) and (2.30).

$$(F^2 + S^2) A \sinh S - 2iFQC \sinh Q = 0 \quad (2.29)$$

$$2iFSA \cosh S + (F^2 + S^2) C \cosh Q = 0$$

$$(F^2 + S^2) B \cosh S - 2iFQD \cosh Q = 0 \quad (2.30)$$

$$2iFSB \sinh S + (F^2 + S^2) D \sinh Q = 0$$

In the rotational potential  $\chi$ , the symmetric wave component is given by the  $A \sinh S$  term. This means that rotation is zero on the plate centre-line, and is of opposite sign in the upper and lower halves of the plate. The effect of this is that the contribution to displacement of the potential is symmetric. The symmetric component of the dilational potential,  $\phi$  is given by the  $C \cosh Q$  term. The remaining terms, which use the constants  $B$  and  $D$  relate to the asymmetric part of the propagating wave. By separating the wave into symmetric and asymmetric components, the two parts of the propagating wave can be examined individually.

Solutions to Equations (2.29) and (2.30) will exist where the corresponding determinants go to zero. This leads to two characteristic equations, for symmetric and asymmetric waves respectively:

$$\frac{4F^2QS}{(F^2 + S^2)^2} = \frac{\tanh S}{\tanh Q} \quad \dots \quad \text{symmetric} \quad (2.31)$$

$$\frac{4F^2QS}{(F^2 + S^2)^2} = \frac{\tanh Q}{\tanh S} \quad \dots \quad \text{asymmetric} \quad (2.32)$$

These equations can be solved to find the possible wavelengths (equivalently wave numbers or wave speeds) at any particular frequency.

Using, Equations (2.29) and (2.30), constants  $C$  and  $D$  can be expressed in

terms of  $A$  and  $B$  respectively. Rewriting  $\chi$  and  $\phi$  in this way gives:

$$\chi = A \sinh SX_3 + B \cosh SX_3 \quad (2.33)$$

$$\phi = \frac{A(F^2 + S^2) \sinh S}{2iFQ \sinh Q} \cosh QX_3 + \frac{B(F^2 + S^2) \cosh S}{2iFQ \cosh Q} \sinh QX_3 \quad (2.34)$$

This allows final expressions for the dimensionless displacements and the stresses to be formulated. These expressions are shown in Equations (2.35) to (2.44).

$$U_{1,\text{symm}} = A \left( -\frac{(F^2 + S^2) \sinh S}{2Q \sinh Q} \cosh QX_3 + S \cosh SX_3 \right) \quad (2.35)$$

$$U_{3,\text{symm}} = iA \left( \frac{(F^2 + S^2) \sinh S}{2F \sinh Q} \sinh QX_3 - F \sinh SX_3 \right) \quad (2.36)$$

$$U_{1,\text{asymm}} = B \left( -\frac{(F^2 + S^2) \cosh S}{2Q \cosh Q} \sinh QX_3 + S \sinh SX_3 \right) \quad (2.37)$$

$$U_{3,\text{asymm}} = iB \left( \frac{(F^2 + S^2) \cosh S}{2F \cosh Q} \cosh QX_3 - F \cosh SX_3 \right) \quad (2.38)$$

$$\sigma_{13,\text{symm}} = \mu A (F^2 + S^2) \left[ \frac{-\sinh S}{\sinh Q} \sinh QX_3 + \sinh SX_3 \right] \quad (2.39)$$

$$\sigma_{33,\text{symm}} = i2\mu A \left[ \frac{(F^2 + S^2)^2 \sinh S}{4QF \sinh Q} \cosh QX_3 - FS \cosh SX_3 \right] \quad (2.40)$$

$$\sigma_{11,\text{symm}} = i\mu A \left[ (F^2 + S^2) \frac{\sinh S}{\sinh Q} \frac{Q^2 - 2F^2}{QF} \cosh QX_3 + 2SF \cosh SX_3 \right] \quad (2.41)$$

$$\sigma_{13,\text{asymm}} = \mu B (F^2 + S^2) \left[ \frac{-\cosh S}{\cosh Q} \cosh QX_3 + \cosh SX_3 \right] \quad (2.42)$$

$$\sigma_{33,\text{asymm}} = i2\mu B \left[ \frac{(F^2 + S^2)^2 \cosh S}{4QF \cosh Q} \sinh QX_3 - FS \sinh SX_3 \right] \quad (2.43)$$

$$\sigma_{11,\text{asymm}} = i\mu B \left[ (F^2 + S^2) \frac{\cosh S}{\cosh Q} \frac{Q^2 - 2F^2}{QF} \sinh QX_3 + 2SF \sinh SX_3 \right] \quad (2.44)$$

## 2.3 Isotropic Dispersion

### 2.3.1 Introduction

To characterise the vibration of an aluminium plate at any given frequency, it is necessary to solve the frequency Equations (2.31) and (2.32). In much of the current analysis, we will restrict ourselves to looking at symmetric vibrations of relatively low frequency ( $\Omega \leq \sqrt{2}$ ). At such frequencies, there are only two possible modes of vibration, one symmetric and one antisymmetric (the  $S_0$  and  $A_0$  modes), and as said before, for now we will restrict ourselves to the former case.

### 2.3.2 Preliminaries

In this section, the basic equations will be rearranged into forms more suitable for analysis. This is done in a similar fashion to that used by Lamb [10]. The preferable dimensionless notation will be used, with the inherent assumption that the Lamé constants are related as  $\lambda = 2\mu$  (true for Aluminium). For the sake of clarity, the earlier expressions from Equations (2.17) and (2.18) are repeated here:

$$Q^2 = F^2 - \Omega^2/4 \quad \text{and} \quad S^2 = F^2 - \Omega^2 \quad (2.45)$$

Following Lamb [10], we introduce a term  $m$  such that:

$$m = \frac{S}{Q} \quad (2.46)$$

Only real values of  $F$  and  $\Omega$  will be considered<sup>2</sup>.  $F$  can be easily expressed in terms of  $Q$  and  $S$ , and then equivalently in terms of  $Q$  and  $m$ , as follows:

$$F^2 = \frac{4Q^2 - S^2}{3} = \frac{4 - m^2}{3}Q^2 \quad (2.47)$$

The dimensionless frequency equation for symmetric vibrations, given by (2.31) earlier in the analysis is repeated here. It has been rewritten using  $mQ$  in place of  $S$  and substituting for  $F$  from (2.47), and then simplified algebraically:

$$\frac{\tanh mQ}{\tanh Q} = \frac{3m(4 - m^2)}{(2 + m^2)^2} \quad (2.48)$$

---

<sup>2</sup>Imaginary values of wavenumber correspond to waves that decay exponentially in the  $x_1$  direction. Similarly imaginary  $\Omega$  corresponds to waves decaying exponentially in time

For antisymmetric vibration, the form of the characteristic equation is only slightly different and one of the fractions is inverted:

$$\frac{\tanh Q}{\tanh mQ} = \frac{3m(4 - m^2)}{(2 + m^2)^2} \quad (2.49)$$

Using (2.45) and (2.47),  $\Omega$  can be expressed purely in terms of  $m$  and  $q$  as follows:

$$\Omega^2 = F^2 - m^2 Q^2 = \frac{4 - 4m^2}{3} Q^2 \quad (2.50)$$

Turning to the definition for dimensionless wave speed in the solid in equation (2.4), and using the connection between wavenumber, frequency and wavespeed, and  $F$  and  $\Omega$  in terms of  $m$ , it is possible to write  $C$  purely as a function of  $m$ :

$$\bar{c}^2 = \left(\frac{c}{c_t}\right)^2 = \left(\frac{\Omega}{F}\right)^2 = \left(\frac{4 - 4m^2}{4 - m^2}\right) \quad (2.51)$$

If  $m$  is allowed to take imaginary values, it is possible to obtain the velocities over a different portion of the frequency speed curve. This corresponds to phase velocities greater than the transverse wave velocity  $c_t$ , but still lower than the longitudinal velocity. It is easier to handle the imaginary  $m$  if by introducing a new term  $n$  defined as

$$m = in \quad (2.52)$$

Using (2.52), the characteristic equations (2.48) and (2.49), along with the expressions for  $F^2$  (2.47),  $\Omega^2$  (2.50) and  $\bar{c}^2$  (2.51) can be rewritten respectively as:

$$\frac{\tan nQ}{\tanh Q} = \frac{3n(4 + n^2)}{(2 - n^2)^2} \quad \text{(Symmetric)} \quad (2.53)$$

$$\frac{\tanh Q}{\tan nQ} = \frac{-3n(4 + n^2)}{(2 - n^2)^2} \quad \text{(Anti-symmetric)} \quad (2.54)$$

$$F^2 = \frac{4 + n^2}{3} Q^2 \quad (2.55)$$

$$\Omega^2 = \frac{4 + 4n^2}{3} Q^2 \quad (2.56)$$

$$\bar{c}^2 = \frac{4 + 4n^2}{4 + n^2} \quad (2.57)$$

Here, the symmetric and anti-symmetric characteristic equations differ not only by the inversion of the left hand side fraction, but also in the sign of the right hand side. This is an effect of the cancellation of the imaginary  $i$  terms.

As will be seen shortly, most modes have velocities in excess of the longitudinal velocity  $c_l$  for some frequencies. In this region,  $S$  and  $Q$  both become complex. To make matters clearer, the imaginary factor  $i$  will be written beside the term  $Q'$ , which is real valued.  $S$  is then written as  $imQ'$ ,  $m$  being a real number once more. Applying this to the relations already presented in Equations (2.48), (2.49), (2.50) and (2.51), gives the following expressions:

$$\frac{\tan mQ}{\tan Q} = \frac{3m(4-m^2)}{(2+m^2)^2} \quad \text{(Symmetric)} \quad (2.58)$$

$$\frac{\tan Q}{\tan mQ} = \frac{3m(4-m^2)}{(2+m^2)^2} \quad \text{(Anti-symmetric)} \quad (2.59)$$

$$\Omega^2 = -\frac{4-4m^2}{3}Q^2 \quad (2.60)$$

$$F^2 = \frac{4-m^2}{3}Q^2 \quad (2.61)$$

$$\bar{c}^2 = \frac{4-4m^2}{4-m^2} \quad (2.62)$$

### 2.3.3 Detailed Calculation of Dispersion Curves

In this section, the dispersion curves are numerically solved for a larger number of points allowing a large portion of the dispersion diagram to be plotted. Depending on the wavenumber in a given region of the diagram, and on whether we want to characterise symmetric or antisymmetric waves, the frequency equations (2.48, 2.49, 2.53, 2.54, 2.58, 2.59) are solved for a given range of values of  $m$  and  $n$  to find corresponding values of  $Q$ . Knowledge of the values of  $m$  (or  $n$ ) and  $Q$  allows us to compute the values of  $\Omega$ ,  $\bar{c}$  and  $F$  through the appropriate equations, which have all been mentioned in Section 2.3.2. The dispersion curves were finally calculated using a program written in Python with the Numerical Python extensions [13]. Plotting has been done using Gnuplot. For notes on plotting of dispersion curves, see Section 2.4.3. The final dispersion curve plotted is shown in Fig. 2.2. The variation of wavelength as a function of frequency for the  $S_0$  mode is shown in Fig. 2.3. It should be noted from Fig. 2.3 how long the  $S_0$  wavelength becomes for small  $\Omega$  (tending to infinity as  $\Omega$  goes to 0). Another point to note is how flat the  $S_0$  dispersion curve in Fig. (2.2) is for  $0 \leq \Omega \leq \sqrt{2}$ . This means that for this range of frequencies, the wave is almost non-dispersive. As will be seen later, the dispersion curves shown here for an isotropic plate are very similar to those obtained for a transversely isotropic composite plate in its plane of isotropy (see Section 2.5 for comparison).

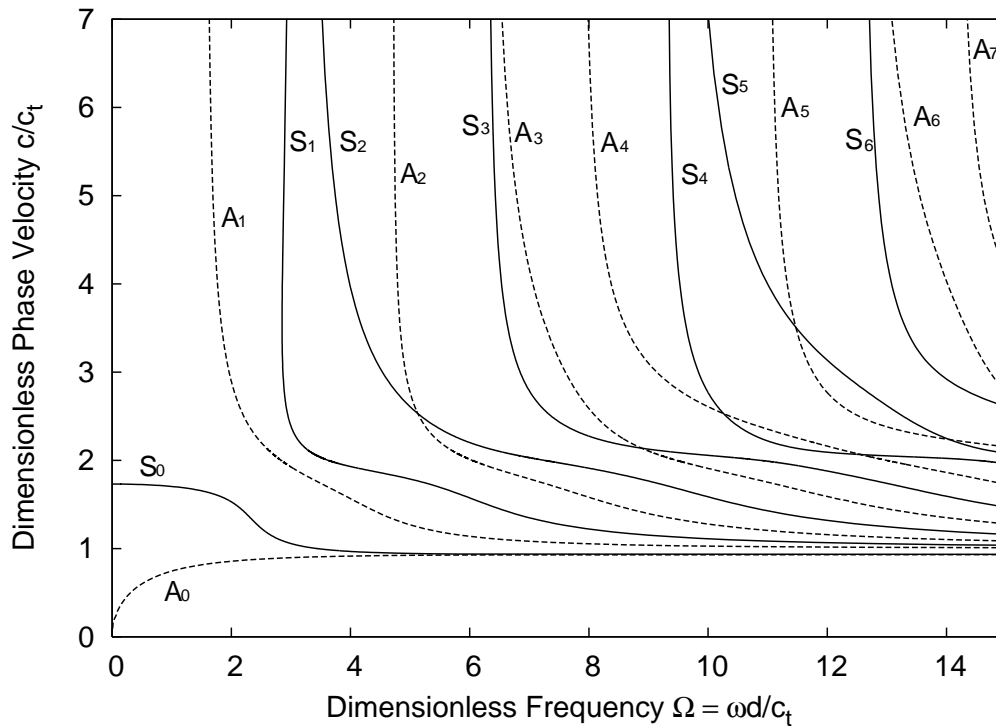


Figure 2.2: Velocity/frequency dispersion plot for aluminium. Solid lines are symmetric modes, dashed lines are antisymmetric modes.

## 2.4 Anisotropic and Inhomogeneous Plates

In this chapter, horizontal defects in anisotropic plates will be discussed. The elastic properties of the plates will be chosen to represent a carbon-fibre reinforced epoxy material. Horizontal defects, i.e. delaminations, are quite commonly found in these materials. Often these occur in the manufacturing process as such materials are typically fabricated from multiple layers. Additionally, this layered construction means that when subjected to damage, it is common for failure to occur at the interfaces between layers.

Four laminated plate models are used. Two of these correspond to unidirectional composite plates. In such plates, the reinforcing fibres are all aligned in the same direction. This produces a material which is transversely isotropic. The bulk wave properties of this material have been mentioned already in Section ???. In such a material, propagation of plate waves will be considered for two propagation directions: normal to the fibre direction and parallel to the fibre direction. It will also be assumed that the fibre direction is parallel to the free surfaces of the

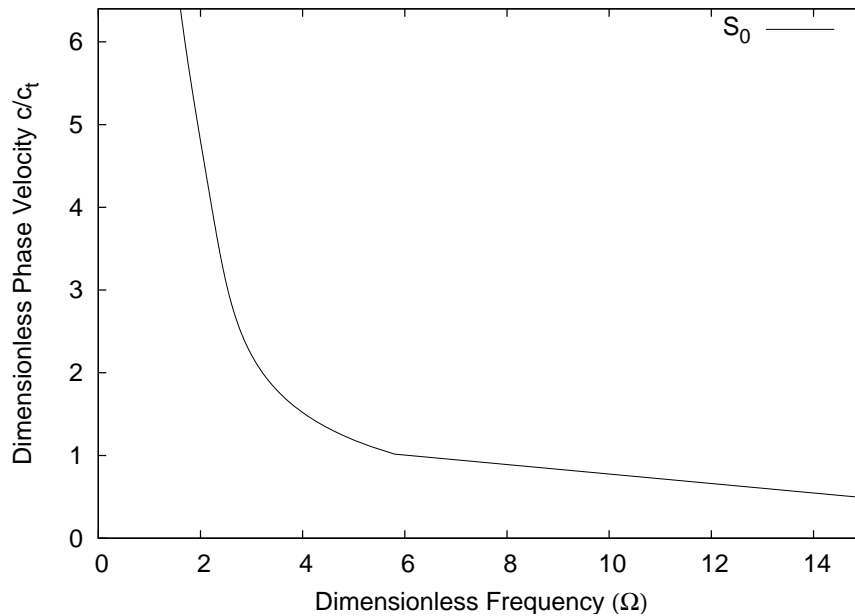


Figure 2.3: Wavelength/Frequency Plot for  $S_0$  Mode

plate. Such a plate is highly anisotropic. Often other material properties are required, and in such a case the direction of fibre orientation is varied from layer to layer. One such plate will be considered here, and the layers will be offset by  $90^\circ$  from each other. This arrangement leads to a somewhat more uniform distribution of stiffness in the in-plane directions, while the plate will be substantially less stiff in the out of plane direction. Such a plate is referred to as a cross-ply laminate. Wave propagation and interaction with defects will be considered in such a plate for two propagation directions.

### 2.4.1 Transverse Isotropy

Since transversely isotropic media are very common in engineering applications, they will here be given a brief examination. It was seen earlier in Section ?? that for propagation normal to the direction of fibres, the material behaves exactly as an isotropic material would. Velocities of the shear and longitudinal waves are independent of propagation direction in this plane, and the modes are always pure modes. For propagation in an arbitrary direction, things are more difficult, however for propagation in a plane parallel with the fibre direction, some simplifications occur. In particular, when looking at plate modes in this case, it is possible to consider only one shear (a quasi  $SV$  mode) and one longitudinal mode. The

remaining shear mode decouples and propagates in the plate as a *SH* mode.

Notwithstanding this simplifications, there are significant complications when compared with the isotropic case. In an isotropic material, the phase velocities of the fundamental component modes were independent of their propagation direction. For the anisotropic material, these velocities depend strongly on the direction of propagation, as can be seen in Fig. 2.6. Nayfeh [1] presents an approach to this problem (also seen in [14, 15, 16]), and this will be used here, specialised to the particular case of propagation polarised in a plane of symmetry of a material with at least orthotropic symmetry. Propagation in any of the planes of symmetry of a composite transversely isotropic plate would meet these criteria.

Propagation will be assumed to be in the  $x_1 - x_3$  plane, and boundaries will be oriented parallel to the  $x_1 - x_2$  plane. This means that the wavenumber vector can be conveniently expressed in the form:

$$\zeta \begin{Bmatrix} n_1 \\ n_2 \\ n_3 \end{Bmatrix} = \zeta n_1 \begin{Bmatrix} 1 \\ 0 \\ \alpha \end{Bmatrix} = k \begin{Bmatrix} 1 \\ 0 \\ \alpha \end{Bmatrix} \quad (2.63)$$

In Equation (2.63),  $\alpha$  is the ratio of  $n_3/n_1$  while  $k$  is the wavenumber in the  $x_1$  direction. Using these specific material properties and the restricted vector  $\mathbf{n}$  in the Christoffel equation as expressed in Equation (1.45) leads to a simplified Christoffel equation as shown below<sup>3</sup>.

$$\begin{pmatrix} A_{11} - \rho v^2 & 0 & A_{13} \\ 0 & A_{22} - \rho v^2 & 0 \\ A_{13} & 0 & A_{33} - \rho v^2 \end{pmatrix} \begin{Bmatrix} \bar{u}_1 \\ \bar{u}_2 \\ \bar{u}_3 \end{Bmatrix} = 0 \quad (2.64)$$

Equation (2.64) has one obvious solution, given by  $A_{22} - \rho v^2 = 0$ . If the term  $A_{22}$  is expanded, and the material property restrictions of Equation (1.32) are applied then the following expression results (written in terms of stiffnesses  $c_{ijkl}$ ):

$$A_{22} = (c_{2112}n_1n_1 + c_{2222}n_2n_2 + c_{2332}n_3n_3) \quad (2.65)$$

Recalling Equation (2.63), and substituting for  $A_{22}$  in the relevant factor of the

---

<sup>3</sup>It is not necessary to pursue the detailed calculations to see how the simplifications arise. Consider  $A_{12}$  By definition,  $A_{12} = c_{1jk2}n_jn_k$ , which is a sum of nine terms. Because of the restrictions on the stiffness tensor, the only two values of  $c_{1jk2}$  which are nonzero are for  $j = 1, k = 2$  and for  $j = 2, k = 1$  (corresponding to  $C_{12}$  and  $C_{66}$  in reduced notation). However, since  $n_2 = 0$ , the corresponding terms in  $A_{12}$  go to zero. The same material restrictions apply to the nonzero terms  $A_{11}, A_{22}, A_{33}, A_{13}$ , but these do not (all) coincide with the zero wavenumber component.

eigenvalue problem gives the result (now using reduced notation):

$$\rho v^2 = n_1^2(C_{66} + \alpha^2 C_{44}) \quad (2.66)$$

This describes an ellipse, and corresponds to the elliptical slowness curve in Fig. 2.6.

For the current discussion, the remaining part of the eigenvalue equation is of more interest, as it describes the (quasi)  $P$  and  $SV$  modes which will be components of Lamb waves. The remaining nonzero  $A_{ij}$  terms in Equation (2.64) are:

$$\begin{aligned} A_{11} &= n_1^2(C_{11} + \alpha^2 C_{55}) \\ A_{33} &= n_1^2(C_{55} + \alpha^2 C_{33}) \\ A_{13} &= n_1^2 \alpha (C_{13} + C_{55}) \end{aligned} \quad (2.67)$$

It should be noted that all terms contain a common factor  $n_1$ . If this is divided out, then the  $\rho v^2$  terms divided by  $n_1$  become  $\rho c^2$ , where  $c = \omega/k$  is the phase velocity projected onto the  $x_1$  axis. Using this, and substituting for the  $A$  terms into the remaining factors of the eigenvalue equation leads to the subsidiary eigenvalue equation:

$$\begin{pmatrix} C_{11} + \alpha^2 C_{55} - \rho c^2 & \alpha(C_{13} + C_{55}) \\ \alpha(C_{13} + C_{55}) & C_{55} + \alpha^2 C_{33} - \rho c^2 \end{pmatrix} \begin{Bmatrix} \bar{u}_1 \\ \bar{u}_3 \end{Bmatrix} = 0 \quad (2.68)$$

At this point, the rationale for the introduction of  $\alpha$  is clear. For a given phase velocity  $c$  in the  $x_1$  direction, values of alpha can be found corresponding to the bulk modes with this property. In fact, Equation (2.68) results in a quadratic equation<sup>4</sup> in terms of  $\alpha^2$  which is shown in Equation (2.69).

$$\begin{aligned} A\alpha^4 + B\alpha^2 + C &= 0 \\ \text{where} \\ A &= C_{33}C_{55} \\ B &= (C_{11} - \rho c^2)C_{33} + (C_{55} - \rho c^2)C_{55} - (C_{13} + C_{55})^2 \\ C &= (C_{11} - \rho c^2)(C_{55} - \rho c^2) \end{aligned} \quad (2.69)$$

Thus, the values of  $\alpha$  appear in matching  $\pm\alpha$  pairs corresponding to upward and downward travelling waves. These four modes will be denoted by an index  $q = 1, 2, 3, 4$ , and the values of  $\alpha$  will satisfy  $\alpha_2 = -\alpha_1$  and  $\alpha_4 = -\alpha_3$ . At this

---

<sup>4</sup>Note that this is equivalent to Equations (5.29-5.30) from Nayfeh [1], but with an error corrected in the expression for  $B$ .

point, the dynamic equations governing bulk waves in a transversely isotropic medium have been rearranged in a form that is convenient for finding bulk modes with a particular phase velocity in the  $x_1$  direction. Introducing free surfaces and applying traction free boundary conditions is the next step required to define Lamb waves and calculate dispersion curves. This requires expressions for the stresses  $\sigma_{13}$  and  $\sigma_{33}$  (the  $\sigma_{23} = 0$  boundary condition is satisfied by the *SH* plate-mode corresponding to the first eigenvalue discussed).

The form of the stress strain relationship applicable to transversely isotropic materials has already been presented in Equation (1.32). Selecting the stress components of interest, substituting for strain in terms of displacement from Equation (1.4), and recalling that there is no dependence on the  $x_2$  direction, gives the following expressions:

$$\sigma_{33} = C_{13} \frac{\partial u_1}{\partial x_1} + C_{33} \frac{\partial u_3}{\partial x_3} \quad (2.70)$$

$$\sigma_{13} = C_{55} \left( \frac{\partial u_3}{\partial x_1} + \frac{\partial u_1}{\partial x_3} \right) \quad (2.71)$$

The displacement components  $u_i$  are the sum of the contributions from the four partial waves mentioned already. It is useful to introduce a term  $w$ , which is the ratio  $\bar{u}_3/\bar{u}_1$  and which can be expressed from Equation (2.68) for mode  $q$  as

$$w_q = \frac{\bar{u}_{3q}}{\bar{u}_{1q}} = \frac{\rho c^2 - C_{11} - \alpha_q^2 C_{55}}{\alpha_q (C_{13} + C_{55})} \quad (2.72)$$

The stresses in Equations (2.70) and (2.71) can then be rewritten

$$\begin{aligned} \sigma_{33} &= \sum_{q=1}^4 (C_{13} + \alpha_q C_{33} w_q) ik \bar{u}_{1q} e^{ik(x_1 + \alpha_q x_3 - ct)} \\ &= \sum_{q=1}^4 D_{3q} ik \bar{u}_{1q} e^{ik(x_1 + \alpha_q x_3 - ct)} \end{aligned} \quad (2.73)$$

$$\begin{aligned} \sigma_{13} &= \sum_{q=1}^4 C_{55} (w_q + \alpha_q) ik \bar{u}_{1q} e^{ik(x_1 + \alpha_q x_3 - ct)} \\ &= \sum_{q=1}^4 D_{1q} ik \bar{u}_{1q} e^{ik(x_1 + \alpha_q x_3 - ct)} \end{aligned} \quad (2.74)$$

Each stress is a summation of four components. These two stresses must each go to zero at the top and bottom surfaces of the plate ( $x_3 = \pm d$ ). These conditions

can be neatly expressed in a matrix form, as follows:

$$ik \begin{pmatrix} D_{11}E_1 & D_{12}E_2 & D_{13}E_3 & D_{14}E_4 \\ D_{31}E_1 & D_{32}E_2 & D_{33}E_3 & D_{34}E_4 \\ D_{11}E_1^{-1} & D_{12}E_2^{-1} & D_{13}E_3^{-1} & D_{14}E_4^{-1} \\ D_{31}E_1^{-1} & D_{32}E_2^{-1} & D_{33}E_3^{-1} & D_{34}E_4^{-1} \end{pmatrix} \begin{Bmatrix} \bar{u}_{11} \\ \bar{u}_{12} \\ \bar{u}_{13} \\ \bar{u}_{14} \end{Bmatrix} e^{ik(x_1-ct)} = \begin{Bmatrix} 0 \\ 0 \\ 0 \\ 0 \end{Bmatrix} \quad (2.75)$$

Where  $E_q = e^{ik\alpha_q d}$ . The  $D_{ij}$  terms are given in Equation (2.76).

$$\begin{aligned} D_{1m} &= C_{55}(w_m + \alpha_m) \\ D_{3m} &= C_{13} + \alpha_m w_m C_{33} \end{aligned} \quad (2.76)$$

Setting the determinant of the  $4 \times 4$  matrix in Equation (2.75) equal to zero gives the characteristic equation governing (quasi) Lamb waves propagating in a plane of symmetry of a transversely isotropic material. In fact, it is possible to further simplify the characteristic equation by a sequence of matrix manipulations<sup>5</sup> to arrive at the characteristic equation below, where the determinant has been separated into two sub-determinants:

$$\begin{vmatrix} iD_{11}S_1 & iD_{13}S_3 & 0 & 0 \\ iD_{31}C_1 & iD_{33}C_3 & 0 & 0 \\ 0 & 0 & D_{11}C_1 & D_{13}C_3 \\ 0 & 0 & D_{31}S_1 & D_{33}S_3 \end{vmatrix} = 0 \quad (2.77)$$

Where  $S_1 = \sin(\alpha_1 k) = \sin(\alpha_1 \omega/c)$  and  $C_1 = \cos(\alpha_1 k) = \cos(\alpha_1 \omega/c)$

In Equation 2.77,  $S_1$  When expanded, these sub-determinants bear a strong resemblance to the characteristic equations already obtained for isotropic materials. Application of the additional restrictions on the material properties of isotropic materials shows that for this case, both sets of expressions are equivalent. An example calculation for this class of material is presented in Section 2.6 along with dispersion curves.

## 2.4.2 Stratified Media

Quite separate to the issue of anisotropic, but homogeneous, material properties is the subject of layered media. The individual layers may be themselves anisotropic, or they may be composed of different isotropic materials. In a sense, the discussion in this chapter has concerned layered media since Section 2.2 when Lamb waves were introduced. In that case the problem addressed consisted of a three

<sup>5</sup>Details of these manipulations for a more general  $6 \times 6$  matrix have been presented by Nayfeh [1], the procedure used here is similar.

layer system: an isotropic elastic layer sandwiched by two infinite layers of vacuum. More generally, the discussion of guided waves in layered media concerns layered plates, embedded in infinite layers of arbitrary material (which may be vacuum, fluid or solid).

The area of wave propagation in layered media has received significant attention, originally from the geophysical community who sought to model wave propagation through the strata of the Earth's crust, but more recently from those interested in the field of nondestructive evaluation. Various approaches have been used, some of which will be mentioned here.

In some cases, one particular layer may be very dominant. An example of this would be where a thin coating or cladding has been added to a plate. In such cases, researchers have found it useful to model the composite structure by simply modifying the boundary conditions to account for the presence of the coating [17, 18]. A similar method can be used to model the presence of a thin interface layer between two much thicker layers by using appropriate interface conditions [19].

In other cases, it has been necessary to explicitly account in detail for all layers present in a stratified material. The most commonly used technique is known as the transfer matrix method, which was first developed for elastic media by Thomson [20] and Haskell [21].

The principle of the transfer matrix is relatively simple, even in the anisotropic case, although the implementation can be very difficult. In broadest terms, a  $6 \times 6$  matrix is formed, relating the stress and displacement boundary conditions at the top of a layer to those at its bottom. The matrices for multiple layers are then combined based on the assumption of continuity at their interfaces. This process leads to the formation of an overall  $6 \times 6$  matrix which relates the boundary conditions at the top of the multilayered medium to those at the bottom.

A six dimensional stress displacement field vector is used,  $\mathbf{s}(x_3)$ , which (in the general case) contains the three displacement components  $u_i$  and the three stress components acting on the interface surface  $\sigma_{i3}$ .

$$\mathbf{s}(x_3) = (u_1, u_2, u_3, \sigma_{13}, \sigma_{23}, \sigma_{33})^T = \begin{pmatrix} \mathbf{u} \\ \boldsymbol{\sigma} \end{pmatrix} \quad (2.78)$$

$\mathbf{s}(x_3)$  is continuous across the interfaces between the layers. This means that for two layers  $m$  and  $m + 1$ , with field vectors  $\mathbf{s}_m$  and  $\mathbf{s}_{m+1}$  respectively, and with their interface at position  $x_3 = z_m$ , the following must hold:

$$\mathbf{s}_{m+1}(z_m) = \mathbf{s}_m(z_m) \quad (2.79)$$

It is necessary to relate the field vector on the bottom of a layer to that on the top. The displacement  $\mathbf{u}$  can be decomposed into the quasi longitudinal and transverse

waves seen in Section 1.4. Six components are used, three propagating in the positive  $x_3$  direction, and three propagating in the negative  $x_3$  direction. These six components will be denoted by the index  $q = 1, 2, \dots, 6$ . We will also use an index  $m$ , denoting the layer number. These components, for a layer  $m$  can thus be summed to give the total displacement vector for a monochromatic plane wave  $\mathbf{u}^m$ .

$$\mathbf{u}^m = \left( \sum_{q=1}^6 \bar{\mathbf{u}}_q e^{i(\mathbf{n}_q \cdot \mathbf{x} - \omega t)} \right)^m \quad (2.80)$$

The vectors  $\bar{\mathbf{u}}_q$  are the polarisation vectors of the relevant components.  $\mathbf{n}_q$  is the wavenumber vector of component  $q$ .  $\bar{\mathbf{u}}$  and  $\mathbf{n}$  are obtained from the Christoffel equation, which was presented earlier in Equation (1.44). Substituting  $\mathbf{u}$  as given in (2.80), into equations for stress (1.2) and (1.4) gives components of stress in layer  $m$  as follows:

$$\boldsymbol{\sigma}^m = \left( i \sum_{q=1}^6 \bar{\boldsymbol{\sigma}}_q e^{i(\mathbf{n}_q \cdot \mathbf{x} - \omega t)} \right)^m \quad (2.81)$$

Where the components of the stress-amplitude vector  $\bar{\boldsymbol{\sigma}}_q$  differ from those of  $\bar{\mathbf{u}}_q$  (in layer  $m$ ) as follows ( $n_t$  and  $\bar{u}_s$  being components of  $\mathbf{n}_q$  and  $\bar{\mathbf{u}}_q$  respectively):

$$(\bar{\sigma}_{i3})_q^m = (c_{i3st} n_t \bar{u}_s)_q^m \quad (2.82)$$

Looking at layer  $m$  which has boundaries at  $x_3 = z_{m-1}$  and at  $x_3 = z_m$ ,  $\mathbf{u}$  and  $\boldsymbol{\sigma} = (\sigma_{13}, \sigma_{23}, \sigma_{33})^T$  can be written as:

$$\begin{aligned} \begin{Bmatrix} \mathbf{u}^m \\ \boldsymbol{\sigma}^m \end{Bmatrix} &= \begin{bmatrix} \bar{\mathbf{u}}_1^m & \bar{\mathbf{u}}_2^m & \dots & \bar{\mathbf{u}}_6^m \\ \bar{\boldsymbol{\sigma}}_1^m & \bar{\boldsymbol{\sigma}}_2^m & \dots & \bar{\boldsymbol{\sigma}}_6^m \end{bmatrix} [\mathbf{H}(x_3 - z_{m-1})]^m e^{i(n_1 x_1 + n_2 x_2 - \omega t)} \\ \{s(x_3)^m\} &= [\mathbf{P}^m] [\mathbf{H}(x_3 - z_{m-1})]^m e^{i(n_1 x_1 + n_2 x_2 - \omega t)} \end{aligned} \quad (2.83)$$

In Equation (2.83), the entries  $\bar{\mathbf{u}}_q$  and  $\bar{\boldsymbol{\sigma}}_q$  are column vectors of length 3 and have the same meaning as in Equations (2.80) and (2.81). Thus the first matrix on the right hand side of the equation is a  $6 \times 6$  square matrix. The dependence of the field vector on position through the thickness,  $x_3$ , manifests in the  $[\mathbf{H}(x_3)]$  term which is a diagonal  $6 \times 6$  matrix with entries  $\mathbf{H}_{ll}(x_3) = \exp(in_{3(q)} x_3)$ ,  $n_{3(q)}$  being the vertical component of the wavenumber of the  $q^{\text{th}}$  partial wave.

The aim now is to look at the value of  $s(x_3)^m$  at the two interfaces of the layer, and to obtain a relation linking them. The first interface is at  $x_3 = z_m$ , the second at  $x_3 = z_{m-1}$ . Substituting these values into Equation (2.83) leads to the following

two relations:

$$\{\mathbf{s}(z_m)^m\} = [\mathbf{P}^m] [\mathbf{H}(z_m - z_{m-1})^m] e^{i(n_1x_1 + n_2x_2 - \omega t)} \quad (2.84)$$

$$\{\mathbf{s}(z_{m-1})^m\} = [\mathbf{P}^m] [\mathbf{I}] e^{i(n_1x_1 + n_2x_2 - \omega t)} \quad (2.85)$$

Note that in (2.85), the  $\mathbf{H}^m$  term has reduced to the identity matrix, while that in (2.84) is a function of the layer thickness. Substituting from (2.85) into (2.84) gives the following relation which relates the field vectors at the two faces of a layer.

$$\begin{aligned} \{\mathbf{s}(z_m)\}^m &= [\mathbf{P}^m] [\mathbf{H}(z_m - z_{m-1})^m] [\mathbf{P}^m]^{-1} \{\mathbf{s}(z_{m-1})\}^m \\ &= [\mathbf{T}^m] \{\mathbf{s}(z_{m-1})\}^m \end{aligned} \quad (2.86)$$

By repeated application of this relation, for all the layers in the system, a matrix can be formed which relates the field vectors at the top and bottom surfaces of the medium. This matrix is the product of all the layer matrices  $[\mathbf{T}^m]$  and is referred to as the transfer matrix. For the general three dimensional analysis presented here, the final transfer matrix will be of dimension  $6 \times 6$ . For a two dimensional analysis (valid for isotropic materials or for propagation along principle axes of materials with symmetry), a  $4 \times 4$  matrix is formed.

The transfer matrix has been used widely in the study of Lamb-like wave propagation in layered plates. Chimenti and Nayfeh [22] used the technique to look at propagation along axes of symmetry in biaxially laminated composite plates, as well as the more general case where the layers were allowed symmetry as low as monoclinic and general angles of incidence were used [23, 24]. Taylor and Nayfeh [25] considered multiple monoclinic layers where slip conditions were allowed between layers. These papers also describe the use of vacuum or fluid loading boundary conditions. The former amounts to a traction free surface, while the latter only requires that shear stress on the surface be zero. An application of this method is presented in Section 2.7, and dispersion curves are calculated for a cross-ply fibre-reinforced composite plate.

Much work involving the transfer matrix has been concerned with tackling the precision issues which arise in its implementation. Specifically when imaginary wave-numbers occur at high frequency-thickness products. This is the situation when a partial wave is incident on a layer at an angle beyond the critical angle (i.e. as grazing incidence is approached), giving rise to the imaginary wavenumber. The presence of this imaginary term leads to exponential growth in the propagator matrix  $[\mathbf{H}]$ , and makes computational implementation of the method very difficult due to loss of precision. One approach taken to avoid this is the Delta Matrix technique, first proposed by Dunkin [26]. In this technique,  $2 \times 2$  subdeterminants

of the transfer matrices are first calculated, and the final expressions for reflection or transmission coefficients are expressed in terms of these subdeterminants. The subdeterminants can be calculated without incurring significant precision losses, and their use improves the stability of the transfer matrix technique. This technique has been used by various researchers, including Kundu and Mal [27] who also highlighted a second precision problem arising in the calculation of the field vector for transmitted waves and proposed some ways to reorder calculations to improve this situation. Lévesque and Piché [28] further improved on the method, producing a technique for multiple isotropic layers which is reported to be highly stable. Hosten and Castaings [29], Castaings and Hosten [30] have published results based on a further generalisation of this method to multilayered media with anisotropic absorbing layers, and have shown good stability. For the case of periodically layered media, Potel and de Belleval [31] have proposed the use of Floquet waves. Floquet waves propagate in an infinite, periodically layered, and are the fundamental modes of an equivalent homogeneous medium. They are found by solving an eigenvalue problem based on the transfer matrix of one period of the thickness. When combined with careful choice of frames of reference for the  $x_3$  coordinate, this method can ameliorate the precision problem when analysing periodic multilayered materials [32]. The method has also been extended to include lossy or dissipative media [33]. Floquet homogenisation has also been used by Wang and Rokhlin [34]. Wang and Rokhlin [35] additionally used a stiffness matrix instead of a transfer matrix, resulting in a better conditioned numerical problem. The stiffness matrix related the length 6 vector of stresses on top and bottom surfaces of the medium to the length 6 vector of displacements.

A more stable, but still exact, method used to study wave propagation in a multilayered medium is the global matrix method [36, 37]. The method involves building a large (global) matrix out of submatrices describing the behaviour of the individual layers. For any given layer, the expression for stress and displacement as a function of the amplitudes of the different components has already been given in Equation (2.83). Rewriting it more compactly, we have:

$$\begin{Bmatrix} \mathbf{u}^m \\ \boldsymbol{\sigma}^m \end{Bmatrix} = [\mathbf{D}^m(x_3)] \{ \mathbf{a}^m \} e^{i(n_1 x_1 + n_2 x_2 - \omega t)} \quad (2.87)$$

Note that  $[\mathbf{D}]$  is a function of  $x_3$ . It differs from the  $6 \times 6$  square matrix in Equation (2.83), because now normalised displacement polarisation vectors are used, which explains the presence of the amplitude  $\{a\}$  vector. As in the case of the transfer matrix analysis, it is necessary to satisfy continuity of displacement and stress on the interface. If two layers,  $m$  and  $m - 1$  share a boundary (at  $x_3 = z_{m-1}$ ), then equating stresses and displacements from (2.87) the following relation must

hold:

$$\begin{aligned} [\mathbf{D}^{m-1}(z_{m-1})] \{\mathbf{a}^{m-1}\} &= [\mathbf{D}^m(z_{m-1})] \{\mathbf{a}^m\} \\ \iff [[\mathbf{D}^{m-1}(z_{m-1})] [-1\mathbf{D}^m(z_{m-1})]] \begin{Bmatrix} \mathbf{a}^{m-1} \\ \mathbf{a}^m \end{Bmatrix} &= \{0\} \end{aligned} \quad (2.88)$$

Equation (2.88) accounts for one interface in the medium. The global matrix is assembled by repeating the same process for all the interfaces in the system. This gives rise to an expression of the following form:

$$\begin{bmatrix} [\mathbf{D}^0(z_0)] & [-\mathbf{D}^1(z_0)] & & & \\ & [\mathbf{D}^1(z_1)] & [-\mathbf{D}^2(z_1)] & & \\ & & \ddots & \ddots & \\ & & & [\mathbf{D}^{n-1}(z_{n-1})] & [-\mathbf{D}^n(z_{n-1})] \end{bmatrix} \begin{Bmatrix} \mathbf{a}^0 \\ \mathbf{a}^1 \\ \vdots \\ \mathbf{a}^n \end{Bmatrix} = \{0\} \quad (2.89)$$

Equation (2.89) is the basic form of the global matrix method. Algebraic rearrangement allows solutions for particular loading conditions or input signals to be obtained. Lowe [36] has conducted an extensive review of the development and merits of the global matrix technique. The main advantage of the global matrix technique is that it is inherently more stable than the transfer matrix as inhomogeneous waves produce only decaying exponentials when the matrix is being computed [36]. It is also convenient that the solution gives rise directly to  $\{\mathbf{a}\}$ , the column of partial wave amplitudes which describe the behaviour of the entire system across all layers. This information can be obtained from the transfer matrix method also (which can even be reformulated in terms of amplitudes [31]), but it always involves a second round of computations after the initial solution is obtained. The main disadvantage of the global matrix method is that as the number of layers increases, the size of the matrices which must be dealt with increases also. This limitation has not stopped the global matrix method finding application in general purpose computer programs for analysis of multilayered media [38, 39].

Another method used to tackle the problem of wave propagation in layered, arbitrarily anisotropic plates is the stiffness, or discrete layer method [40, 41]. This method involves approximating the plate by dividing it into discrete layers. Within each layer, the displacements are approximated by interpolation functions of generalised coordinates. These generalised coordinates can be displacements and/or tractions at particular points through the thickness of the layer. Different interpolation functions can be used, for example cubic [41, 42], quadratic [40, 43, 44, 45] or linear [40] polynomials. It should be noted, that the sublayers in this technique are quite distinct from any physical layers which may be present in the plate being modelled, and for accuracy each physical lamina of a composite plate is generally modelled by several sublayers [43]. Once the displacements through the plate

have been approximated, the approximation is used with the constitutive relations for the material to formulate the Lagrangian per unit length for each lamina. The Lagrangian for the entire plate is obtained by summing the individual layers. Finally, application of Hamilton's principle results in an eigenvalue problem, which can be solved iteratively at particular frequencies/wavenumbers. The resulting eigenvectors describe the mode shapes. These contain the generalised coordinates, which can be substituted into the interpolation functions. The eigenvalues provide the wavenumbers/frequencies, depending on how the algebra has been arranged.

An advantage of this method is that it is computationally quite economical [40], and the difficulty in finding roots of the exact dispersion relation is avoided as now only an eigenvalue problem needs to be solved. Accuracy is preserved though, both for unlayered [40] and for layered media [43], and results obtained agree closely with those obtained from methods without approximation. Indeed, the results from the approximated method can be used to seed a more accurate technique with useful initial guesses for roots [43]. Finally, the overall solutions provided by the stiffness method may be coupled with finite element analysis of specific regions for greater flexibility [46, 47].

It is worth noting that for many laminated materials (such as fibre reinforced polymer composites), as the number of layers increases and the frequency decreases (wavelength increases), very approximate methods can provide quite accurate results. In this way, it is possible to treat layered plates as homogeneous anisotropic plates with appropriate material properties, as was done by Karunasena et al. [43].

### **2.4.3 Plotting Dispersion Curves**

To actually plot the dispersion curve, we need to find combinations of frequency and phase-velocity (or wavenumber) where the determinants already discussed go to zero. One way to do this [36] is to locate one point on each of the higher order curves by scanning across frequency for a fixed wavenumber in the long wavelength case (this would be a horizontal line near the top of the plot on the dispersion curves shown here). Then, using curve-following techniques, we can compute further points on the curves at shorter wavelengths. Difficulties arise since the curves will in general cross each other and will also become very close together at higher frequencies. However, this technique is computationally efficient, and makes it straight-forward to identify and plot individual dispersion curves. The technique is also quite general. Unfortunately, it is rather difficult to reliably code such an algorithm.

For the case of dispersion curves in simple materials where it is easy to see the behaviour of the governing characteristic equations (e.g. Isotropic dispersion2.3),

it is possible to set up a tailored solution scheme that can isolate specific curves (e.g. using knowledge of the tangent terms occurring in characteristic equations such as (2.53)). This has the significant disadvantage of being very non-general.

Another possibility, also discussed in [36], is to calculate the value of the relevant determinant everywhere in the frequency-wavenumber space of interest, and then to highlight the points/curves where it becomes zero. This is obviously quite computationally intensive. However, it is a very simple method to implement, in particular if a program code that can automatically handle complex numbers and produce contour plots with little fuss. Satisfactory systems for implementing such a solution include Matlab<sup>6</sup> or Python and Gnuplot. By doing a contour plot with 3D data, and plotting only the contours for  $z = 0$ , the relevant dispersion curves are produced. Although it is not possible to automatically plot individual dispersion curves in this way, it is possible to plot the symmetric and antisymmetric parts of the spectrum separately for materials with a central plane of symmetry (since the relevant characteristic equations decouple in this case).

## 2.5 Propagation Normal to Fibres

### 2.5.1 Material Properties

We will look here at a transversely isotropic material. As has been mentioned, an example of such a material is unidirectional graphite fibre reinforced epoxy. This term is very broad and describes a wide range of materials. Sample material property data have been provided by Potel and de Belleval [32], and are shown below.

$$C_{11} = 13.5\text{GPa} \qquad C_{12} = 6.3\text{GPa} \qquad (2.90)$$

$$C_{13} = 5.5\text{GPa} \qquad C_{33} = 125.9\text{GPa} \qquad (2.91)$$

$$C_{44} = 6.2\text{GPa} \qquad \rho = 1600\text{kg/m}^3 \qquad (2.92)$$

Two planes of propagation are particularly interesting when looking at a material such as this one. The first is the plane of transverse isotropy (i.e. propagation in the plane normal to the fibre direction and axis of symmetry). This is the plane denoted  $B$  in Fig. 2.4. This gives the slowness curves shown in Fig. 2.5. As can be seen, the slowness (and hence velocity) is independent of the propagation direction. This is why the plane is referred to as a plane of transverse isotropy.

---

<sup>6</sup>Thanks to Catherine Potel [48] for pointing out this approach's usefulness even for plotting dispersion curves for isotropic materials in personal correspondence via a visiting student in UCD, Johnny Caron

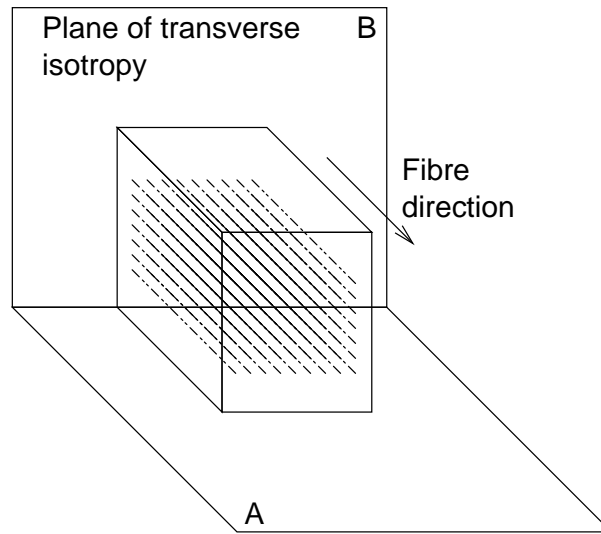


Figure 2.4: Schematic of propagation directions

Three distinct velocities are observed, with the longitudinal wave being the fastest (smallest slowness).

Also of interest is to look at propagation in a plane normal to the plane of transverse isotropy (and hence parallel to the fibre direction). Such a plane has been highlighted in Fig. 2.4 and is denoted A. In fact, any plane normal to plane B would be equivalent. The slowness curves for this case are shown in Fig. 2.6. In this case the propagation direction has a very powerful effect on the velocity of propagation. The direction of the fibres is parallel to the vertical axis in the illustration. In this direction, the slowness of the longitudinal and first shear modes is at a minimum. This is so for the longitudinal mode because in this direction of propagation it is stretching the fibres which are far stiffer than the epoxy matrix. Similarly, the shear mode is shearing normal to the fibres, which is the stiffest shear modulus of the plate. Also worth noting is that for propagation along the fibres, the two shear modes have equal slowness/velocity. This is because for this direction of propagation, they are equivalent (both involving shearing normal to the fibres). For other propagation directions, each shear mode has quite a different interaction with the plate and thus a different slowness.

For the perpendicular direction (normal to the fibres), the slownesses become identical to those seen in the plane of transverse isotropy (this is a direction shared by both planes of interest).

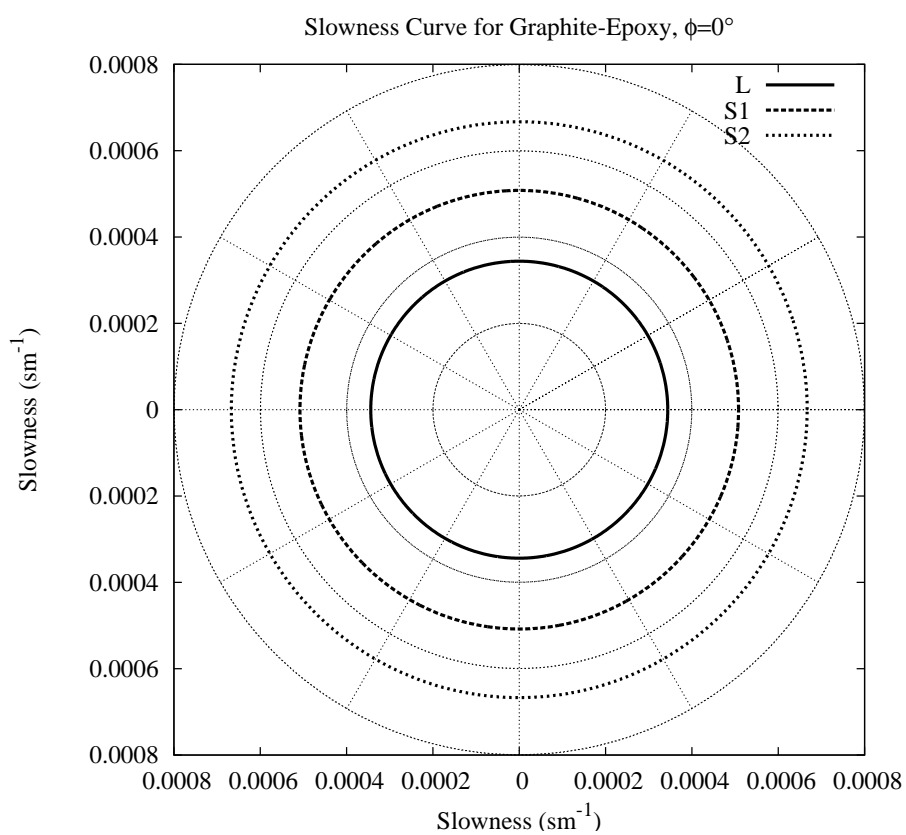


Figure 2.5: Slowness curves for propagation in the plane normal to the fibres

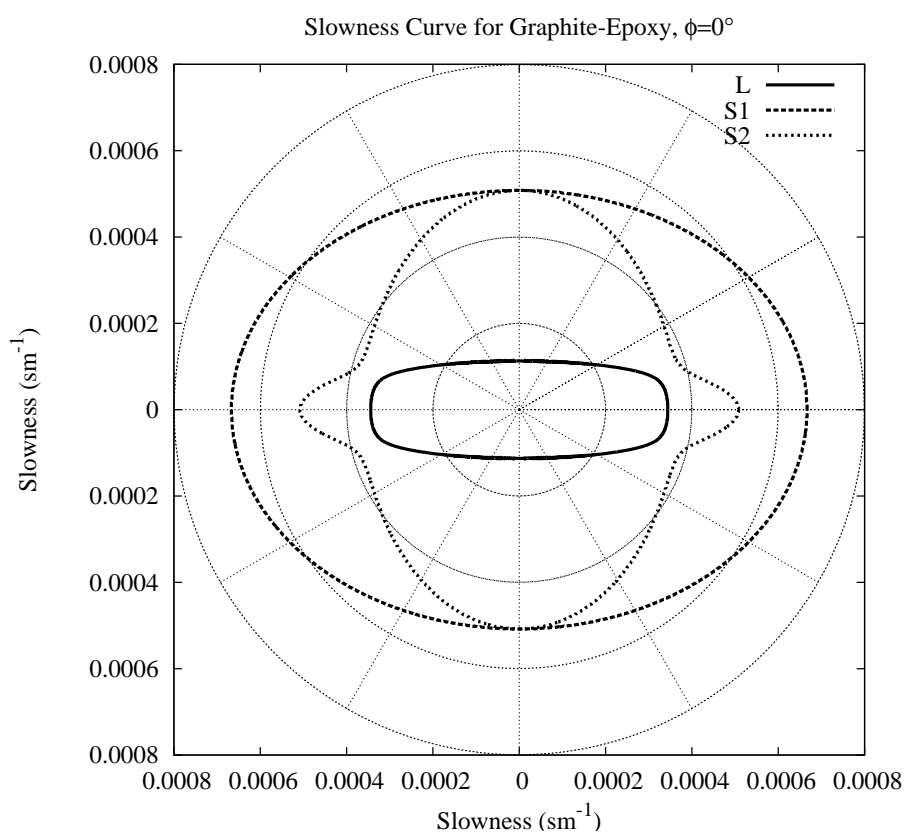


Figure 2.6: Slowness curves for propagation in a plane parallel to the fibres

## 2.5.2 Dispersion Curve

Wave propagation in a plane normal to the fibre direction in a transversely isotropic composite is equivalent to propagation in an isotropic plate, and this simplifies greatly the calculation of a dispersion curve for the material. This property can be seen in the slowness curves shown in Fig. 2.5 for graphite-epoxy composite. Earlier, in Fig. 1.24, we saw the same property in the propagation of waves in Cadmium-Sulphide, another transversely isotropic material. In each case, the slowness curves are all circles, indicating that the slowness (and hence phase velocity) is independent of propagation direction for waves polarised in this plane. A dispersion curve for Lamb waves in a plate of such a transversely isotropic material is presented in Fig. 2.7. The material used is the graphite fibre reinforced composite mentioned in Section 1.4.3 (also a transversely isotropic material, although I did not plot slowness curves to highlight the plane of transverse isotropy). The dispersion curve is plotted for propagation where all motion is restricted to the plane corresponding to the slowness curve of Fig. 2.5. For such a polarisation, the material behaves exactly like an isotropic material. The effective moduli, however, are different to those of aluminium, which were used in the calculation of Fig. 2.2. The plane of transverse isotropy being the  $X_1 - X_2$  plane, the effective values of the Lamé constants are, by Equation (1.35),

$$\begin{aligned}\lambda &= C_{12} = 6.3\text{GPa} \\ \mu &= C_{66} = \frac{1}{2}(C_{11} - C_{12}) = \frac{1}{2}(13.5 - 6.3)\text{GPa} = 3.6\text{GPa}\end{aligned}\tag{2.93}$$

The effective Poisson's ratio is, by Equation (1.38),  $(C_{11}/C_{12} + 1)^{-1} = 0.318$ . The fact that this is different from the Poisson's ratio of aluminium means that the dispersion curve will have a somewhat different shape to that observed for aluminium. The generated curve is shown in Fig. 2.7. This plot has been produced using the contour technique described earlier for isotropic materials like aluminium. At first glance, the dispersion curves look the same as those obtained for aluminium. This is unsurprising given that Poisson's ratio is quite similar for both materials (and remembering, of course, that the curve for the composite material applies only to a single plane of polarisation). However, there are some interesting points of difference between the curves for the materials. Note, for example, the crossing of  $A_3$  and  $S_3$  which occurs at approximately  $\Omega = 6.3$  and  $c/c_t = 6.5$ . In the case of aluminium, these modes also cross, but do so only at  $\Omega = 2\pi$  and in the limit as  $c/c_t \rightarrow \infty$ .

An effect of the change of Poisson's ratio is that the analytical points on the curves (e.g. the cut-off values of  $\Omega$ ) no longer happen at such mathematically neat locations on the graph. Just as making the assumption  $\lambda = 2\mu$  simplified the

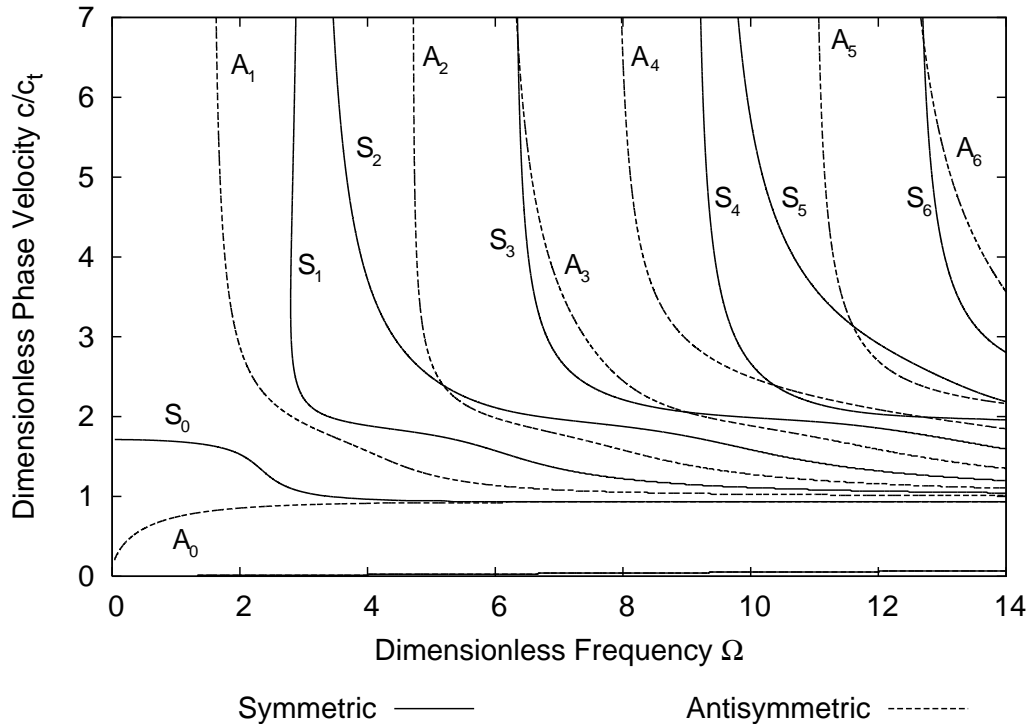


Figure 2.7: Velocity/frequency dispersion plot for unidirectional graphite fibre-reinforced epoxy, in plane of transverse isotropy. Solid lines are symmetric modes, dashed lines are antisymmetric modes.

writing of the equations governing the behaviour of a free plate, it also simplified the computation of the final dispersion curves.

Finally, although the use of dimensionless notation has simplified the previous discussion, it is important to realise that the  $c_t$  term used in the definition of dimensionless wave-speed and frequency is a function of material properties ( $c_t^2 = \mu/\rho$ ). For aluminium,  $c_t = 3.15\text{km/s}$ , while for the  $X_1 - X_2$  plane of the composite material discussed the velocity is  $c_t = 1.50\text{km/s}$ . These velocities can also be obtained by examining the slowness curves in Figs 1.7 and 2.5, and inverting the value of slowness corresponding to the shear mode.

## 2.6 Propagation Parallel to Fibres

### 2.6.1 Dispersion Curve

In this instance, the guided waves are propagating parallel to the fibre direction. This is equivalent to rotating the plate orientation of the preceding Section 2.5 90 degrees about the plate normal. The analysis of the propagation of waves in this system has been discussed in Section 2.4.1. A sample calculation will be presented here, which will give a dispersion diagram for guided waves propagating in the material subject to this orientation.

The same material properties will be used as in the previous section. These have been detailed in Equations (1.32) and (2.90). As for the case of a plane of transverse isotropy, the contour method will be used to generate the dispersion curves. Although this method is quite simple, its application is not as straightforward in the current case as it is for isotropic or transversely isotropic materials.

Due to the additional anisotropy in the plane of propagation, the characteristic equation must be reformulated for each value of phase velocity  $c$ . This is done by solving the quadratic Equation 2.69 to find the admissible values of  $\alpha$  (2.63). Two values of  $\alpha^2$  are found corresponding to four values of  $\alpha_q$ . These are denoted  $\pm\alpha_1$  and  $\pm\alpha_3$ . Having found the values of  $\alpha$  which apply to a particular phase velocity (i.e. those bulk modes with the appropriate wavenumber in the  $x_1$  direction) it is possible to solve the characteristic Equation (2.77). This is rewritten explicitly as:

$$\frac{\sin(\alpha_1 \omega/c) \cos(\alpha_3 \omega/c)}{\cos(\alpha_1 \omega/c) \sin(\alpha_3 \omega/c)} = \frac{D_{13} D_{31}}{D_{11} D_{33}} \quad (2.94)$$

$$\frac{\sin(\alpha_1 \omega/c) \cos(\alpha_3 \omega/c)}{\cos(\alpha_1 \omega/c) \sin(\alpha_3 \omega/c)} = \frac{D_{11} D_{33}}{D_{13} D_{31}} \quad (2.95)$$

The former of these describes the relation between phase velocity and frequency for symmetric modes, while the latter relates to antisymmetric modes of propagation. In these expressions, the only influence of frequency is through  $\omega$  in the trigonometric terms. The  $\alpha$  and  $D$  terms are purely functions of the phase velocity  $c$  and the material properties. Thus for each value of  $c$  in the desired range,  $\alpha_1$ ,  $\alpha_3$ ,  $D_{11}$ ,  $D_{33}$ ,  $D_{13}$  and  $D_{31}$  are calculated. Then, the residual is calculated for a range of values of frequency ( $\omega$ ), thus plotting one horizontal stripe on the dispersion curve. Once the calculation has been performed for the entire frequency-velocity space, the zero contour is plotted, corresponding to the dispersion curves. In Fig. 2.8, dimensionless frequency and velocity are again used. The definition of these quantities is somewhat more arbitrary here than it was in the case of isotropic materials, or in the case of transversely isotropic materials for propagation in the plane of isotropy. Now, there is no single meaning to the ve-

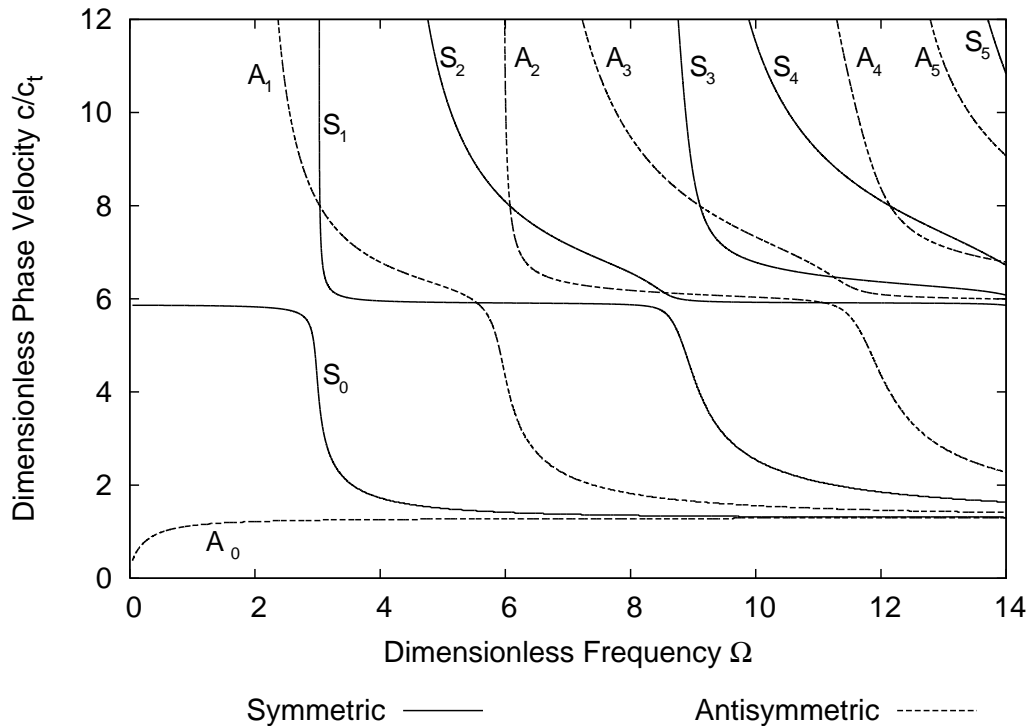


Figure 2.8: Velocity/frequency dispersion plot for graphite fibre reinforced composite, in plane parallel to fibres. Solid lines are symmetric modes, dashed lines are antisymmetric modes.

locity  $c_t$ , as the velocity of the shear mode varies with bulk propagation direction (recall Fig. 2.6). To aid comparison with the dispersion curves for waves propagating in the same material in the plane of transverse isotropy, the same value of  $c_t$  will be used, which corresponds to a velocity of 1500m/s.

Comparing Figs 2.8 and 2.7, there are obviously some profound differences. Most notable is that the  $S_0$  mode now has much higher phase velocities in its initial non-dispersive region. Additionally, this flattened region is even more flat and linear than it was for propagation in the plane of transverse isotropy. Also notable is that the plateaus in the dispersion curves are far more distinct, and flatter than for the earlier propagation direction. This is especially clear for the symmetric modes. Another difference is that the cutoff frequencies have been shifted upward, meaning that now fewer curves appear on the plot, even though the range of frequencies used is the same and the range of velocities plotted in Fig. 2.8 is in fact greater than that used in Fig. 2.7. The mode that shows the least difference is the  $A_0$  mode, which has the same shape for both materials, and similar (though

somewhat higher) phase velocity. In many other ways, both dispersion curves are qualitatively quite similar, for example in the limiting behaviour as frequency or phase velocity tend to infinity.

## 2.7 Cross Ply Composite

### 2.7.1 Dispersion Curve

A natural progression from the previous two sections is to look at a cross-ply laminate plate. Such a composite is formed from multiple layers of fibre-reinforced polymer material. As opposed to the plates just described, here the fibre direction is alternated from layer to layer. This gives a plate which has a more uniform in-plane strength. The out of plane strength is the same as for a unidirectional plate formed from the same laminae. While it would be possible to look at propagation in any arbitrary direction, matters simplify considerably if the analysis is restricted to propagation in a plane coinciding with the planes of symmetry of the component laminae.

By restricting the propagation to planes of symmetry, it is possible to use the simplified expressions of Section 2.4.1 to describe the behaviour of the individual layers. The dispersion characteristics will be determined using the transfer matrix method, which has been described in Section 2.4.2. Due to the choice of propagation direction and material properties, the current analysis will be simpler than that outlined in the earlier exposition of the transfer matrix.

As before, propagation will be restricted to the  $X_1 - X_3$  plane. Wavenumber will again be expressed in terms of a term  $\alpha$ , as shown in Equation (2.63). Since propagation is in a plane of symmetry, the Christoffel equation allows easy separation of the shear-horizontal component from the shear-vertical and longitudinal displacements as shown in Equation (2.64). This means that the quadratic Equation (2.69) can be used to find the values of  $\alpha$  corresponding to a particular  $X_1$  phase velocity. To arrive at the final dispersion relation, it remains to account for the interfaces between the discrete layers comprising the overall plate.

As noted earlier in the discussion of stratified media, it is useful to formulate a displacement-stress vector, as shown in Equation (2.78). Since the displacements are polarised in the  $X_1 - X_3$  plane, and the only applicable stresses are  $\sigma_{13}$  and  $\sigma_{33}$ , the expression can be simplified somewhat. This  $s$  vector can be written in terms of the component  $U_1$  amplitudes of the various components as follows for a

particular layer  $m$ :

$$\{\mathbf{s}(x_3)^m\} = \begin{Bmatrix} u_1^m \\ u_3^m \\ \sigma_{13}^m \\ \sigma_{33}^m \end{Bmatrix} = \begin{bmatrix} 1 & 1 & 1 & 1 \\ w_1 & -w_1 & w_3 & -w_3 \\ D_{11} & -D_{11} & D_{13} & -D_{13} \\ D_{31} & D_{31} & D_{33} & D_{33} \end{bmatrix}^m [\mathbf{H}(x_3 - z_{m-1})] \begin{Bmatrix} U_{11}^m \\ U_{12}^m \\ U_{13}^m \\ U_{14}^m \end{Bmatrix} \quad (2.96)$$

This is equivalent to Equation (2.83), though it has been simplified for the current analysis. As in the previous expression, the  $[\mathbf{H}]$  term is a diagonal matrix (here of dimension  $4 \times 4$ ) with entries  $H_{mm}(l) = \exp(ik\alpha_m x_3)$ . The  $w_1$ ,  $w_3$  and  $D_{11}$ ,  $D_{13}$ ,  $D_{31}$ ,  $D_{33}$  terms are as given in Equations (2.72) and (2.76) respectively. Writing this expression for both the top ( $x_3 = z_{m-1}$ ) and bottom ( $x_3 = z_m$ ) interfaces of the layer, and substituting from one into the other (as was shown in Section 2.4.2) leads to the following expression, where  $d$  is the thickness of the layer  $m$ , and  $[\mathbf{P}^m]$  is the square matrix from Equation (2.96).

$$\{\mathbf{s}(z_m)^m\} = [\mathbf{P}^m] [\mathbf{H}(d)^m] [\mathbf{P}^m]^{-1} \{\mathbf{s}(z_{m-1})^m\} = [\mathbf{T}^m] \{\mathbf{s}(z_{m-1})^m\} \quad (2.97)$$

Since the stress and displacement at the bottom of one layer must be the same as the stress and displacement at the top of the next layer, repeated application of this procedure allows the stresses and displacement at the top of the plate to be related to the bottom of the plate:

$$\{\mathbf{s}(0)\} = [\mathbf{T}^1] [\mathbf{T}^2] \dots [\mathbf{T}^n] \{\mathbf{s}(n)\} = [\mathbf{T}] \{\mathbf{s}(n)\} \quad (2.98)$$

At this point, there are two options regarding the calculation of dispersion curves for a free plate. The first option is to set the stresses at the top and bottom surfaces equal to zero. This results in the following equation:

$$\begin{Bmatrix} u_1^0 \\ u_3^0 \\ 0 \\ 0 \end{Bmatrix} = \begin{bmatrix} T_{11} & T_{12} & T_{13} & T_{14} \\ T_{21} & T_{22} & T_{23} & T_{24} \\ T_{31} & T_{32} & T_{33} & T_{34} \\ T_{41} & T_{42} & T_{43} & T_{44} \end{bmatrix} \begin{Bmatrix} u_1^n \\ u_3^n \\ 0 \\ 0 \end{Bmatrix} \quad (2.99)$$

This gives a characteristic equation:

$$T_{31}T_{42} - T_{32}T_{41} = 0 \quad (2.100)$$

Solving Equation (2.100) provides the dispersion characteristics for the plate.

If the plate is restricted to symmetric construction (i.e. midplane of the laminate is a plane of mirror symmetry), then alternative characteristic equations are available. The bottom of the plate is still a free surface, but it is only necessary

to account for layers up to the plate midplane. If  $n$  layers are included, then this relates to a plate with  $2n$  layers in total. Two sets of boundary conditions for the plate midplane are appropriate, and these correspond to symmetric and antisymmetric modes of the plate.

Looking first at the case of symmetric modes, it has been noted repeatedly that this requires vertical ( $u_3$ ) out-of-plane displacements to be zero on the midplane of the plate. It is also necessary for the plate centreline to have zero shear stress. This produces the equation

$$\begin{pmatrix} u_1^0 \\ u_3^0 \\ 0 \\ 0 \end{pmatrix} = \begin{bmatrix} T_{11} & T_{12} & T_{13} & T_{14} \\ T_{21} & T_{22} & T_{23} & T_{24} \\ T_{31} & T_{32} & T_{33} & T_{34} \\ T_{41} & T_{42} & T_{43} & T_{44} \end{bmatrix} \begin{pmatrix} u_1^n \\ 0 \\ 0 \\ \sigma_{33}^n \end{pmatrix} \quad (2.101)$$

$$T_{31}T_{44} - T_{41}T_{34} = 0$$

Alternatively, for antisymmetric motion, in-plane displacements ( $u_1$ ) must be zero on the midplane, and normal stresses must go to zero. This gives the characteristic equation:

$$\begin{pmatrix} u_1^0 \\ u_3^0 \\ 0 \\ 0 \end{pmatrix} = \begin{bmatrix} T_{11} & T_{12} & T_{13} & T_{14} \\ T_{21} & T_{22} & T_{23} & T_{24} \\ T_{31} & T_{32} & T_{33} & T_{34} \\ T_{41} & T_{42} & T_{43} & T_{44} \end{bmatrix} \begin{pmatrix} 0 \\ u_3^n \\ \sigma_{13}^n \\ 0 \end{pmatrix} \quad (2.102)$$

$$T_{32}T_{43} - T_{42}T_{33} = 0$$

In every case, the total transfer matrix  $[T]$  is reformulated for each value of the  $x_1$  phase velocity  $c$ . Then, values of frequency which set the required residual to zero are determined. The number of computations required increases significantly as the number of layers increases, because in general a transfer matrix must be computed for each layer. This makes computations considerably slower than in the case of a transversely isotropic material. If there are several identical layers with the same material orientation and properties and the same thickness, then it is possible to only compute the  $[T]$  for these layers once, and then include it repeatedly as appropriate in the calculation of the global transfer matrix.

In the current analysis, symmetric plates will be considered. Thus, the characteristic Equations (2.101) and (2.102) can be used. The material used in the individual layers will be the same as that discussed already in the two orientations of unidirectional plate. The composition is as indicated in Fig. 2.9, which shows two views on the same composite lay-up of alternated  $0^\circ$  and  $90^\circ$  layers. The diagram depicts the plate geometry in two planes of propagation. Half the plate is shown. The cross-section shown in Fig. 2.9(b) is taken in a plane perpendicular

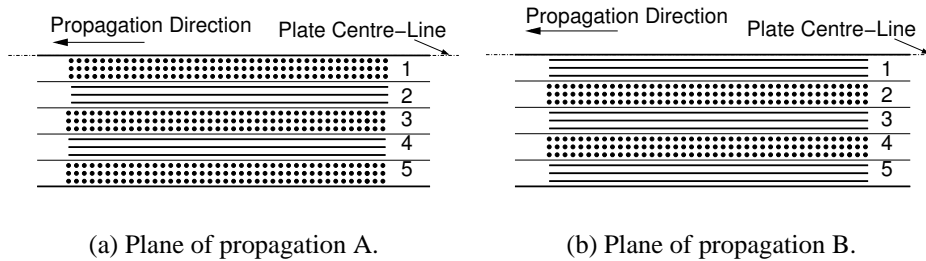


Figure 2.9: Crossply plate geometry is of stacking sequence (a)  $(90, 0, 90, 0, 90)_s$ , (b)  $(0, 90, 0, 90, 0)_s$ .

to that of the cross-section in Fig. 2.9(a). The pattern of dots denotes laminae for which propagation is in the plane of transverse isotropy, while the horizontal line denotes layers for which propagation is parallel to the fibre direction. The appropriate material properties, when used in the calculation scheme discussed earlier in this section, produces the dispersion behaviour shown in Fig 2.10 for propagation in the plane shown in Fig. 2.9(a). The definitions of the dimensionless quantities use the same value of  $c_t$  as was used in the previous two unidirectional composite plate dispersion curves. As in Section 2.6, this selection is somewhat arbitrary, but it greatly facilitates comparison between the different plate orientations and geometries.

Clearly, the dispersion behaviour shown in Fig. 2.10 is different to that of a plate composed entirely of either of the two constituent material-orientations. First, it is apparent that the magnitude of the low frequency phase velocity of the  $S_0$  mode is located between that found for propagation in the plane of transverse-isotropy, and that for propagation parallel to the fibres. Similarly, the plateaus in the other curves occur at velocities between those seen in the previous two material orientations. This is unsurprising given that the plate studied here is a mixture of the properties of the plates studied in the previous two subsections. The number of curves appearing on the dispersion plot (13) also places the crossply between the previous two cases (12 and 14), indicating that the location of cut-off frequencies is higher than in the isotropic case, but lower than the parallel-to-fibres case.

The relatively sharp first bend in the  $S_0$  curve seen in Fig. 2.10 is similar to that seen in the case of parallel to fibre propagation. However, for higher order modes, the shapes of the curves are more reminiscent of those seen for propagation in the plane of transverse-isotropy, as the plateaus are not so horizontal as those in Fig. 2.8.

The noisy band at the bottom of the dispersion plot is an annoyance. A similar,

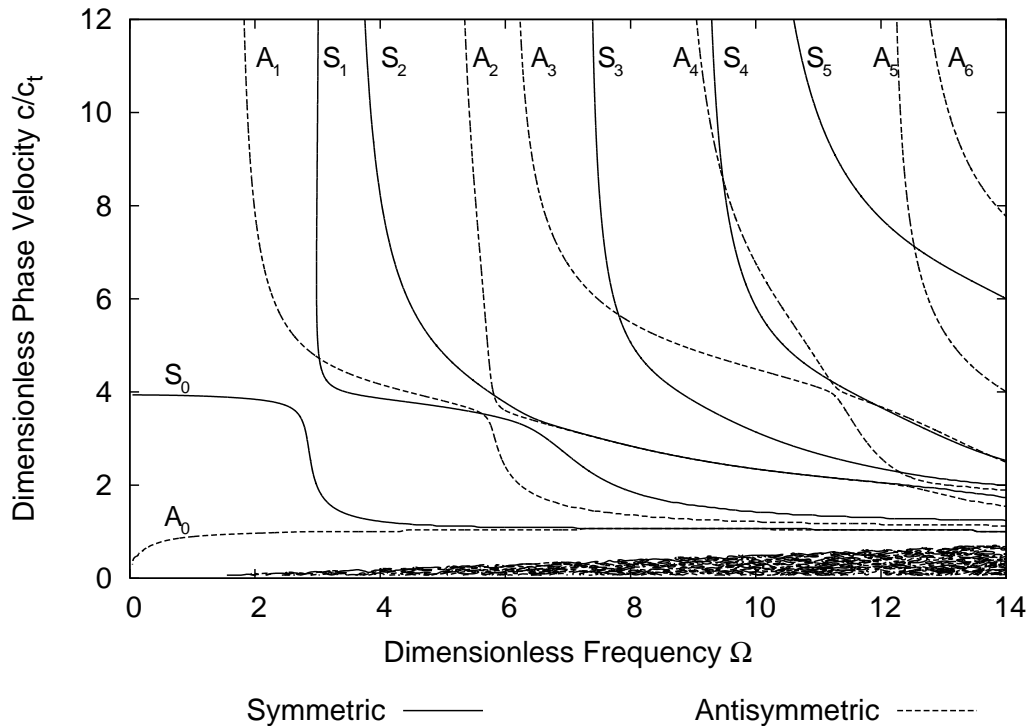


Figure 2.10: Velocity/frequency dispersion plot for graphite fibre reinforced cross-ply composite as shown in Fig. 2.9(a). Solid lines are symmetric modes, dashed lines are antisymmetric modes.

but less obtrusive, effect occurred even in the case of the transversely-isotropic plot shown in Fig. 2.7. In that case it manifested as a single additional line close to the bottom of the plot. This is a consequence of plotting the data using a contour method, and also perhaps an artifact of the computation scheme. It only becomes truly problematic if dimensionless frequencies in the range  $\Omega > 16$  are to be plotted.

Finally, it is worthwhile to consider the dispersion behaviour for the same plate shown in Fig. 2.9(a), but for propagation in a plane at right angles to the propagation plane used to generate Fig. 2.10. For this direction, the layers where formerly propagation was in the plane of transverse isotropy now have propagation parallel to the fibres. Similarly, planes that had propagation parallel to the fibres are now isotropic. This is as shown in Fig. 2.9(b). The dispersion curve produced is shown in Fig. 2.11.

The dispersion curve produced is quite similar to that observed for the first propagation direction. The main difference observed is that the velocity of the

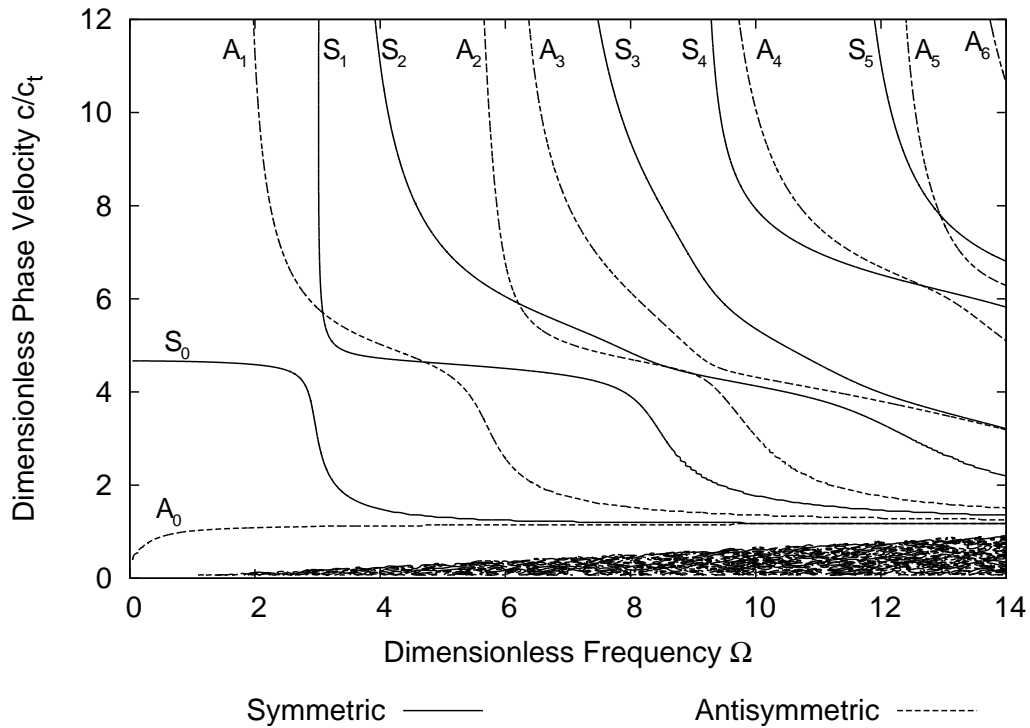


Figure 2.11: Velocity/frequency dispersion plot for graphite fibre reinforced cross-ply composite as shown in Fig. 2.9(b). Solid lines are symmetric modes, dashed lines are antisymmetric modes.

$S_0$  mode, and the plateau velocities of the higher order modes, are higher than they were for the first propagation direction, while still being lower than those observed for a unidirectional plate with propagation parallel to the fibres. This is unsurprising given that now 60% of the layers have their fibres aligned in the propagation direction, compared to 40% before. This makes the plate somewhat stiffer in the propagation direction, leading to an increase in the phase velocity.

# Bibliography

- [1] A. H. Nayfeh. *Wave Propagation in Layered Anisotropic Media with Applications to Composites*. Elsevier, Amsterdam, 1995.
- [2] B. A. Auld. *Acoustic Fields and Waves in Solids*, volume 1. John Wiley and Sons, New York, 1973.
- [3] S. G. Lekhnitskii. *Theory of Elasticity of an Anisotropic Elastic Body*. Holden-Day, San Francisco, 1963.
- [4] F. I. Fedorov. *Theory of Elastic Waves in Crystals*. Plenum Press, New York, 1968.
- [5] C. Hammond. *The Basics of Crystallography and Diffraction*. Oxford University Press, Oxford, 1997.
- [6] M. A. Jaswon and M. A. Rose. *Crystal Symmetry: Theory of Colour Crystallography*. Ellis Horwood Limited, Chichester, 1983.
- [7] W. A. Wooster. *Tensors and Group Theory for the Physical Properties of Crystals*. Clarendon Press, Oxford, 1973.
- [8] J. E. Gubernatis. Long-wave approximations for the scattering of elastic waves from flaws with applications to ellipsoidal voids and inclusions. *Journal of Applied Physics*, 50:4046–4058, 1977.
- [9] Lord-Rayleigh. On the free vibrations of an infinite plate of homogeneous isotropic matter. *Proceedings of the London Mathematical Society*, 20:225–234, 1889.
- [10] H. Lamb. On waves in an elastic plate. *Proceedings of the Royal Society, London*, 93:114–128, 1917.
- [11] R. D. Mindlin. Waves and vibrations in isotropic, elastic plates. In J. N. Goodier and N. J. Hoff, editors, *Structural Mechanics, Proceedings of the*

- First Symposium on Naval Structural Mechanics*, pages 199–232, Oxford, 1960. Pergamon Press.
- [12] J. C. Jaeger. *Elasticity, Fracture and Flow with Engineering and Geological Applications*. Chapman & Hall, London, 1969.
- [13] D. Ascher, P. F. Dubois, K. Hinsien, J. Hugunin, and T. Oliphant. *Numerical Python*. Lawrence Livermore National Laboratory, Livermore, CA 94566, USA, Mar 2001.
- [14] A. H. Nayfeh. Ultrasonic wave reflection from liquid-coupled orthotropic plates with application to fibrous composites. *Transactions of the ASME Journal of Applied Mechanics*, 55:210–217, 1988.
- [15] A. H. Nayfeh and D. E. Chimenti. Free wave propagation in plates of general anisotropic media. *Transactions of the ASME Journal of Applied Mechanics*, 56:881–886, 1989.
- [16] L. P. Solie and B. A. Auld. Elastic waves in free anisotropic plates. *Journal of the Acoustical Society of America*, 54:50–65, 1973.
- [17] P. C. Xu and S. K. Datta. Guided waves in a bonded plate: A parametric study. *Journal of Applied Physics*, 67:6779–6787, 1990.
- [18] A. J. Niklasson, S. K. Datta, and M. L. Dunn. On approximating guided waves in plates with thin anisotropic coatings by means of effective boundary conditions. *Journal of the Acoustical Society of America*, 108:924–933, 2000.
- [19] A. J. Niklasson, S. K. Datta, and M. L. Dunn. On ultrasonic guided waves in a thin anisotropic layer lying between two isotropic layers. *Journal of the Acoustical Society of America*, 108:2005–2011, 2000.
- [20] W. T. Thomson. Transmission of elastic waves through a stratified solid medium. *Journal of Applied Physics*, 21:89–93, 1950.
- [21] N. A. Haskell. The dispersion of surface waves on multilayered media. *Bulletin of the Seismological Society of America*, 43:17–34, 1953.
- [22] D. E. Chimenti and A. H. Nayfeh. Ultrasonic reflection and guided wave propagation in biaxially laminated composite plates. *Journal of the Acoustical Society of America*, 87:1409–1415, 1990.

- [23] A. H. Nayfeh. The general problem of elastic wave propagation in multilayered anisotropic media. *Journal of the Acoustical Society of America*, 89: 1521–1531, 1991.
- [24] A. H. Nayfeh and D. E. Chimenti. Elastic wave propagation in fluid-loaded multi-axial anisotropic media. *Journal of the Acoustical Society of America*, 89:542–549, 1991.
- [25] T. W. Taylor and A. H. Nayfeh. Dynamic internal response of fluid-loaded multilayered anisotropic media. *Journal of the Acoustical Society of America*, 91:2519–2528, 1992.
- [26] J. W. Dunkin. Computation of modal solutions in layered elastic media at high frequencies. *Bulletin of the Seismological Society of America*, 55:335–358, 1965.
- [27] T. Kundu and A. K. Mal. Elastic waves in a multilayered solid due to a dislocation source. *Wave Motion*, 7:459–471, 1985.
- [28] D. Lévesque and L. Piché. A robust transfer matrix formulation for the ultrasonic response of multilayered absorbing media. *Journal of the Acoustical Society of America*, 92:452–467, 1992.
- [29] B. Hosten and M. Castaings. Transfer matrix of multilayered absorbing and anisotropic media. measurements and simulations of ultrasonic wave propagation through composite materials. *Journal of the Acoustical Society of America*, 94:1488–1495, 1993.
- [30] M. Castaings and B. Hosten. Delta operator technique to improve the Thomson–Haskell-method stability for propagation in multilayered anisotropic absorbing plates. *Journal of the Acoustical Society of America*, 95:1931–1941, 1994.
- [31] C. Potel and J.-F. de Belleval. Propagation in an anisotropic periodically layered medium. *Journal of the Acoustical Society of America*, 93:2669–2677, 1993.
- [32] C. Potel and J.-F. de Belleval. Acoustic propagation in anisotropic periodically multilayered media: A method to solve numerical instabilities. *Journal of Applied Physics*, 74:2208–2215, 1993.
- [33] C. Potel and J.-F. de Belleval. Surface waves in an anisotropic periodically multilayered medium: Influence of the absorption. *Journal of Applied Physics*, 77:6152–6161, 1995.

- [34] L. Wang and S. I. Rokhlin. Floquet wave homogenization of periodic anisotropic media. *Journal of the Acoustical Society of America*, 112:38–45, 2002.
- [35] L. Wang and S. I. Rokhlin. Stable reformulation of transfer matrix method for wave propagation in layered anisotropic media. *Ultrasonics*, 39:413–424, 2001.
- [36] M. J. S. Lowe. Matrix techniques for modeling ultrasonic waves in multi-layered media. *IEEE Transactions on Ultrasonics, Ferroelectrics and Frequency Control*, 42:525–542, 1995.
- [37] H. Schmidt and F. B. Jensen. Efficient numerical solution technique for wave propagation in horizontally stratified environments. *Computers and Mathematics with Applications*, 11:699–715, 1985.
- [38] B. Pavlakovic, M. Lowe, D. Alleyne, and P. Cawley. Disperse: a general purpose program for creating dispersion curves. In D. O. Thompson and D. E. Chimenti, editors, *Review of Progress in Quantitative Nondestructive Evaluation*, volume 16A, pages 185–192, New York, 1997. Plenum Press.
- [39] B. Pavlakovic and M. Lowe. A general purpose approach to calculating the longitudinal and flexural modes of multi-layered, embedded, transversely isotropic cylinders. In D. O. Thompson and D. E. Chimenti, editors, *Review of Progress in Quantitative Nondestructive Evaluation*, volume 18A, pages 239–246, New York, 1999. Plenum Press.
- [40] S. B. Dong and R. B. Nelson. On natural vibrations and waves in laminated orthotropic plates. *Transactions of the ASME Journal of Applied Mechanics*, 39:739–745, 1972.
- [41] S. K. Datta, A. H. Shah, R. L. Bratton, and T. Chakraborty. Wave propagation in laminated composite plates. *Journal of the Acoustical Society of America*, 83:2020–2026, 1988.
- [42] W. M. Karunasena, R. L. Bratton, S. K. Datta, and A. H. Shah. Elastic wave propagation in laminated composite plates. *Transactions of the ASME Journal of Engineering Materials and Technology*, 113:411–418, 1991.
- [43] W. Karunasena, A. H. Shah, and S. K. Datta. Wave propagation in a multilayered laminated cross-ply composite plate. *Transactions of the ASME Journal of Applied Mechanics*, 40:1028–1032, 1991.

- [44] T. Liu, W. Karunasena, S. Kitipornchai, and M. Veidt. The influence of backward wave transmission on quantitative ultrasonic evaluation using Lamb wave propagation. *Journal of the Acoustical Society of America*, 107:306–314, 2000.
- [45] S. K. Datta, A. H. Shah, and W. Karunasena. Edge and layering effects in a multilayered composite plate. *Computers and Structures*, 37:151–162, 1990.
- [46] W. M. Karunasena, A. H. Shah, and S. K. Datta. Plane-strain-wave scattering by cracks in laminated composite plates. *ASCE Journal of Engineering Mechanics*, 117:1738–1754, 1991.
- [47] W. Karunasena, A. H. Shah, and S. K. Datta. Guided waves in a jointed composite plate. *Journal of the Acoustical Society of America*, 95:1206–1212, 1994.
- [48] Catherine Potel. *Propagation des Ultrasons dans les Milieu Multicouches Anisotropes – Modelisation et Experimentations*. PhD thesis, Université de Technologie de Compiègne, January 1994.